VOL.107 NO.GT2. FEB. 1981

JOURNAL OF THE GEOTECHNICAL ENGINEERING DIVISION

PROCEEDINGS OF
THE AMERICAN SOCIETY
OF CIVIL ENGINEERS

VOL. 107 NO. GT2. FEB. 1981

JOURNAL OF THE GEOTECHNICAL ENGINEERING DIVISION

PROCEEDINGS OF
THE AMERICAN SOCIETY
OF CIVIL ENGINEERS

Copyright© 1981 by
American Society
of Civil Engineers
All Rights Reserved
ISSN 0093-6405

AMERICAN SOCIETY OF CIVIL ENGINEERS

BOARD OF DIRECTION

President
Irvan F. Mendenhall

Past President
Joseph S. Ward

President Elect
James R. Sims

Vice Presidents
Robert D. Bay — Lyman R. Gillis
Francis J. Connell — Albert A. Grant

Directors
Martin G. Abegg — Paul R. Munger
Floyd A. Bishop — William R. Neuman
L. Gary Byrd — Leonard S. Oberman
Larry J. Feeser — John D. Parkhurst
John A. Focht, Jr. — Celestino R. Pennoni
Sergio Gonzalez-Karg — Robert B. Rhode
James E. Humphrey, Jr. — S. Russell Stearns
Richard W. Karn — William H. Taylor
Leon D. Luck — Stafford E. Thornton
Arthur R. McDaniel — Robert E. Whiteside
Richard S. Woodruff

EXECUTIVE OFFICERS

Eugene Zwoyer, *Executive Director*
Julie E. Gibouleau, *Assistant to the Executive Director*
Louis L. Meier, *Washington Counsel/Assistant Secretary*
William H. Wisely, *Executive Director Emeritus*
Michael N. Salgo, *Treasurer*
Elmer B. Isaak, *Assistant Treasurer*

STAFF DIRECTORS

Donald A. Buzzell, *Managing Director for Education and Professional Affairs*
Robert A. Crist, Jr., *Managing Director for Publications and Technical Affairs*
Alexander Korwek, *Managing Director for Finance and Administrative Services*
Alexandra Bellow, *Director, Human Resources*
David Dresia, *Director, Publications Production and Marketing*
Barker D. Herr, *Director, Membership*
Richard A. Jeffers, *Controller*
Carl E. Nelson, *Director, Field Services*
Don P. Reynolds, *Director, Policy, Planning and Public Affairs*
Bruce Rickerson, *Director, Legislative Services*
James M. Shea, *Director, Public Communications*
Albert W. Turchick, *Director, Technical Services*
George K. Wadlin, *Director, Education Services*
R. Lawrence Whipple, *Director, Engineering Management Services*

COMMITTEE ON PUBLICATIONS

Stafford E. Thornton, *Chairman*
Martin G. Abegg — Richard W. Karn
John A. Focht, Jr. — Paul R. Munger
William R. Neuman

GEOTECHNICAL ENGINEERING DIVISION

Executive Committee
Robert Schuster, *Chairman*
Ernest T. Selig, *Vice Chairman*
William F. Swiger — Harvey E. Wahls
Robert T. Darragh, Jr., *Secretary*
Elio D'Appolonia, *Management Group E Contact Member*

Publications Committee
William F. Marcuson III, ***Chairman***
O. B. Andersland — Fred H. Kulhawy
Warren J. Baker — C. C. Ladd
Don C. Banks — Poul V. Lade
Chandra S. Brahama — Leonard J. Langfelder
John T. Christian — Felipe A. Len-Rios
G. W. Clough — Gholamreza Mesri
Tuncer B. Edil — Donald J. Murphy
Herbert H. Einstein — S. V. Nathan
Arley G. Franklin — Thom L. Neff
D. H. Gray — Michael W. O'Neill
Bobby Hardin — Jean H. Prevost
Cornelius J. Higgins — Adel Saada
William H. Highter — Surendra K. Saxena
Robert D. Holtz — Robert L. Schiffman
Izzat M. Idriss — Woodland G. Schockley
L. H. Irwin — Marshall L. Silver
Reuben H. Karol — Glen S. Tarbox
H. Y. Ko — G. R. Thiers
William D. Kovacs — D. D. Treadwell
Leland M. Kraft — Charles R. Ullrich
Raymond J. Krizek — J. Lawrence Von Thun
R. N. Yong
E. T. Selig, *Exec. Comm. Contact Member*

PUBLICATION SERVICES DEPARTMENT

David Dresia, *Director, Publications Production and Marketing*

Technical and Professional Publications

Richard R. Torrens, *Manager*
Joseph P. Cerami, *Chief Copy Editor*
Linda Ellington, *Copy Editor*
Thea C. Feldman, *Copy Editor*
Meryl Mandle, *Copy Editor*
Joshua Spieler, *Copy Editor*
Shiela Menaker, *Production Co-ordinator*
Richard C. Scheblein, *Draftsman*

Information Services

Elan Garonzik, *Editor*

PERMISSION TO PHOTOCOPY JOURNAL PAPERS

Permission to photocopy for personal or internal reference beyond the limits in Sections 107 and 108 of the U.S. Copyright Law is granted by the American Society of Civil Engineers for libraries and other users registered with the Copyright Clearance Center, 21 Congress Street, Salem, Mass. 01970, provided the appropriate fee is paid to the CCC for all articles bearing the CCC code. Requests for special permission or bulk copying should be addressed to the Manager of Technical and Professional Publications, American Society of Civil Engineers.

CONTENTS

Offshore Gravity Structures: Centrifugal Modeling
by Jean H. Prevost, Bernard Cuny, and Ronald F. Scott 125

Offshore Gravity Structures: Analysis
by Jean H. Prevost, Bernard Cuny, Thomas J. R. Hughes, and Ronald F. Scott 143

Construction Vibrations: State-of-the-Art
by John F. Wiss 167

Response of Buried Structures to Traveling Waves
by Richard N. Hwang and John Lysmer 183

At-Rest Lateral Pressure of Peat Soils
by Tuncer B. Edil and Abdulmohsin W. Dhowian 201

This Journal is published monthly by the American Society of Civil Engineers. Publications office is at 345 East 47th Street, New York, N.Y. 10017. Address all ASCE correspondence to the Editorial and General Offices at 345 East 47th Street, New York, N.Y. 10017. Allow six weeks for change of address to become effective. Subscription price to members is $16.00. Nonmember subscriptions available; prices obtainable on request. Second-class postage paid at New York, N.Y. and at additional mailing offices. GT.

The Society is not responsible for any statement made or opinion expressed in its publications.

TECHNICAL NOTES

Proc. Paper 16009

Statistical Analysis of Marine Clay Deposits
by Hin Fatt Cheong and R. V. Subrahmanyam 221

Limit Plasticity Approach to Slope Stability Problems
by Ryszard J. Izbicki 228

DISCUSSION

Proc. Paper 16003

Static Shear and Liquefaction Potential,* by Yoginder P. Vaid and W. D. Liam Finn (Oct., 1979).
by Yoshiaki Yoshimi and Kohji Tokimatsu 237

INFORMATION RETRIEVAL

The key words, abstract, and reference "cards" for each article in this Journal represent part of the ASCE participation in the EJC information retrieval plan. The retrieval data are placed herein so that each can be cut out, placed on a 3 × 5 card and given an accession number for the user's file. The accession number is then entered on key word cards so that the user can subsequently match key words to choose the articles he wishes. Details of this program were given in an August, 1962 article in CIVIL ENGINEERING, reprints of which are available on request to ASCE headquarters.

*Discussion period closed for this paper. Any other discussion received during this discussion period will be published in subsequent Journals.

16044 OFFSHORE GRAVITY STRUCTURES: MODELING

KEY WORDS: **Centrifugation;** Eccentric loading; **Geotechnical engineering;** Offshore structures; Testing

ABSTRACT: Offshore gravity structure foundations, including their analysis and design, are investigated. The results of an experimental study on the interaction of such structures with their soil foundations when subjected to wave forces are reported. The experimental tests were performed in a centrifuge at 100 g centrifugal acceleration with a 10-cm diam model structure bearing on a normally consolidated desposit of Santa Barbara silt. Therefore, the experimental test results apply to a 10-m diam prototype structure. The model structure was subjected to both monotonic and cyclic, as well as inclined and eccentric loading conditions; and its resulting movements (sinking, sliding and tilting) were recorded.

REFERENCE: Prevost, Jean H., Cuny, Bernard, and Scott, Ronald F., "Offshore Gravity Structures: Centrifugal Modeling," *Journal of the Geotechnical Engineering Division,* ASCE, Vol. 107, No. GT2, **Proc. Paper 16044**, February, 1981, pp. 125-141

16045 OFFSHORE GRAVITY STRUCTURES: ANALYSIS

KEY WORDS: Analysis; **Centrifugation;** Constitutive equations; Cyclic loads; Finite elements; **Geotechnical engineering;** Numerical analysis; **Offshore structures;** Plasticity; Strength; Stress strain characteristics

ABSTRACT: Experimental and analytical studies are described on the offshore gravity structure foundations with their soil foundations when subjected to wave forces. The experimental tests were performed in a centrifuge at 100g centrifugal acceleration with a 10-cm diam model structure bearing on a normally consolidated deposit of Santa Barbara silt, and therfore apply to a 10-m diam prototype structure. The analytical predicitions, for the particular prototype situation considered in this study, were obtained by using a finite element program which incorporates a three-dimensional nonlinear soil model capable of describing the behavior of the Santa Barbara silt under both monotonic and cyclic loading conditions. The results of both two-dimensional (plane strain) and three-dimensional calculations are reported, and the are compared with the experimental test results obtained in the centrifuge.

REFERENCE: Prevost, Jean H., Cuny, Bernard, Hughes, Thomas J.R., and Scott, Ronald F., "Offshore Gravity Structures: Analysis," *Journal of the Geotechnical Engineering Division,* ASCE, Vol. 107, No. GT2, **Proc. Paper 16045**, February, 1981, pp. 143-165

16030 CONSTRUCTION VIBRATIONS: STATE-OF-THE-ART

KEY WORDS: **Blasting;** Concrete; **Construction equipment;** Demolition; **Dynamics; Pile driving;** Pipelines; **Vibration**

ABSTRACT: The generation and propagation of vibrations due to construction are discussed. The relative intensity of the vibration produced by many construction sources is identified. A brief summary of the development of suitable vibration-measuring instruments is related. Differences in current damage criteria are revealed. Future research is needed on the effects of both transient and steady-state vibrations on structures, uncured concrete, soils and underground utilities; additional research is needed on fatigue of building materials. Human response evaluation of transient vibrations also requires further research.

REFERENCE: Wiss, John F., "Construction Vibrations: State-of-the-Art," *Journal of the Geotechnical Engineering Division,* ASCE, Vol. 107, No. GT2, **Proc. Paper 16030**, February, 1981, pp. 167-181

16052 RESPONSE OF BURIED STRUCTURES TO WAVES

KEY WORDS: Dynamics; **Finite element method; Pipelines; Seismic design; Soil-structure interaction; Tunnels;** Wave propagation; Waves

ABSTRACT: The response of buried long structures to waves traveling in the longitudinal direction of the structures was studied. The structures and the surrounding soils were represented by three-dimensional finite elements. The three-dimensional models, however, were reduced to two-dimensional models by using a special type of wave-transmitting element which faithfully accounts for the effects of wave propagation. The results obtained for a linear system indicate that, for large structures, soil-structure interaction effects on the computed stresses and strains are indeed significant; therefore, it will be overly conservative to use free field strains in the design. Also, the assumption of vertically propagating waves is not adequate in predicting response; therefore, appropriate considerations should be given to traveling waves.

REFERENCE: Nwang, Richard N., and Lysmer, John, "Response of Buried Structures to Traveling Waves," *Journal of the Geotechnical Engineering Division,* ASCE, Vol. 107, No. GT2, **Proc. Paper 16052**, February, 1981, pp. 183-200

16063 AT-REST PRESSURE OF PEAT SOILS

KEY WORDS: At rest pressure; **Coefficient of earth pressure;** Compressibility (soils); Fibers; **Lateral pressure; Peat;** Soil classification; **Soil compression tests**

ABSTRACT: The results are presented of an experimental program directed toward evaluating K_0 (the coefficient of lateral earth pressure under conditions of no lateral formation) and its dependence on stress history and other parameters of peat soils. Three peats with different fiber contents were consolidated in a custom-built K_0-test tube. During loading and rebound, the axial deformations, pore pressure, and both axial and radial stresses were measured. A sand and clay sample compared well with previously reported values and empirical predictions. The values of K_0 for the peat sample were found to remain essentially constant during the loading phase, but their values (which increased gradually during unloading) never exceeded unity. Several indirect approaches were tried to compute the K_0 of the peats from effective shear strength parameters. Peat type appeared to exert a significant influence on the measured values of K_0 during loading.

REFERENCE: Edil, Tuncer B., and Dhowian, Abdulmohsin W., "At-Rest Lateral Pressure of Peat Soils," *Journal of the Geotechnical Engineering Division,* ASCE, Vol. 107, No. GT2, **Proc. Paper 16063**, February, 1981, pp. 201-217

JOURNAL OF THE GEOTECHNICAL ENGINEERING DIVISION

OFFSHORE GRAVITY STRUCTURES: CENTRIFUGAL MODELING

By Jean H. Prevost,[1] M. ASCE, Bernard Cuny,[2] and Ronald F. Scott,[3] M. ASCE

INTRODUCTION

The fast-growing need for new oil and gas supplies has led to the development of numerous new offshore fields. Until the last decade most offshore petroleum industry activity was confined to areas of shallow water depths. A few years ago active offshore drilling and production began in the North Sea and is now being contemplated in both the North Atlantic and Arctic waters. At these sites the waves are larger and the water depths are greater than in areas previously exploited. New types of offshore platforms have thus had to be designed in order to withstand such difficult site conditions. Some of these structures are of unprecedented dimensions, and many of the problems encountered in their design have never been tackled before. In particular, the design of their foundations poses a new and very complicated geotechnical problem, as explained later.

Prior to North Sea oilfield development, the majority of offshore structures has been of tubular steel design, pinned to the sea floor by piles, e.g., in the Gulf of Mexico. Initially, platform structures developed for the North Sea were also of this type, but of substantially stronger construction than those built in the Gulf of Mexico. The soil conditions found in some other parts of the offshore world are different in general from those in the Gulf of Mexico, and often from a foundation point of view are so excellent that, if encountered on land, would not have required piles for the foundations of even heavy structures. Offshore, the piles are needed because of the very large lateral

[1]Asst. Prof. of Civ. Engrg., Princeton Univ., Princeton, N.J. 08544.
[2]Grad. Student, California Inst. of Tech., Pasadena, Calif.
[3]Prof. of Civ. Engrg., California Inst. of Tech., Pasadena, Calif.

Note.—Discussion open until July 1, 1981. Separate discussions should be submitted for the individual papers in this symposium. To extend the closing date one month, a written request must be filed with the Manager of Technical and Professional Publications, ASCE. Manuscript was submitted for review for possible publication on March 5, 1980. This paper is part of the Journal of the Geotechnical Engineering Division, Proceedings of the American Society of Civil Engineers, ©ASCE, Vol. 107, No. GT2, February, 1981. ISSN 0093-6405/81/0002-0125/$01.00.

and overturning loads generated by waves. The stability of such platforms depends on the presence of the piles. However, it is extremely difficult and time consuming to drive piles in deep and rough waters.

Consequently, there is a potentially hazardous period in regions where bad weather is prevalent, after the placement of the platform, and before sufficient piles are driven to ensure the safety of the structure. This period may be months long. There were, therefore, good reasons to consider alternative design solutions for major offshore structures in the North Sea—designs for which the structure would be stable within days after installation. Studies demonstrated that at many locations it should be possible to place gravity-type concrete structures directly on the sea floor without the use of piles. A number of such concrete structures have now been designed and built. By 1978, 13 concrete gravity platforms had been installed in the North Sea in water depths ranging from 100 m–150 m. The structures are built on shore, floated to the site, sunk and seated on the sea floor by ballasting. They are designed to resist wave forces

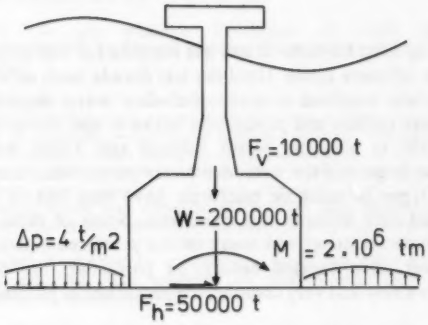

FIG. 1.—Gravity Platform Load Conditions and Definitions of Terms

by the combined action of their weight and large foundation dimensions (typically of the order of several hundred thousand tons and 10,000 m^2, respectively).

In terms of size these gravity structures are one order of magnitude larger than platforms previously built, and this also applies to the environmental forces to which they are subjected. Fig. 1, as an example, gives the order of magnitude of the forces acting on a gravity structure in a water depth of 150 m as a result of its interaction with a wave whose height is 30 m and period 15 sec. When such a wave passes the structure, the forces first act in one direction and a few seconds later in the opposite direction with almost the same magnitudes. Under such cyclic loading conditions, soils exhibit very significant dissipative and softening characteristics (1,3). The effect of cyclic structural forces on soil foundations is thus a type of fatigue problem, and it is of great concern to determine to what extent the behavior of soils under cyclic loading may influence the safety of these structures.

Field data on the performance of full scale structures under severe loading conditions are urgently needed, but until now have remained proprietary. Further

data are unlikely to be obtained soon due to the scale of the structures involved, the cost of testing, and the low probability of having a particular instrumented structure subjected to design loads. Consequently, some form of model study seems inevitable to enable alternative design or analysis methods to be checked.

A program whereby this possibility could be implemented was suggested to Chevron Oil Company. It would utilize centrifugal model tests of a gravity platform structure placed on a normally consolidated deposit of soil to be carried out at California Institute of Technology. The centrifuge model tests would include both monotonic and cyclic loading of the model structure. Centrifuge tests were proposed because in them, model scaling relations are adequately satisfied as considered later. The soil involved was a clayey silt, obtained from the ocean floor off the southern California coast. Centrifuge tests on the behavior of a gravity platform placed on a homogenous clay deposit have been reported before in Ref. 7.

This proposal was accepted by Chevron Oil Company, and work was initiated. This report describes the apparatus, the tests and test results. Their analysis is reported in Refs. 5 and 6.

Centrifugal Model Testing

If the scaling relations required to characterize tests of geotechnical models are established, it is found that, because of the general dependence of the mechanical properties of soil on the ambient stress conditions, and the importance of gravity-induced stresses, scaling can only be satisfied under special conditions. In the special case of soil, it is inconvenient or impossible to construct a model material, and a real soil is usually employed in model tests. In that case, the scaling conditions require that the soil model be subjected to a higher gravitational acceleration than the prototype. The ratio of the accelerations in model and prototype structures is inversely proportional to the ratio of their linear dimensions; that is to say, a 1/100-scale soil model must be subjected to 100 times the earth's gravitational acceleration, and so on. To obtain the necessary accelerations, a centrifuge is required. Considering the size and mass of soil in model experiments, even at 1/100 scale, the centrifuge has to be quite large.

If the ratio of linear prototype dimensions to those of the centrifuge model is h, then the ratio of area is h^2 and volumes h^3. The scaling relations indicate that forces in the prototype are h^2 times those in the model, so that stresses (force per unit area) are unchanged. Deformation in the prototype is h times larger than in the model, but strains (deformation per unit length) are the same. Thus, the presence of the same material in both prototype and model results in identical stresses and strains at homologous points. Where dynamic problems are involved, it turns out that time in the prototype is h times the time in the model. Consequently, model frequencies are higher by the factor h, but velocities are unchanged. Energy in the prototype is h^3 times the energy in the model but energy density (energy per unit volume) is the same. Table 1 gives a more complete list of the relations between prototype and model (centrifuge) parameters.

The attractiveness of the centrifugal method is that the stresses in the model are identical to those in the prototype so that it avoids problems associated with testing, at earth gravity, small soil models involving material with strongly

nonlinear and stress-dependent behavior. The disadvantages are associated with performing the tests on models which are rotating at rates of 100 rpm–500 rpm in a centrifuge. Power and signals have to be passed in and out through electrical and hydraulic sliprings. Up till now, electrical noise has presented a problem in recording the results of a variety of experiments, especially where strain gauges have been employed. The noise comes from ambient sources, the electric motor driving the centrifuge, from motors used to control the tests, and centrifuge vibration.

A number of centrifuges have been built and used for soil testing. There are three in the United Kingdom, two at Cambridge and one at Manchester, with radii up to 5 m and acceleration capabilities up to 200 *g*. In the Soviet Union, a recent paper (4) refers to the employment of "several dozen" centrifuges for soil testing purposes. So far, only one or two small centrifuges have been

TABLE 1.—Scaling Relations

Quantity (1)	Full scale (prototype) (2)	Centrifugal model, at n gravities (3)
Linear dimension, displacement	1	$1/n$
Area	1	$1/n^2$
Volume	1	$1/n^3$
Stress	1	1
Strain	1	1
Force	1	$1/n^2$
Mass	1	$1/n^3$
Acceleration	1	n
Energy	1	$1/n^3$
Density	1	1
Energy density	1	1
Velocity	1	1
Time: in dynamic terms	1	$1/n$
Time: in diffusion cases	1	$1/n^2$
Time: in viscous flow cases	1	1
Frequency in dynamic problems	1	n

used for such tests in the United States, although the technique was apparently originated here (2); the reasons for this limited usage have not been determined. Centrifuges are currently used for geotechnical research in Sweden, Denmark, France, and Japan, apart from the Soviet Union and the United Kingdom. A compilation of references on centrifugal testing, worldwide, extends to more than 150 papers and a number of books.

Soil Tested

The soil tested in this investigation is a sandy clayey silt ("Santa Barbara silt") obtained in soil investigations off the California coast in the vicinity of Santa Barbara and supplied by Dames and Moore, San Francisco, through the courtesy of Chevron Oil Research Company, La Habra, Calif. The scale tests

were carried out on the soil in a rectangular container 14.5 in. × 11.5 in. × 10 in. mounted on the centrifuge platform. The Santa Barbara silt as initially obtained, was supplied in the form of dried out chunks of soil, left over from laboratory tests performed by Dames and Moore. Later, extra quantities of this material were received in moist condition in plastic sample tubes, from which the soil was moved by jacking with a piston extractor. It was not convenient or correct in either case, to place the soil in the test containers in the form in which it was received, since it was desirable to install the platform on a normally consolidated soil deposit to simulate an ocean floor test site. Consequently, both dry and wet as-received samples of Santa Barbara silt were mixed

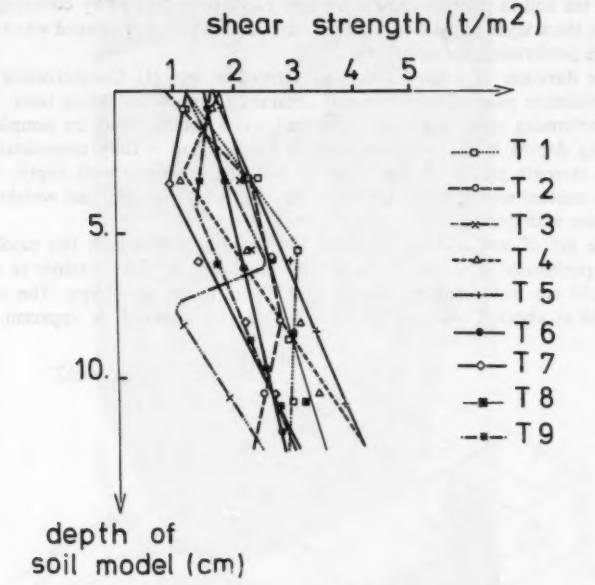

FIG. 2.—Centrifuge Model Shear Strength Profiles in Series T Tests

with tapwater in a mixing machine until the resulting material was smooth and lump-free at a water content slightly higher than the liquid limit of the soil ($w_L \approx 30\%$).

The soil slurry was then poured into the test container, taking care to avoid the inclusion of air bubbles. To prepare the test specimen the container was centrifuged at 100 g, the test acceleration, until it had consolidated. Drainage was facilitated by the presence of a sand layer at the bottom of the container, overlaid by blotting paper to prevent mixing of the silt and sand, and by a layer of porous plastic placed inside the wall of the test container.

The question of the similarity of the centrifuge test specimen of soil to that of the larger prototype section, and in particular, the identification of the stress

paths in model and prototype is complicated. Absolutely similar stress histories and stress paths cannot be obtained during testing, but a reasonable facsimile can be achieved in the centrifuge (8).

The soil at the site is slightly overconsolidated with a field shear strength at the mud line of about 2.5 ton/m^2. The strength increases linearly with depth to a value close to 5 ton/m^2 at a depth of about 12.5 m in the prototype. The field strengths were measured by performing "Tor-vane" tests on the samples as they were obtained on the deck of the drilling vessel. As such, they are not very precise and depend largely on the local nature of the soil exposed at the end of each sample tube for testing.

In order to effect a close simulation of the real material properties in the field, the soil in the container was slightly overconsolidated by covering it with a 1-in. thick layer of sand during the consolidation phase. The sand was removed before performing the model tests.

The duration of centrifuging was arrived at by: (1) Consideration of the consolidation properties of the soil obtained from consolidation tests; and (2) by performing miniature vane shear and water content tests on samples from varying depths in the test container. When the soil is fully consolidated, the shear strength profile should increase essentially linearly with depth, and the water content should decrease with depth. Both dry and total unit weight should increase with depth.

One set of soil test results from the containers in which the model tests were performed is shown in Fig. 2. The silt occupied the container to a depth of 12.50 cm, representing a depth of 12.50 m in the prototype. The soil was probed at about 5 cm from the sides of the container. It is apparent that in

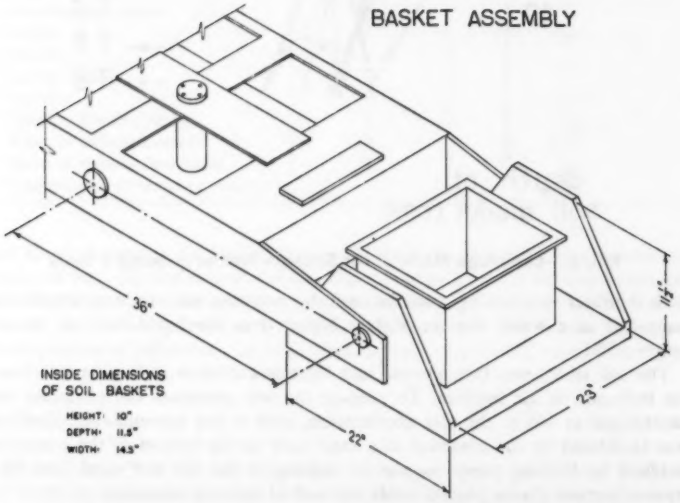

FIG. 3.—Perspective View of Centrifuge Test Container

most cases adequate consolidation has been achieved although the soil strength appears to be slightly lower than in the field. This appears to be related to the changing soil-water chemistry caused by continually diluting the original salt content of the soil by the addition of tapwater.

Equipment and Instrumentation

Centrifuge.—The centrifuge used is a Model A1030 Genisco "G-accelerator," which consists of an 80-in. diam aluminum alloy arm which rotates in the horizontal

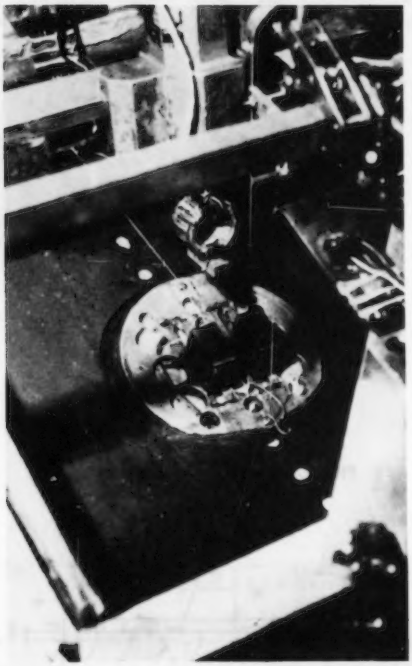

FIG. 4.—Centrifuge Model Platform and Loading Devices

plane and is rated at 10,000 *g*-lb payload capacity. At each end of the arm is located an 18 in. × 22 in. magnesium mounting basket capable of carrying a 100-lb payload to 100 *g* or a 60-lb payload to 175 *g*. The acceleration range at the approx 40-in. radius of the baskets is from 1*g*–175*g*. A variable speed transmission based on the Rouverol ball-galaxy principle allows continuous variation of the acceleration throughout the range. The transmission is driven by a 3 hp 1,800 rpm 220 V three-phase double-ended electric drive motor. For accurate determination of the rotational speed, a 600 tooth gear wheel

is located on the main drive shaft and this produces 600 electrical pulses per revolution on a magnetic pickoff. These pulses are read by an electronic counter which converts them to an LED display of RPM accurate to 0.1 prm. The drift and wow of the system at any given setting is 0.05%. The acceleration

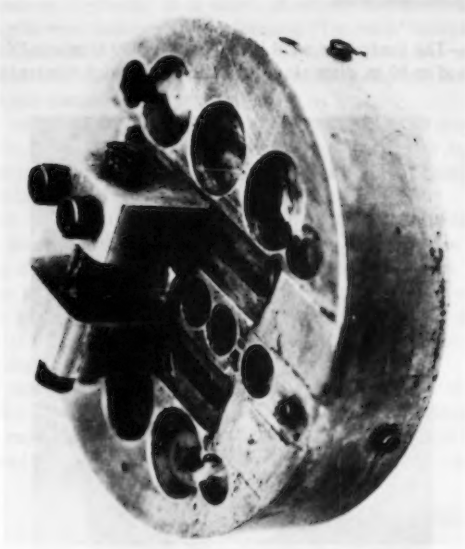

FIG. 5.—Centrifuge Model Platform

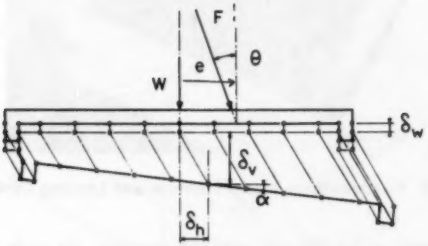

FIG. 6.—Definition of Test Parameters

arm is housed in an extruded aluminum enclosure, with all controls and instrumentation, in the interests of safety, located remotely.

Electrical power and signals to and from the rotating arm or basket are conducted through 44 sliprings, of various capacities in the 10 amp–30 amp range. Externally generated hydraulic or air pressure is transmitted through either two or four

lines by means of rotary unions (hydraulic sliprings). Operations on the centrifuge can be observed by means of a television camera mounted on the rotating arm close to the axis; its signal is conveyed either through the aforementioned sliprings or through coaxial cable and related, separate sliprings, to a monitor television in the instrumentation house.

The centrifuge layout is shown in Fig. 3, with a more detailed view of the arm in the test configuration of this report in Fig. 4, which will be described later.

Specialized Test Apparatuses.—Fig. 4 shows one of the two apparatuses which were constructed to apply an inclined and eccentric force to the model platform. Loading was achieved by directly pushing on the model platform with a small

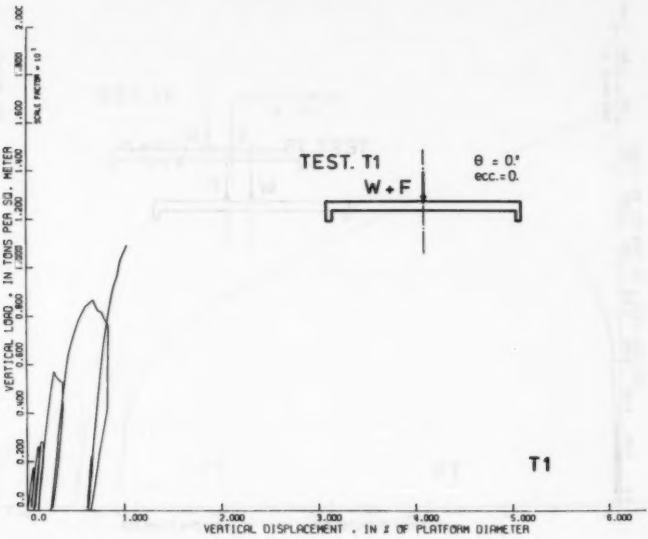

FIG. 7.—Test T1: Test Results

hydraulic piston attached to the aluminum loading frame shown in Fig. 4. This loading frame is bolted to the aluminum container.

The model platform was machined out of aluminum to a 10-cm diam as shown in Fig. 5. Its weight was adjusted so that at 100 g it corresponded to a bearing pressure of 4.3 ton/m^2. The platform was mounted with skirts (0.4 cm thick) whose depth could be varied (0 cm–0.6 cm) by adjusting the position of the movable base of the structure. The bearing surface consisted of an aluminum plate on which sand had been glued so that it would be rough to simulate field conditions.

The applied force and the resulting movements of the model platform were recorded by a load cell and displacement transducers. The cell consists of a ring of stainless steel ("proving ring"), 1.0-in. × 0.5-in. height × 0.025-in. wall

thickness, to which were bonded four strain gauges (BLH FDE-06S-35ET, G.F. + 3.10 ± 0.5 ohms, Serial No. 1-A-KH, Lot No. A-D-135) using an epoxy adhesive (BLH EPY-150). Two of the gauges were located on the outside of the ring diametrically opposite one another, while the other two gauges were placed in the same location, but on the inside. This arrangement provided reasonable output and good temperature compensation when wired into a complete bridge. Displacements were recorded through nylon strings attached to the platform and connected to displacement transducers made of a small cantilever strip of metal on which strain gauges had been glued. They formed the legs of a Wheatstone bridge. The displacement transducers were preloaded slightly to avoid any slack in the strings.

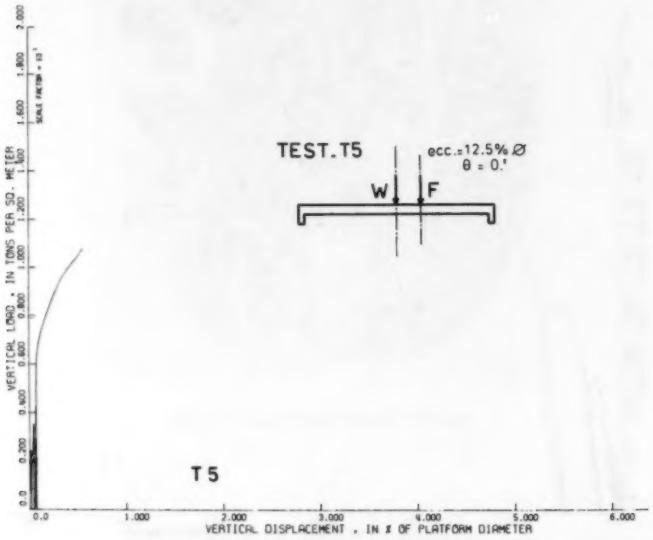

FIG. 8.—Test T5: Test Results for Vertical Load Versus Vertical Displacement

Data Acquisition Systems.—The recording instruments used were: (1) A Honeywell Model 1858 CRT visicorder, which allows inertialess recording from DC to 5,000 Hz; and (2) a Hewlett-Packard Model 7045A X-Y recorder. The X-Y recorder was used primarily to check that the tests were proceeding as expected; accordingly only the load and one displacement component were recorded on it. The load and all displacements were also recorded on the visicorder.

All pretest calibrations were carried out using the entire electronic circuitry, i.e., the calibration signals were routed through those terminals, amplifier channels, and sliprings which they would use during the actual testing. To calibrate the load cell, brass tester weights were suspended from the cell and the output recorded on both the X-Y recorder and visicorder. The calibration of the displacement transducers was accomplished with the aid of a Federal dial gauge

accurate to 0.001 in. The output was again recorded on both the X-Y recorder and the visicorder.

Test Procedures.—The Santa Barbara soil was thoroughly mixed with water, as previously described, and placed in the prepared soil container. The preparation consisted of placing 1 cm of saturated sand in the bottom of the container and covering both the sand and the vertical walls of the cylinder with porous, permeable plastic material. This facilitated the drainage of water at 100 *g* to maximize consolidation. Once the soil was introduced the centrifuge was brought to 100 *g* acceleration and allowed to operate at this setting for several hours to consolidate the soil. The centrifuge was then stopped, and for the initial tests vertical marker columns of wax were installed in the middle plane of

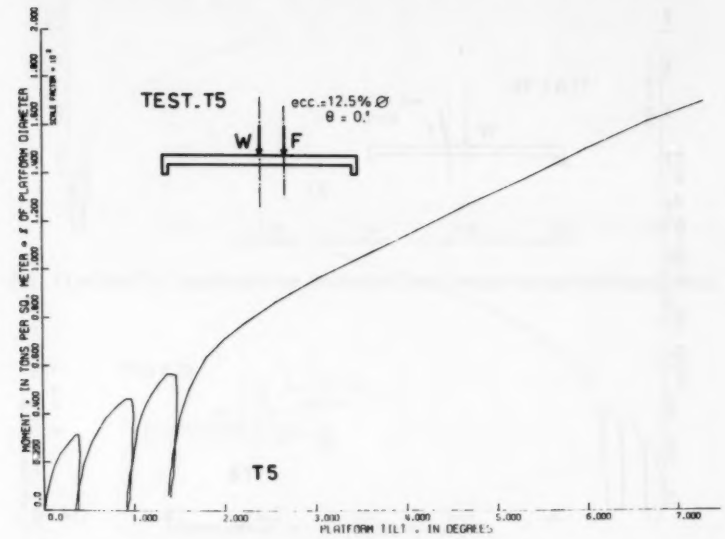

FIG. 9.—Test T5: Test Results for Moment Versus Tilt

the bucket by pouring hot wax in predrilled holes about 2 cm apart. Later, modeling clay cylinders were used in place of the wax. The soil deposit was thereafter covered with a 2-1/2-cm layer of sand on top of blotting paper, and the centrifuge was again brought to 100 *g* acceleration for several hours. The consolidation duration was established from consolidation tests on the clay and trial runs in the centrifuge with shear strength measurements. After consolidation, the centrifuge was stopped, the sand layer removed, the aluminum loading frame bolted to the top of the container, and the model platform installed on top of the silt deposit. Electrical connections were established and the centrifuge returned to 100 *g* acceleration. The system was allowed to stabilize at this acceleration for a few minutes, during which time the recording instruments were allowed to warm up, and the calibrated excitation voltages were set (typically:

load cell = 6.00 V d-c; displacement transducers = 1.57 V d-c). The centrifuge was then stopped again, and the loading device was set at the desired inclination and eccentricity of the applied force. The displacement transducers were connected to the platform and the centrifuge brought again to 100 *g* acceleration ready for testing. The tests are described in the next section.

Data Reduction.—The strip chart from the visicorder was digitized onto punched cards (Benson-Lehner 099 data reducer & 282E Telecordex IBM 29 cardpunch) which were used with a computer program to yield various plots of load versus displacement of the model platform. After a test had been completed, the centrifuge was stopped, the loading frame dismounted, and the soil deposit cut in half through the plane of the wax or modeling clay columns to investigate

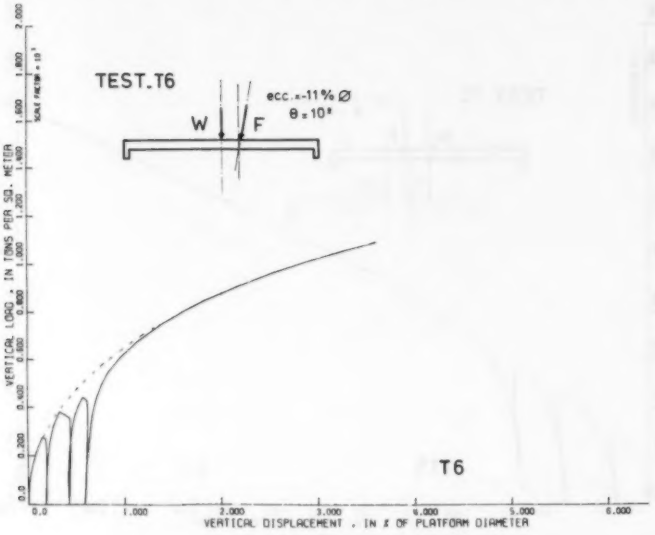

FIG. 10.—Test T6: Test Results for Vertical Load Versus Vertical Displacement

the resulting movements in the soil foundation. Miniature Tor-vane, water content, and dry density tests were conducted at various depths in the soil deposit.

Model Tests: Description and Results

A total of 18 tests (6) were performed at various inclinations and eccentricities of the applied external (wave, or ice) force **F**. Fig. 6 shows the notation and defines the parameters used in the interpretation of these tests. The load **F** is conveniently identified by means of its horizontal and vertical components, F_h and F_v, respectively, giving rise to the moment $M = F_v \cdot e$. Under the action of the load **F**, the platform sinks, slides and tilts, and δ_v, δ_h and α [in Fig.

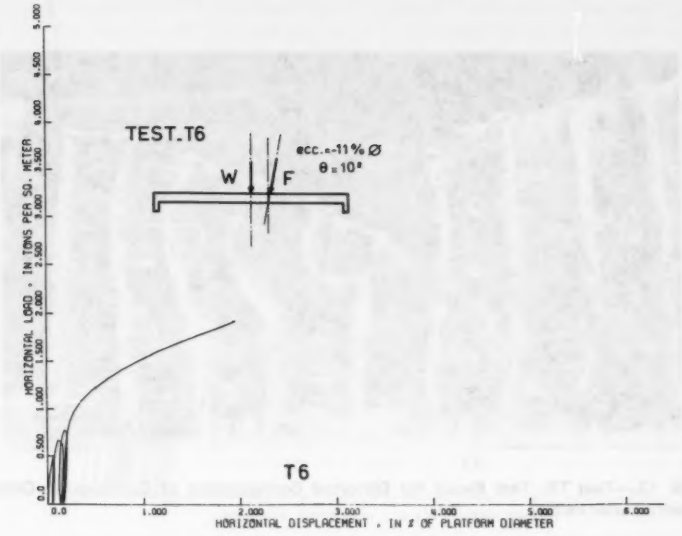

FIG. 11.—Test T6: Test Results for Horizontal Load Versus Horizontal Displacement

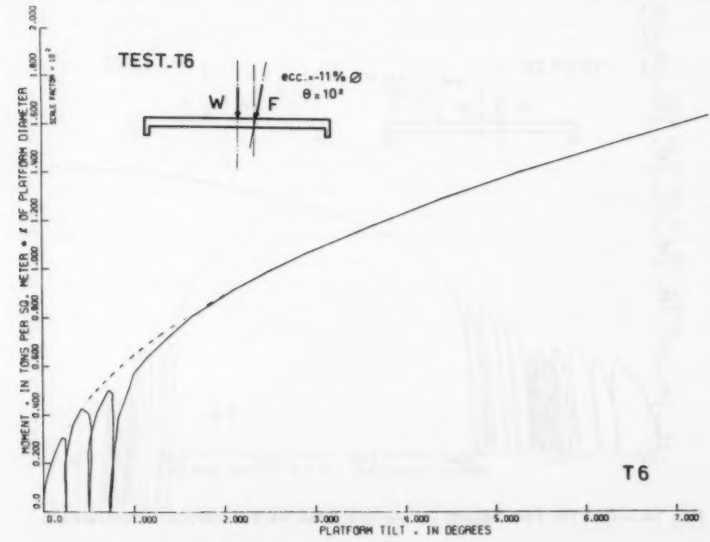

FIG. 12.—Test T6: Test Results for Moment Versus Tilt

FIG. 13.—Test T6: Test Result for Distorted Configuration of Soil Deposit Cross Section after Failure

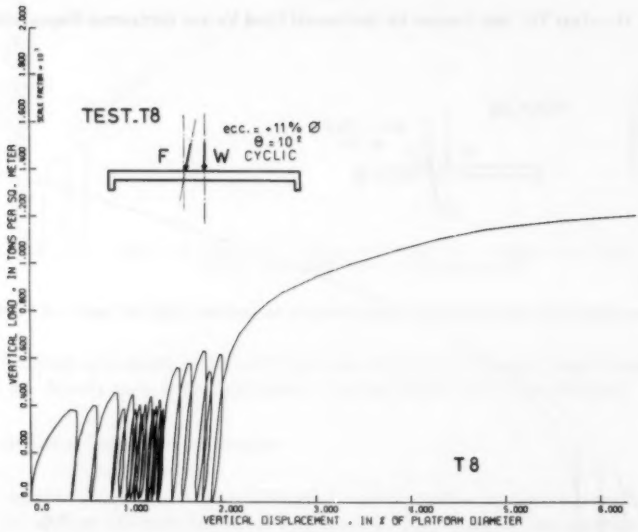

FIG. 14.—Test T8: Test Results for Vertical Load Versus Vertical Displacement

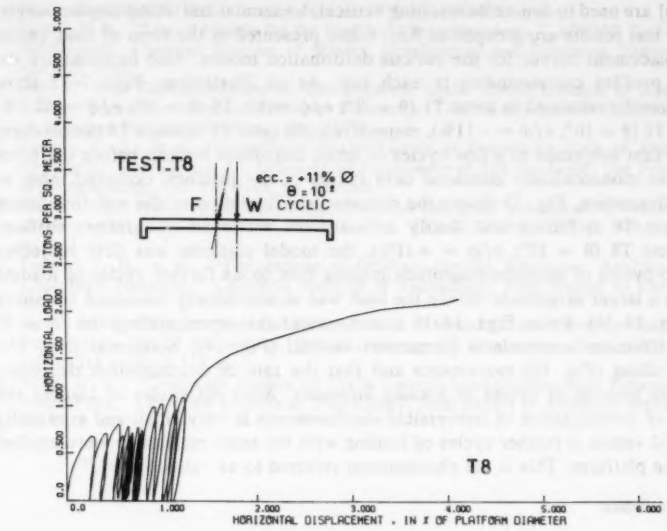

FIG. 15.—Test T8: Test Results for Horizontal Load Versus Horizontal Displacement

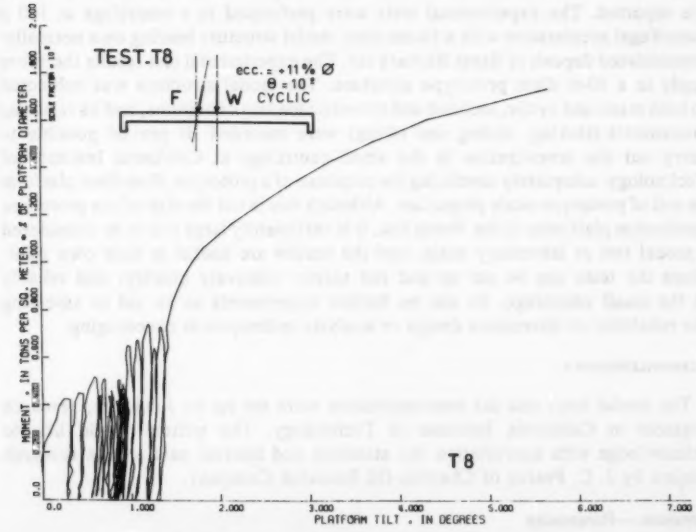

FIG. 16.—Test T8: Test Results for Moment Versus Tilt

6(*b*)] are used to denote its resulting vertical, horizontal and tilting displacements. The test results are grouped in Ref. 6 and presented in the form of load versus displacement curves for the various deformation modes. Also included are the soil profiles corresponding to each test. As an illustration, Figs. 7–13 show the results obtained in tests T1 ($\theta = 0°$; $e/\phi = 0$), T5 ($\theta = 0°$; $e/\phi = 12.5\%$) and T6 ($\theta = 10°$; $e/\phi = -11\%$), respectively. In tests T1 through T6 the platform was first subjected to a few cycles of small magnitude loading before the force F was monotonically increased until failure of the platform occurred, and, as an illustration, Fig. 13 shows the distorted configuration of the soil foundation in test T6 at failure and clearly indicates the existence of a failure surface. In test T8 ($\theta = 10°$; $e/\phi = +11\%$), the model platform was first subjected to 15 cycles of constant magnitude loading then to six further cycles of loading with a larger magnitude before the load was monotonically increased to failure (Figs. 14–16). From Figs. 14–16 it is apparent that upon cycling the force F, the structure accumulates permanent vertical (Fig. 14), horizontal (Fig. 15), and tilting (Fig. 16) movements and that the rate of accumulation decreases as the number of cycles of loading increases. After six cycles of loading the rate of accumulation of irreversible displacements is very small and eventually would vanish if further cycles of loading with the same magnitude were applied to the platform. This is the phenomenon referred to as "shakedown."

Conclusions

This investigation concerns offshore gravity structure foundations, their analysis and design. The results of an experimental study on the interaction of such structures with their soil foundation when subjected to wave (or ice) forces are reported. The experimental tests were performed in a centrifuge at 100 *g* centrifugal acceleration with a 10-cm diam model structure bearing on a normally-consolidated deposit of Santa Barbara silt. The experimental test results therefore apply to a 10-m diam prototype structure. The model structure was subjected to both static and cyclic, inclined and eccentric loading conditions, and its resulting movements (sinking, sliding and tilting) were recorded. It proved possible to carry out the investigation in the small centrifuge at California Institute of Technology, adequately simulating the response of a prototype 10-m diam platform on soil of prototype-scale properties. Although this is not the size of the prototype production platforms in the North Sea, it is sufficiently large not to be considered a model test at laboratory scale, and the results are useful in their own right. Since the tests can be set up and run safely, relatively quickly, and reliably in the small centrifuge, its use on further experiments as an aid to assessing the reliability of alternative design or analysis techniques is encouraging.

Acknowledgments

The model tests and the instrumentation were set up by John Lee, research engineer at California Institute of Technology. The writers would like to acknowledge with appreciation the attention and interest paid to this research project by J. C. Pearce of Chevron Oil Research Company.

Appendix.—References

1. Andersen, K. H., "Behavior of Clay Subjected to Undrained Cyclic Loading,"

Proceedings, BOSS '76 Conference, Vol. 1, 1976, pp. 392–403.

2. Bucky, P. B., "Use of Models for the Study of Mining Problems," *AIMME Technical Publications*, American Institute of Mining, Metallurgical and Petroleum Engineers, No. 425, 1931.
3. Lee, K. H., "Characterization of Soil Behavior Under Cyclic Loading as Applied to the Foundation Design of Offshore Structures," *UCLA-ENG-7735*, Final Report to American Petroleum Institute, Mar., 1977.
4. Polshin, D. E., et al., "Centrifugal Model Testing of Foundation Soils of Building Structures," *Proceedings*, 8th International Conference of Soil Mechanics and Foundation Engineering, Vol. 1.3, 1973, pp. 203–208.
5. Prevost, J. H., et al., "Offshore Gravity Structures: Analysis," *Journal of the Geotechnical Engineering Division*, ASCE, Vol. 107, No. GT2, Proc. Paper 16045, Feb., 1981, pp. 143–165.
6. Prevost, J. H., et al., "Foundations of Offshore Gravity Structures: Analysis and Centrifugal Modeling," California Institute of Technology, Final Report to Chevron Oil Co., 1979.
7. Rowe, R. W., "Displacement and Failure Modes of Model Offshore Gravity Platforms Founded on Clay," *Proceedings*, Offshore Europe '75 Conference, Sept., 1975, pp. OE-75 218.1–OE-75 218.16.
8. Scott, R. F., "Centrifuge Studies of Cyclic Lateral Load-Displacement Behavior of Single Piles," California Institute of Technology, Final Report to American Petroleum Institute, 1977.

JOURNAL OF THE GEOTECHNICAL ENGINEERING DIVISION

OFFSHORE GRAVITY STRUCTURES: ANALYSIS

By Jean H. Prevost,[1] M. ASCE, Bernard Cuny,[2] Thomas J. R. Hughes,[3] M. ASCE, and Ronald F. Scott,[4] M. ASCE

INTRODUCTION

In terms of size, offshore gravity structures are one order of magnitude larger than platforms previously built, and this also applies to the environmental forces to which they are subjected. When a wave passes such a structure, the forces first act in one direction and a few seconds later in the opposite direction with almost the same magnitudes. It is therefore not sufficient to check the stability of the structure for the maximum forces introduced by say, a 100-yr wave acting as a static load, but it must also be considered that, before the maximum wave occurs, the structure has already been subjected to a great number (several thousand) of lesser waves causing cyclic loading of the soil foundation. Under such cyclic loading conditions, soils exhibit very significant dissipative and softening characteristics (1,9). The effect of cyclic structural forces on soil foundations is thus a type of fatigue problem, and it is of great concern to determine to what extent the behavior of soils under cyclic loading may influence the safety of these structures.

In order that the design of the foundation be rational the interaction between the structure and its soil foundation under cyclic, inclined, and eccentric loading conditions must be analyzed. The complexity of the problem dictates that the method of analysis be numerical in nature.

To make accurate predictions, a realistic analytical model of soil stress-strain-strength behavior is essential. Indeed, it must be emphasized that the solution provided by even the most complex finite element program will never be better or more realistic than the constitutive equations adopted in the program to

[1]Asst. Prof. of Civ. Engrg., Princeton Univ., Princeton, N.J.
[2]Grad. Student, California Inst. of Tech., Pasadena, Calif.
[3]Assoc. Prof. of Structural Mechanics, California Inst. of Tech., Pasadena, Calif.
[4]Prof. of Civ. Engrg., California Inst. of Tech., Pasadena, Claif.

Note.—Discussion open until July 1, 1981. Separate discussions should be submitted for the individual papers in this sumposium. To extend the closing date one month, a written request must be filed with the Manager of Technical and Professional Publications, ASCE. Manuscript was submitted for review for possible publication on March 5, 1980. This paper is part of the Journal of the Geotechnical Engineering Division, Proceedings of the American Society of Civil Engineers, ©ASCE, Vol. 107, No. GT2, February, 1981. ISSN 0093-6405/81/0002-0143/$01.00.

model soil behavior. In particular, the cyclic wave forces subject the foundation materials to three-dimensional stress-strain histories involving cycles of loading, unloading, and subsequent reloading. Consequently, for the analysis of the foundation-structure interaction to be realistic, the dependence of the constitutive equations on their stress-strain history must be taken into account. However, most of the stress-strain strength soil models that have been used so far in geotechnical engineering cannot cope adequately with such complex loading histories. Various simplified methods of analysis have thus been proposed and are currently in use.

The first category of methods is based on failure concepts. It is common practice in soil engineering to design structure foundations with an adequate factor of safety against "failure," which in a general sense must be interpreted as the structure's loss of equilibrium with uncontrolled displacements. For a gravity structure, three modes of failure can be identified, namely, bearing, sliding, and overturning. The corresponding failure loads are computed by assuming that the actual three-dimensional field situation can be idealized to a two-dimensional (plane strain) representation, that the soil foundation behavior

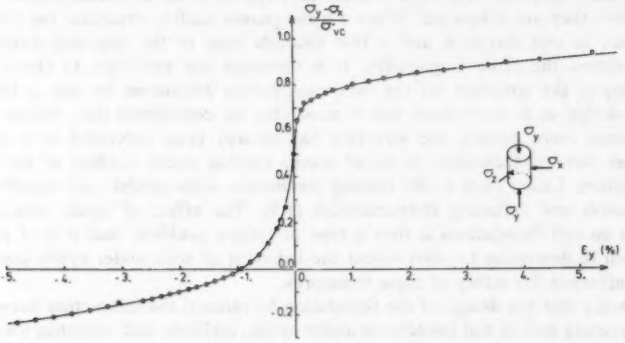

FIG. 1.—Santa Barbara Silt: Compression and Axial Extension Tests Results

can be taken to be isotropic and, rigid-perfectly plastic, and by using limit equilibrium techniques (see e.g., Refs. 4, 6, 11, 12, and 26). The results of the failure analysis are usually presented in the form of an interaction diagram (26). The soil strength to be used in interpreting such a diagram for design purposes is a "reduced" strength to account for the effects of cyclic loading. This method of analysis is evidently very crude and its results are rather uncertain since it requires so many simplifications of the actual field conditions. It is therefore not clear to what extent analytical predictions based on such drastic simplifying assumptions are related to actual field performances. Furthermore, the method does not provide information about deformations prior to failure.

In an attempt to provide this, more complicated analytical methods have been proposed based on finite element representations of the soil foundation underneath the structure. In the studies, soil is modeled either as an isotropic, linear, or nonlinear (3,5) elastic material, or an isotropic, elastic-perfectly plastic

(25) or elastic-plastic hardening (27) material. In order to account for the effects of cyclic loading on the soil foundation, soil specimens in the laboratory are subjected to the cyclic shear stresses predicted by the finite element analysis, and the results of these tests are used to predict the resulting deformations of the platform foundation. This method of analyses is therefore in essence a "stress path" procedure (8). Although the stress path method may have proven useful in soil engineering, its limitations should be recognized, namely that the estimation of the stress (or strain) path followed by any soil element in the gound is strongly dependent on the particular soil model used for these predictions. This stress path is then employed in a test on the soil to determine its strain response, which is usually widely different from that used in the stress calculation. It is therefore evident that the meaning of such a procedure is at best limited.

Recently a more rational analysis procedure has been proposed in Refs. 18 and 20. The method is based on a finite element analysis of the soil-structure

TABLE 1.—Santa Barbara Silt: Yield Surface Parameters, $G = 133.333\ \sigma'_{vc}$

M (1)	$\alpha_{11}^{(m)}/\sigma'_{vc}$ (2)	$\alpha_{12}^{(m)}/\sigma'_{vc}$ (3)	$\alpha_{22}^{(m)}/\sigma'_{vc}$ (4)	$k^{(m)}/\sigma'_{vc}$ (5)	$H^{(m)}/\sigma'_{vc}$ (6)
1	0.167	0.0	−0.333	0.000	266.667
2	0.170	0.0	−0.340	0.090	69.565
3	0.152	0.0	−0.303	0.205	37.037
4	0.140	0.0	−0.280	0.270	21.739
5	0.130	0.0	−0.260	0.330	13.605
6	0.120	0.0	−0.240	0.360	9.697
7	0.123	0.0	−0.245	0.393	6.617
8	0.115	0.0	−0.230	0.415	4.737
9	0.117	0.0	−0.233	0.465	2.614
10	0.123	0.0	−0.245	0.502	1.821
11	0.134	0.0	−0.267	0.550	0.0

interaction problem by using a soil model (14–16) which describes the nonlinear, anisotropic, elastoplastic, path-dependent stress strain-strength properties of soil when subjected to complicated, and in particular to cyclic, three-dimensional loading paths. This formation allows the solution to the complicated wave-structure-soil interaction to be obtained directly because it incorporates the material stress-strain-strength properties, including their progressive softening with strain. However, although this formulation has been carefully checked against laboratory experimental test results, its accuracy in predicting field performances has not yet been tested. This is a common problem in geotechnical engineering. It exists because of the paucity of field test information. Field data on the performance of full-scale structures under severe loading conditions are urgently needed, but until now have remained proprietary. Further data are unlikely to be obtained soon because of the scale of the structures involved, the cost of testing, and the low probability of having a particular instrumented structure subjected to design loads. Consequently, some form of model study seems inevitable to enable alternative design or analysis methods to be checked.

A program whereby this possibility could be implemented was suggested to Chevron Oil Company. It would utilize: (1) Some of the results of laboratory

tests on a particular soil performed at University of California at Los Angeles (UCLA) (9); (2) centrifugal model tests of a model structure placed on a normally consolidated deposit of the same soil carried out at California Institute of Technology (17,19); and (3) analytical calculations performed in parallel with these model tests using the computer code DIRT (7) with the best possible estimate of the soil parameters obtained in the laboratory tests. Centrifuge tests were proposed because in them, model scaling relations are adequately satisfied as covered in Refs. 17 and 19.

The proposal was accepted by Chevron Oil Company, and work was initiated. The soil involved was a clayey silt obtained from the ocean floor off the southern California coast. The centrifuge model tests included both monotonic and cyclic

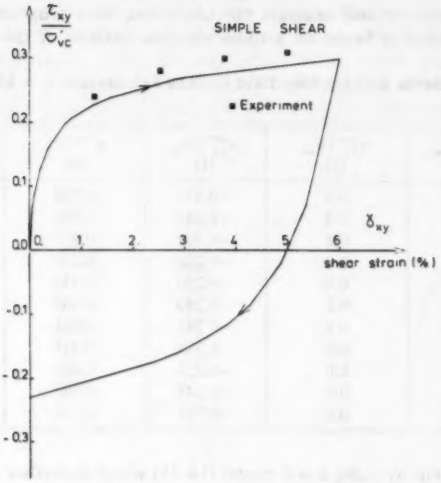

FIG. 2.—Santa Barbara Silt: Comparison of Prediction and Test Results in Simple Shear

loading of the model structure, and the results have been reported in Refs. 17 and 19. This report describes the analytical results and compares them with the experimental test results.

Soil Model

Soils in general undergo both elastic and plastic deformations simultaneously upon shearing. In order to separate the contributions of the elastic and plastic properties in the total deformations, it is assumed that the elasticity of the material is linear and isotropic, and that nonlinearity and anisotropy result from its plasticity. To account for the effects of unloading-reloading events on the material behavior, the model combines properties of isotropic and kinematic plasticity by allowing the yield surface to be translated in stress space by the

stress point and to change in size simultaneously. Also, in order to allow for the adjustment of the plastic hardening rule to any kind of experimental nonlinear hardening law obtained for instance in triaxial or simple shear soil tests, a collection of nested yield surfaces is used.

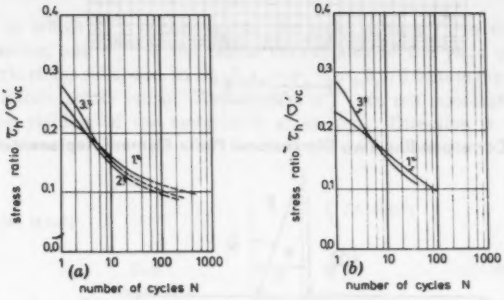

FIG. 3.—Santa Barbara Silt: (*a*) Derived Cyclic Simple Shear Strain-Controlled Test Results; (*b*) Predicted Cyclic Simple Shear Test Behavior from Analytical Model (Figures on Curves give Strain as a percentage)

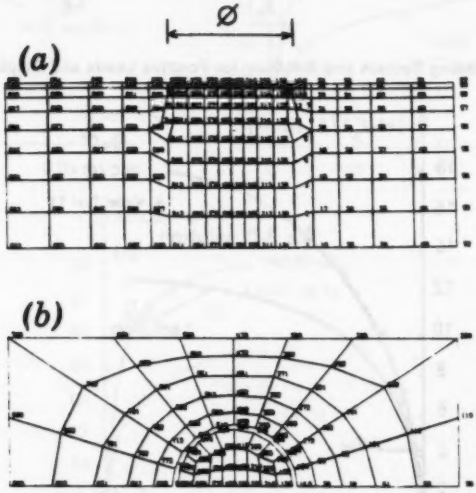

FIG. 4.—General Three-Dimensional Finite Element Representation of Centrifuge Model: (*a*) Side View; (*b*) Top View at Surface

Since the duration of the loading applied to the model structure was short, it was found appropriate to assume that deformations in the soil foundation occurred with no volume changes. Therefore, a simple version of the more general formulation reported in Ref. 14 was used. For undrained loading

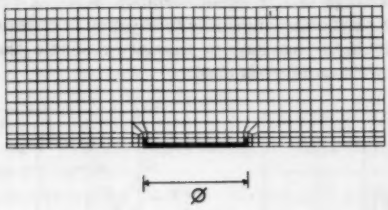

FIG. 5.—Corresponding Two-Dimensional Finite Element Representation

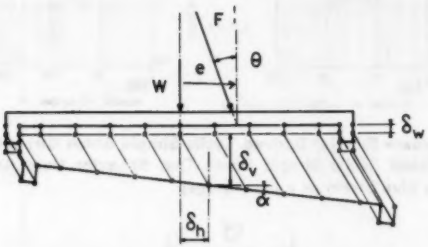

FIG. 6.—Loading System and Notation for Positive Loads and Displacements

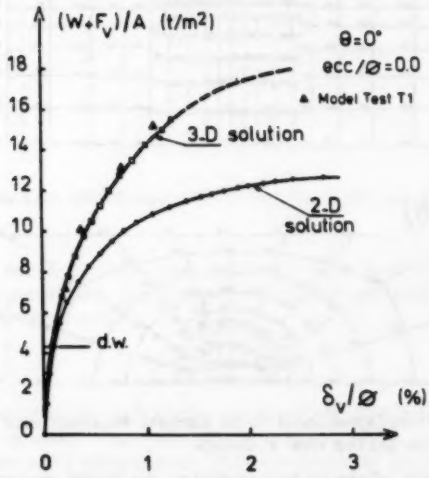

FIG. 7.—Vertical Force Versus Vertical Displacement; Comparison of Computed Results for Three-Dimensional and Two-Dimensional Cases with Experimental Points for Centrifuge Model Test T1

conditions, the yield surfaces are represented by equations of the following form (14)

$$\frac{3}{2}(s_{ij}-\alpha_{ij}^{(m)})(s_{ij}-\alpha_{ij}^{(m)})=[k^{(m)}]^2 \quad \ldots\ldots\ldots\ldots\ldots\ldots\ldots\ldots\ldots\ldots (1)$$

for all m, in which $k^{(m)}$ = the size of the yield surface f_m in the deviatoric stress subspace; and $\alpha_{ij}^{(m)}$ = the center coordinates of the yield surface f_m in the deviatoric stress subspace. In Eq. 1, $s_{ij}=\sigma_{ij}-\sigma_{kk}\delta_{ij}/3$ denote the components of the deviatoric stress tensor. Because the $\alpha_{ij}^{(m)}$ are not necessarily all equal to zero, the yielding of the material is anisotropic. Direction is therefore of

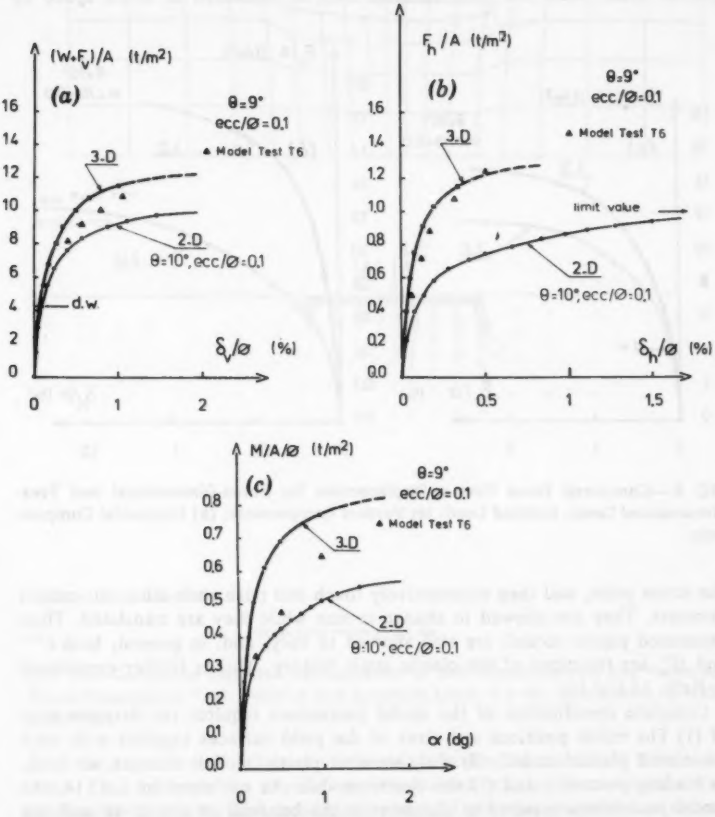

FIG. 8.—Computed and Experimental (Test T6) Force Versus Displacement for Three-Dimensional and Two-Dimensional Cases, Inclined and Eccentric Load: (*a*) Vertical Components; (*b*) Horizontal Components; (*c*) Moment and Rotation

great importance and the physical reference axes (x, y, z) are fixed with respect to the soil element and specified to coincide with the principal axes of stress in the material's past consolidation history. The initial positions and sizes of the yield surfaces reflect the past stress-strain history of the material element, and, in particular, their translations are a direct expression of the material's memory of its past loading history as it is associated with the direction of loading as shown in Refs. 14–16. In the following the y-axis is vertical, $\alpha_{xy}^{(m)} = \alpha_{yz}^{(m)} = \alpha_{zx}^{(m)} = 0$ for all m initially, and $\alpha_x^{(m)} = \alpha_z^{(m)} = -\alpha_y^{(m)}/2$.

A plastic modulus H'_m is associated with each of the yield surfaces, and the associated flow rule is used to compute the plastic strain rate tensor components. The total strain rate is set equal to the sum of the elastic and plastic strain rates. All yield surfaces may be translated in stress space by

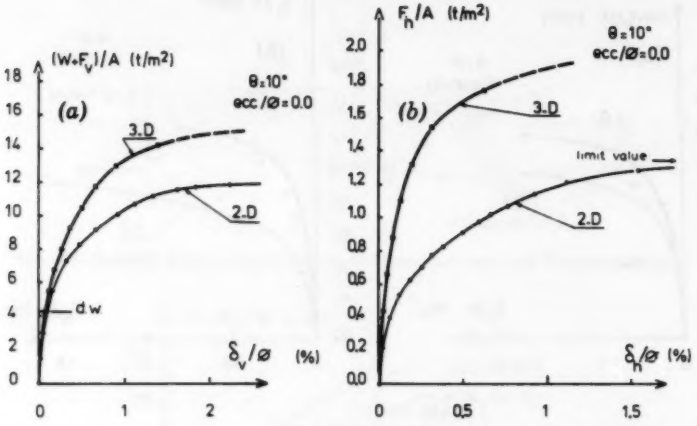

FIG. 9.—Computed Force Versus Displacement for Three-Dimensional and Two-Dimensional Cases, Inclined Load: (*a*) Vertical Components; (*b*) Horizontal Components

the stress point, and they consecutively touch and push each other but cannot intersect. They are allowed to change in size while they are translated. Their associated plastic moduli are also allowed to vary, and, in general, both $k^{(m)}$ and H'_m are functions of the plastic strain history. This is further considered in Refs. 14 and 16.

Complete specification of the model parameters requires the determination of (1) The initial positions and sizes of the yield surfaces together with their associated plastic moduli; (2) their sizes or plastic moduli changes, or both, as loading proceeds; and (3) the elastic moduli. As explained in Ref. 14, the model parameters required to characterize the behavior of any given soil can be derived entirely from the results of conventional soil tests. The actual number of yield surfaces to be used is a function of the desired degree of accuracy to be achieved in the material behavior representation.

Model Parameters

The model parameters required to characterize the undrained behavior of the Santa Barbara silt are described in this section. As explained in Refs. 15 and 16, the initial positions and sizes of the yield surfaces together with their associated plastic moduli, and the elastic shear modulus are determined solely

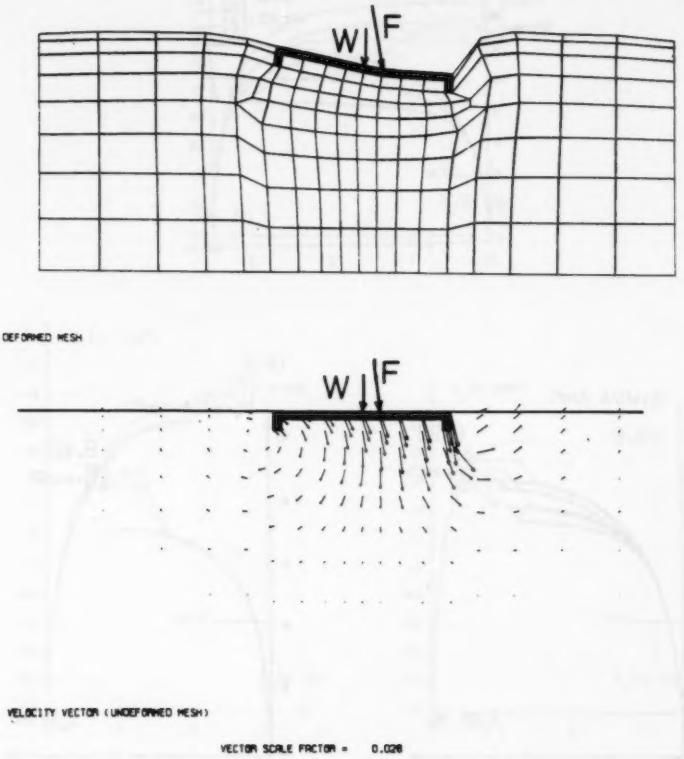

FIG. 10.—Computed Distorted Configuration of Soil, Displacements and Velocities; Three-Dimensional Test; Inclined and Eccentric Load; $\theta = 9°$; Eccentricity/$\phi = 0.1$; Side View

from the experimental behavior of the soil measured in undrained triaxial soil tests. Fig. 1 shows the experimental undrained triaxial stress-strain curves obtained for the Santa Barbara silt (σ_{vc} = vertical effective consolidation stress). Note that the curves obtained in compression and extension are very different. Eleven yield surfaces were used to fit the experimental stress-strain curves closely, and Table 1 lists the parameter values for the Santa Barbara silt, with

$G = 133.33\ \sigma'_{nc}$. The model was thereafter applied to *predict* the results of a simple shear test performed on the same soil, and Fig. 2 shows a comparison of stress-strain behavior calculated with the proposed model with that measured (9) experimentally in an undrained simple shear test [$\tau_{xy} = 1.11\ \tau_h$(21) in which τ_h = the average shear stress measured in the test]. The two sets of curves

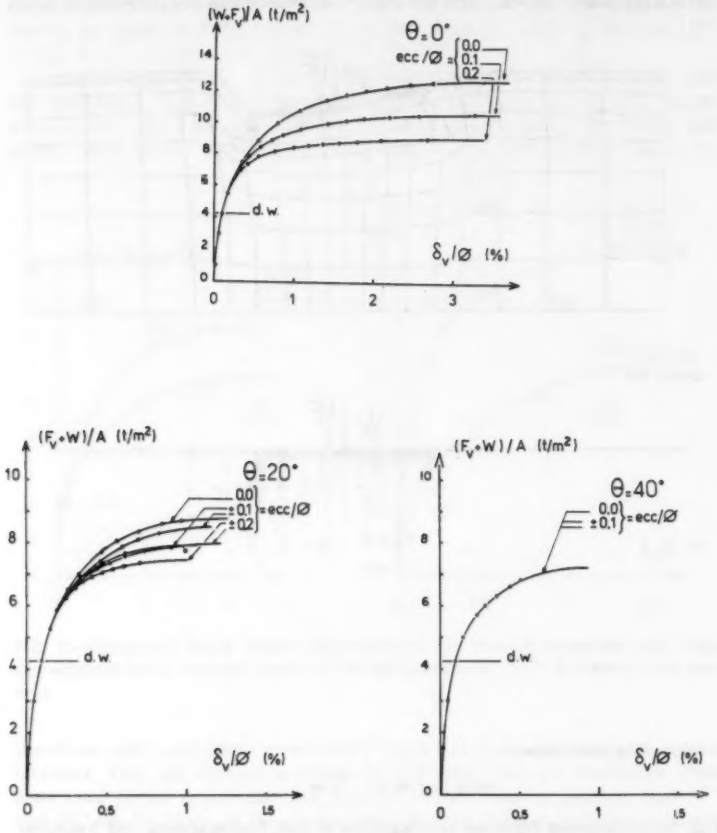

FIG. 11.—Computed Two-Dimensional Solution for Vertical Components

agree well. These results demonstrate the ability of the model to account for the behavior of the Santa Barbara silt upon shearing with rotation of the principal stress axes.

In the course of cyclic loading the yield surfaces all decrease in size. As shown in Ref. 16, the change in size of the yield surfaces as cyclic loading proceeds is determined by using the experimental results from undrained cyclic strain-controlled simple shear tests. Unfortunately, the only cyclic test results

available (9) had been performed under stress-controlled loading conditions. The strain-controlled results had therefore to be derived from the stress-controlled results by using the procedure explained in Ref. 22, and Fig. 3(*a*) shows the corresponding strain-controlled results. The curves shown in Fig. 3(*a*) were used to determine the cyclic parameters (16) of the Santa Barbara silt, and

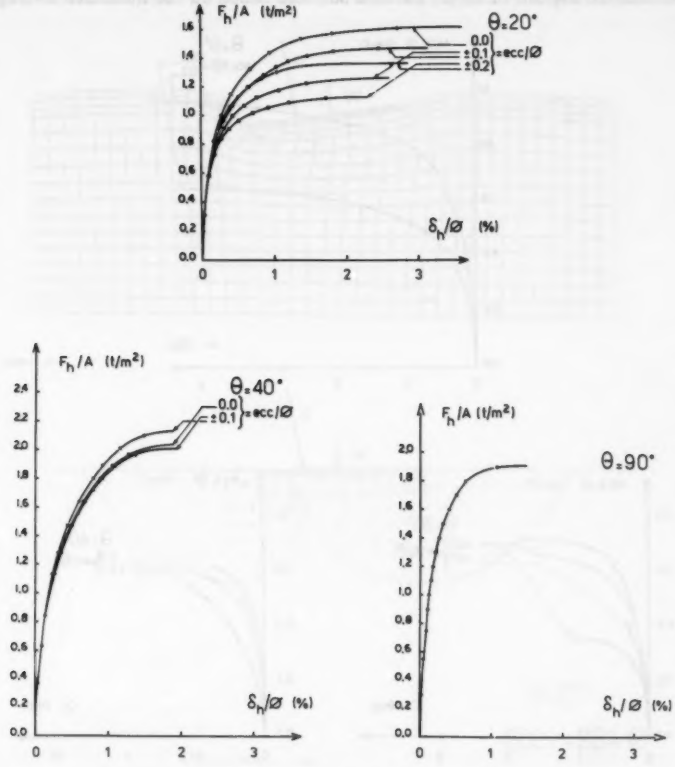

FIG. 12.—Computed Two-Dimensional Solutions for Horizontal Components

Fig. 3(*b*) shows the calculated decrease in shear stress amplitudes using the proposed model. They agree very well with the reconstructed experimental curves shown in Fig. 3(*a*).

Analysis of Interaction of Model Structure with Its Soil Foundation

The soil model described has been coded and incorporated into a finite element program (7). With respect to undrained loading conditions, it should be mentioned that the finite element program incorporates novel features such as penalty

function and reduced integration techniques which allow a simple and effective implementation of the incompressibility constraint (10). The use of the formulation in solving boundary value problems is illustrated by applying it to analyze the interaction of the model structure with its soil foundation when subjected to both monotonic and cyclic forces. The foundation material consists of a normally consolidated deposit of Santa Barbara silt, and based on the measured average

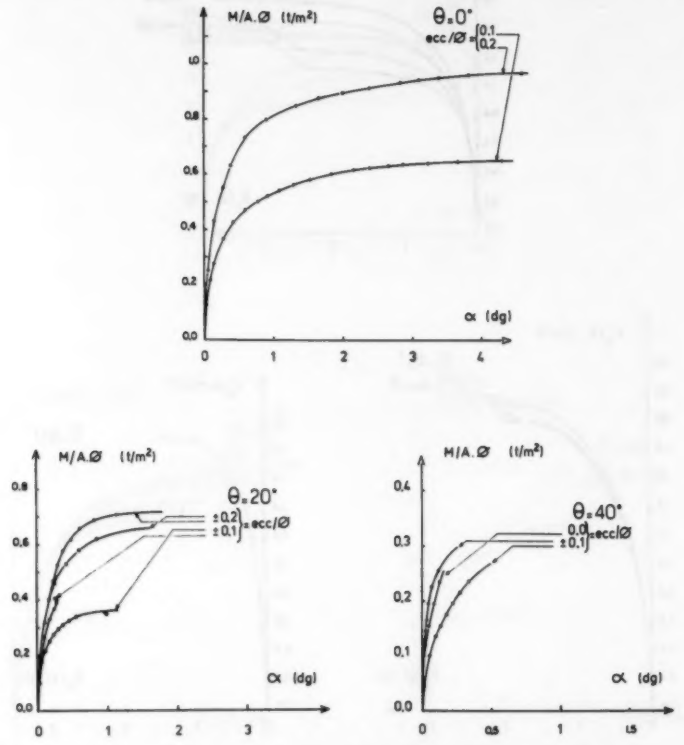

FIG. 13.—Computed Two-Dimensional Solutions for Moment and Rotation

densities in the bucket of the centrifuge in which the model tests were performed, an equation for the vertical effective stress σ'_{vc} can be written (at prototype scale).

$$\sigma'_{vc} = 2.50 + (0.871 + 0.007Z)Z \text{ (in tons per square meter)} \quad \ldots\ldots\ldots\ldots (2)$$

in which Z = the depth, in meters, measured from the surface of the soil. The (prototype scale) platform has a diameter of 10 m (area $A = 78.54$ m^2) and is mounted with skirts 0.6 m long. Its dead weight W is such that $W/A = 4.3$ ton/m^2.

Finite Element Representation.—Fig. 4 shows the three-dimensional finite element representation of the problem geometry. The complete grid (for use in the case of eccentric loading) spans over 1/2 of the bucket geometry, and consists of binlinear isoparametric brick elements as shown in Fig. 4. The axisymmetric grid (for use in the case of vertical loading only) spans over 1/4 of the bucket geometry and consists of bilinear isoparametric brick elements.

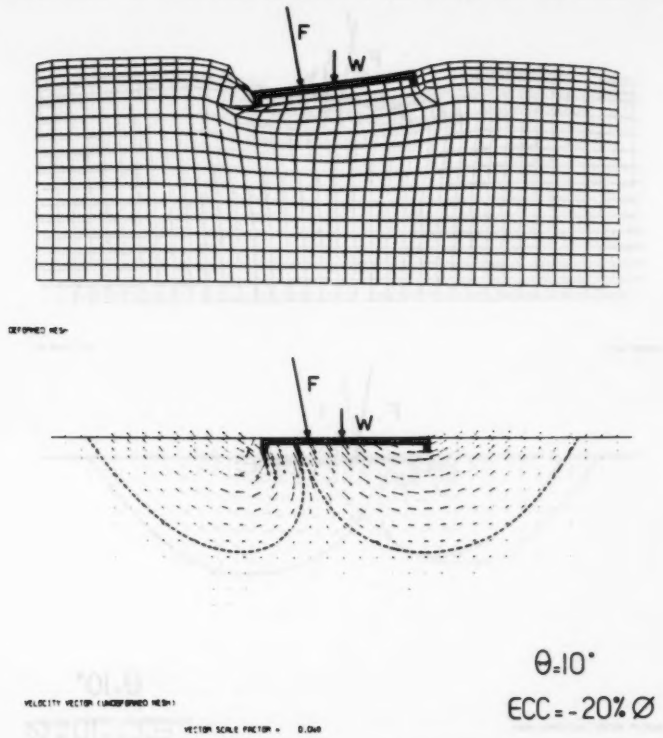

FIG. 14.—Computed Two-Dimensional Distorted Configurations for Inclined and Eccentric Loads, Side View, when $\theta = 10°$, $ecc/\phi = -0.2$

Three-dimensional calculations are several orders of magnitude more expensive than their two-dimensional counterparts. Due to the necessity of working within a limited computation budget only a few three-dimensional calculations were performed and most of the calculations were performed in two dimensions. For that purpose the problem geometry was transposed into two dimensions by assuming that deformation occurred in plane strain, and the corresponding two-dimensional finite element representation is shown in Fig. 5. The grid consists of 554 bilinear isoparametric quadrilateral elements.

The structure's foundation is represented by a circular and a strip footing in the three-dimensional and two-dimensional idealizations, respectively. The footing consists of a 0.4-m thick layer of elements, and the skirt, where present, is represented by an additional layer (row) of elements 0.6 m deep and 0.4 m wide, attached to the footing. The foundation elements are chosen 1,000 times stiffer than the supporting soil to represent the model test conditions. Fig. 6 shows the load system and notation. In addition to the static load W

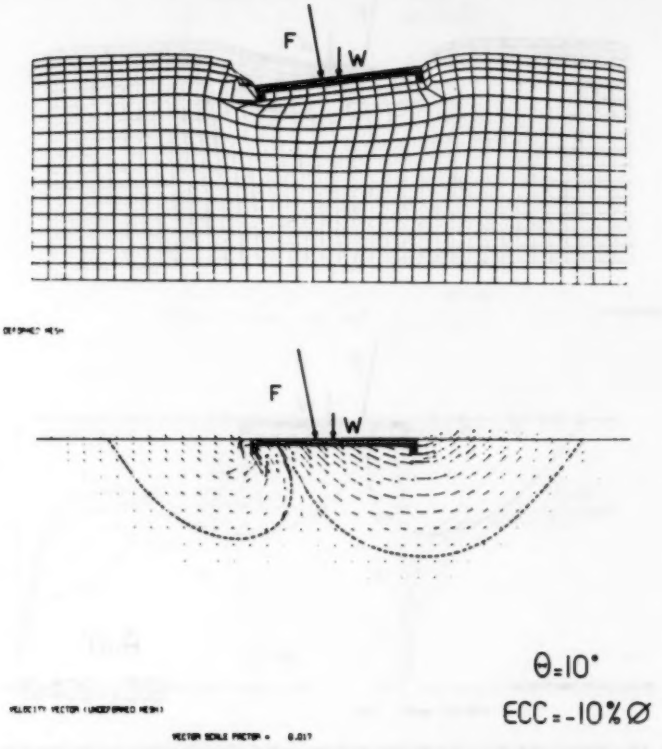

FIG. 15.—Computed Two-Dimensional Distorted Configurations for Inclined and Eccentric Loads, Side View, when $\theta = 10°$ and $ecc/\phi = -0.1$

due to the dead weight of the structure, the foundation is also subjected to the cyclic inclined eccentric load F due to the wave (ice) forces. The load F, is identified in the following by means of its vertical component F_v acting with the eccentricity e given rise to the moment $M = F_v \cdot e$, and its horizontal component F_h.

For the case of centered vertical loading only (i.e., $e = F_h = 0$) the structure settles uniformly and δ_v denotes its vertical settlement. Under inclined or eccentric

loading conditions, or both, the structure slides and tilts as well, as shown in Fig. 6. Its center is displaced by the amount δ_v and δ_h in the vertical and horizontal directions, respectively. The tilt is measured by the angle of rotation α of the slab.

Analysis of Foundation Movements When Subjected to Inclined Eccentric Force of Monotonically Increasing Magnitude.—Figs. 7 and 8 show the computed load

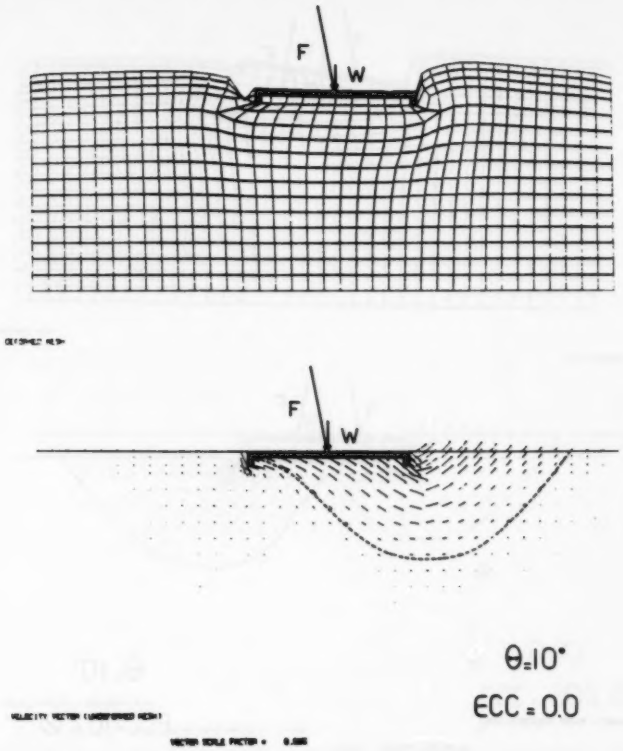

FIG. 16.—Computed Two-Dimensional Distorted Configurations for Inclined and Eccentric Loads, Side View, when $\theta = 10°$ and $ecc/\phi = 0.0$

versus displacement curves for the deformation modes generated by various inclinations and eccentricities of the wave (ice) force **F**, under both three-dimensional and two-dimensional conditions. It is of importance to note that for all cases, the two-dimensional idealization leads to a much softer response of the soil structure interacting system than its three-dimensional (and correct) representation. Also, for comparison, the corresponding centrifuge model test results are shown in Figs. 7 and 8, and it is apparent that the three-dimensional analytical

predictions agree very well with the measured experimental model test results. The experimental results corresponding to $\theta = 10°$, $e/\phi = 0.0$ (Test T2) have not been reported in Fig. 9 because of the poor consolidation state achieved in this test (19). As an illustration, Fig. 10 shows the computed three-dimensional distorted configuration of the soil foundation and the direction of its flow. It is apparent by comparing Fig. 10 with Fig. 13 of the companion paper that

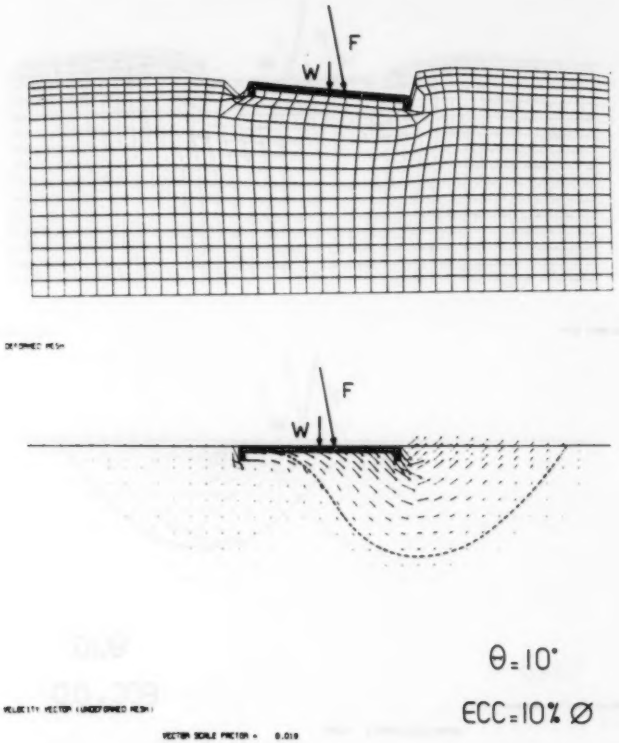

FIG. 17.—Computed Two-Dimensional Distorted Configurations for Inclined and Eccentric Loads, Side View, when $\theta = 10°$ and $ecc/\phi = 0.1$

the three-dimensional finite element representation does adequately capture the failure state displacements in the soil foundation.

Even though it appears from Figs. 7 and 8 that only three-dimensional calculations are capable of representing correctly the three-dimensional model test situations, the remaining calculations, due to the necessity of working within a limited computation budget, were performed by using a two-dimensional

idealization of the problem geometry as shown in Fig. 5. It was felt by the writers that, though such calculations obviously could not provide exact quantitative information about the behavior of the soil-structure system, they would still provide useful answers regarding relative magnitudes of loads and displacements. Figs. 11–13 show the computed load-displacement curves for the deformation modes under various inclinations and eccentricities of the force **F**, and,

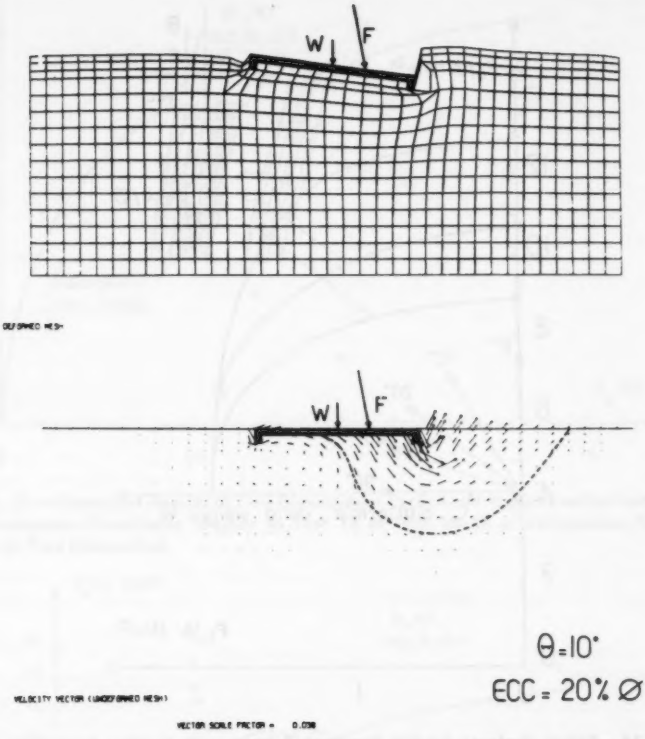

FIG. 18.—Computed Two-Dimensional Distorted Configurations for Inclined and Eccentric Loads, Side View, when $\theta = 1.0°$ and $ecc/\phi = 0.2$

as an illustration, Figs. 14–18 show the computed distorted configurations of the soil foundation and the directions of flow at failure when $\theta = 10°$ and for various eccentricities. For inclined and eccentric loading, failure involves all three failure modes. At failure, a very distinct discontinuity occurs in the velocity magnitude which reveals the existence of a failure surface. Its trace is easily obtained from the vectors shown in Figs. 14–18 and is marked with dotted lines in these plots. This information can be used to check the foundation

stability by using upper bound techniques [see e.g., Ref. (12)], since the latter require the determination of the failure surface's trace. In the ($W + F_v$, F_h, e) space, the various states of loading conditions at failure describe a surface which plays the role of a failure surface for the soil-structure interacting system. Its intersection with planes e/ϕ = constant is shown in the interaction diagram of Fig. 19 for positive eccentricity by projections onto the plane $e = 0$.

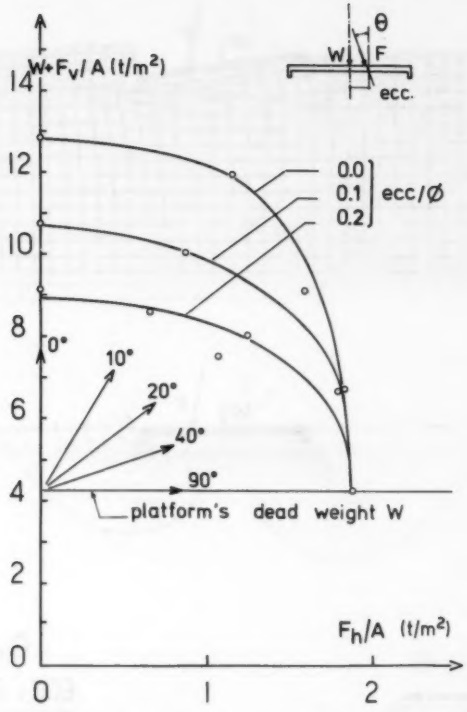

FIG. 19.—Failure Surfaces for Soil-Structure System with Positive Eccentricity of Load

Analysis of Foundation Movements when Subjected to Cyclic Inclined and Eccentric Force.—Since the behavior of the foundation material is strongly path-dependent, the loading applied onto the structure must follow the real wave (ice) loading history as closely as possible to enable predictions of deformation to be made. In order to make the present study specific, the cyclic loading applied to the structure in test T8 (17,19) was selected as an example problem. The computed load-displacement curves for that particular cyclic loading case are shown in Figs. 20–22 from which the progress of the various deformations

can be traced. It is of importance to emphasize that the calculations were performed in two dimensions and therefore the results do not strictly apply to the real three-dimensional conditions of the model test. However, the analytical results do exhibit the same qualitative behavior as observed in the test. From

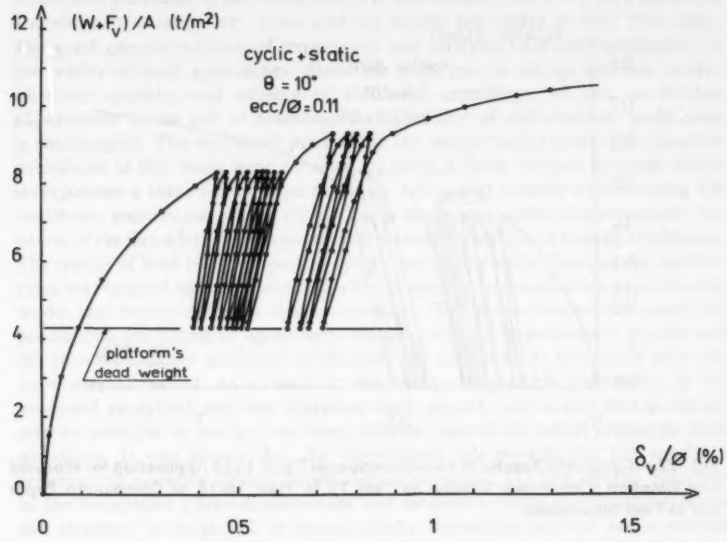

FIG. 20.—Computed Results of Two-Dimensional Cyclic Load Application for Vertical Components (Conditions Similiar to Test T8 in Figs. 14–16 of Companion Paper but in Two Dimensions

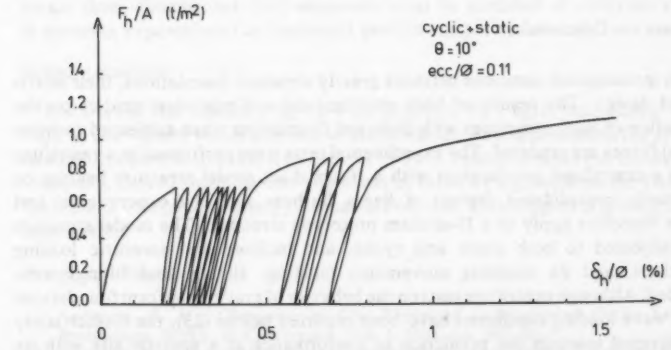

FIG. 21.—Computed Results of Two-Dimensional Cyclic Load Application for Horizontal Components (Conditions Similiar to Test T8 in Figs. 14–16 of Companion Paper but in Two Dimensions

Figs. 20–22 it is apparent that upon cycling the force F, the structure accumulates permanent vertical and horizontal displacements, and a permanent tilt, and that the rate of accumulation decreases as the number of cycles of loading increases, again illustrating the "shakedown" phenomenon (17). It is apparent by comparing

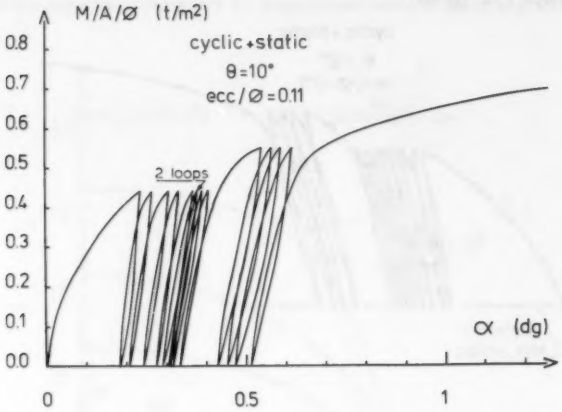

FIG. 22.—Computed Results of Two-Dimensional Cyclic Load Application for Moment and Rotation (Conditions Similiar to Test T8 in Figs. 14–16 of Companion Paper but in Two Dimensions

Figs. 20–22 with Figs. 14–16 of the companion paper that the analytical predictions do exhibit a very strong similarity to, and are consistent with the experimental results obtained in the centrifuge.

Summary and Conclusions

This investigation concerns offshore gravity structure foundations, their analysis and design. The results of both experimental and analytical studies on the interaction of such structures with their soil foundation when subjected to wave (or ice) forces are reported. The experimental tests were performed in a centrifuge at 100 *g* centrifugal acceleration with a 10-cm diam model structure bearing on a normally consolidated deposit of Santa Barbara silt. The experimental test results therefore apply to a 10-m diam prototype structure. The model structure was subjected to both static and cyclic, and inclined and eccentric loading conditions, and its resulting movements (sinking, sliding, and tilting) were recorded. Although centrifuge tests on the behavior of gravity platform foundations under wave loading conditions have been reported before (23), the former study was directed towards the prediction of performance at a specific site with its unique soil conditions. In the present investigation, a different point of view was taken—that of validating a numerical analysis on a relatively well-characterized material. The soil did come from an offshore location, but that condition

was incidental to the tests performed. It proved possible to carry out the investigation in the small centrifuge at California Institute of Technology, adequately simulating the response of a prototype 10-m diam platform on soil of prototype scale properties. Although this is not the size of the prototype production platforms in the North Sea, it is sufficiently large not to be considered a model test at laboratory scale, and the results are useful in their own right. The good correspondence of experiment and analysis reinforce confidence in the results of both approaches. Since the tests can be set up and run safely, relatively quickly, and reliably in the small centrifuge, its use on further experiments as an aid to assessing the reliability of calculational techniques is encouraging. The analytical predictions for the particular prototype situation considered in this study were obtained by using a finite element program which incorporates a three-dimensional nonlinear soil model capable of describing the nonlinear, anisotropic, elasto-plastic, path-dependent stress-strain-strength behavior of the Santa Barbara silt under both monotonic and cyclic loading conditions. The results of both two-dimensional (plane strain) and three-dimensional calculations are reported and are compared with the appropriate equivalent experimental model test results obtained in the centrifuge. The three-dimensional analytical predictions are found to agree very closely with the experimental results and the two-dimensional analytical predictions are shown to be consistent with the experimental results. As a result of this study considerable confidence in the proposed analytical tool has therefore been gained, and is felt that it should now be possible to use it to perform reliable analysis of actual prototype field situations. It was shown that the calculations can provide for the structure reliable and accurate design information concerning: (1) The overall response of the foundation (force-displacement and moment-rotation relationships) when the structure is subjected to monotonically increasing inclined and eccentric forces at various angles of inclinations; (2) its various possible failure modes (bearing, sliding, tilting) and the trace of the failure surface for each case; and (3) the overall response of the foundation when the structure is subjected to cyclic wave forces. Further, as a result of this study, it is now clear that actual three-dimensional field situations must be modeled or analyzed as such if accurate experimental or analytical predictions are to be made.

Acknowledgments

The triaxial test results (Fig. 1) were provided by Fugro, Inc. (Long Beach, Calif.). The writers would also like to acknowledge with appreciation the attention and interest paid to this research project by J. C. Pearce of Chevron Oil Research Company. Part of the computer costs was covered by a grant from the California Institute of Technology Energy Research Program. This support is most gratefully appreciated.

Appendix.—References

1. Anderson, K. H., "Behavior of Clay Subjected to Undrained Cyclic Loading," *Proceedings*, BOSS '76 Conference, Vol. 1, 1976, pp. 392–403.
2. Bucky, P. B., "Use of Models for the Study of Mining Problems," *AIMME Technical Publication*, American Institute of Mining, Metallurgical, and Petroleum Engineers, No. 425, 1931.
3. Duncan, J. M., and Chang, C. Y., "Nonlinear Analysis of Stress and Strain in Soils,"

Journal of the Soil Mechanics and Foundation Engineering, ASCE, Vol. 96, No. SM5, Proc. Paper 7513, Sept., 1970, pp. 1629–1653.

4. Garber, M., and Baker, R., "Bearing Capacity by Variational Method," *Journal of the Geotechnical Engineering Division*, ASCE, Vol. 103, No. GT11, Proc. Paper 13330, Nov., 1977, pp. 1209–1225.
5. Girijavallabahn, C. V., and Reese, L. C., "Finite-Element Method for Problems in Soil Mechanics," *Journal of the Soil Mechanics and Foundation Engineering*, ASCE, Vol. 94, No. SM2, Proc. Paper 5864, Mar., 1968, pp. 473–496.
6. Hansen, J. B., "A Revised and Extended Formula for Bearing Capacity," *Danish Geotechnical Institute Publication*, No. 28, Copenhagen, Denmark, 1970.
7. Hughes, T. J. R., and Prevost, J. H., "DIRT: A Finite Element Program for the Static Analysis of Nonlinear Anisotropic Elastoplastic Hysteretic Continua Subjected to Complicated Loading Paths," *California Institute of Technology*, May, 1977.
8. Lambe, W. T., "Stress Path Method," *Journal of the Soil Mechanics and Foundation Engineering*, ASCE, Vol. 93, No. SM6, Proc. Paper 5613, Nov., 1967, pp. 309–331.
9. Lee, K. H., "Characterization of Soil Behavior under Cyclic Loading as Applied to the Foundation Design of Offshore Structures," *UCLA-ENG-7735*, Final Report to American Petroleum Institute, March, 1977.
10. Malkus, D. S., and Hughes, T. J. R., "Mixed Finite Element Methods—Reduced and Selective Integration Techniques: A Unification of Concepts," *Computer Methods in Applied Mechanics and Engineering*, Vol. 15, No. 1, 1978, pp. 63–81.
11. Meyerhof, G. G., "Some Recent Research in the Bearing Capacity of Foundations," *Canadian Geotechnical Journal*, Vol. 1, No. 1, 1963, pp. 16–26.
12. Murff, J. D., and Miller, T. W., "Foundation Stability on Nonhomogeneous Clays," *Journal of the Geotechnical Engineering Division*, ASCE, Vol. 103, No. GT10, Proc. Paper 13302, Oct., 1977, pp. 1083–1095.
13. Polshin, D. E., et al., "Centrifugal Model Testing of Foundation Soils of Building Structures," *Proceedings*, 8th International Conference on Soil Mechanics and Foundation Engineering, Vol. 1.3, 1973, pp. 203–208.
14. Prevost, J. H., "Plasticity Theory for Soil Stress Behavior," *Journal of the Engineering Mechanics Division*, ASCE, Vol. 104, No. EM5, Proc. Paper 14069, Oct., 1978, pp. 1177–1194.
15. Prevost, J. H., "Anisotropic Undrained Stress-Strain Behavior of Clays," *Journal of the Geotechnical Engineering Division*, ASCE, Vol. 104, No. GT8, Proc. Paper 13942, Aug., 1978, pp. 1075–1090.
16. Prevost, J. H., "Mathematical Modeling of Monotonic and Cyclic Undrained Clay Behavior," *International Journal of Numerical Analytical Methods in Geomechanics*, Vol. 1, No. 2, 1977, pp. 195–216.
17. Prevost, J. H., et al., "Offshore Gravity Structures: Centrifugal Modeling," *Journal of the Geotechnical Engineering Division*, ASCE, Vol. 107, No. GT2, Proc. Paper 16044, Feb., 1981, pp. 125–141.
18. Prevost, J. H., Hughes, T. J. R., and Cohen, M., "Analysis of Gravity Offshore Structure Foundations," *Journal of Petroleum Technology*, Feb., 1980, pp. 199–209.
19. Prevost, J. H., et al., "Foundations of Offshore Gravity Structures: Analysis and Centrifugal Modeling," *California Institute of Technology*, Final Report to Chevron Oil Co., 1979.
20. Prevost, J. H., and Hughes, T. J. R., "Analysis of Gravity Offshore Structure Foundations Subjected to Cyclic Wave Loading," *Proceedings*, Offshore Technology Conference, Vol. 1, May, 1978.
21. Prevost, J. H., and Hoeg, K., "Reanalysis of Simple Shear Soil Testing," *Canadian Geotechnical Journal*, Vol. 13, 1976, pp. 418–429.
22. Prevost, J. H., and Hoeg, K., "Mathematical Model for Static and Cyclic Undrained Clay Behavior, Part II: Experimental Investigations and Model Predictions," *Norwegian Geotechnical Institute, Internal Report 52412*, Nov., 1975.
23. Rowe, R. W., "Displacement and Failure Modes of Model Offshore Gravity Platforms Founded on Clay," *Proceedings*, Offshore Europe '75 Conference, Sept., 1975 pp. OE-75 218.1–OE-75 218.16.
24. Scott, R. F., "Centrifuge Studies of Cyclic Lateral Load-Displacement Behavior of Single Piles," *California Institute of Technology*, Final Report to American Petroleum Institute, 1977.

25. Smith, I. M., "Aspects of the Analysis of Gravity Offshore Structure," *Proceedings, International Conference on Numerical Methods in Geomechanics*, Vol. 2, 1977, pp. 947–972.
26. Young, A. G., Kraft, L. M., and Focht, J. A., "Geotechnical Considerations in Foundation Design of Offshore Gravity Structure," *Proceedings*, Offshore Technology Conference, Proc. Paper OTC 2371, 1975.
27. Zienkiewicz, O. C., et al., "A Unified Approach to the Soil Mechanics Problems of Offshore Foundations," *Numerical Methods in Offshore Engineering*, O. C. Zienkiewicz, et al., ed., John Wiley and Sons, Inc., New York, N.Y., 1978, pp. 361–411.

JOURNAL OF THE GEOTECHNICAL ENGINEERING DIVISION

CONSTRUCTION VIBRATIONS: STATE-OF-THE-ART[a]

By John F. Wiss,[1] F. ASCE

INTRODUCTION

Vibrations produced during construction operations become of concern when they can be felt. They may be sufficiently intense to annoy the recipients, or they may have detrimental effects on structures or equipment. This presentation will consider the sources of construction vibrations, the transmitting medium, and the effects upon the receivers of the vibration. Instrumentation and criteria will be analyzed, as well as the need for further research.

SOURCES OF CONSTRUCTION VIBRATION

Construction vibrations are of three different types: (1) Transient or impact vibration; (2) steady-state or continuous; and (3) pseudo-steady-state vibrations. All are shown in Fig. 1. Examples of transient construction vibrations are those that occur from blasting with explosives, impact pile driving, demolition, and wrecking balls. Steady-state vibrations may be generated by vibratory pile drivers, large pumps as used in jacking underground pipes, and compressors. Pseudo-steady-state vibrations are so called because they are of a random nature or a series of impact vibrations that are at short enough intervals to approach essentially a steady-state condition. Examples of these are jackhammers, pavement breakers, trucks, bulldozers, cranes, and scrapers.

[a]Presented at the April 14–18, 1980, ASCE Convention and Exposition, held at Portland, Oreg.

[1]Chmn., Wiss, Janney, Elstner and Assoc., Inc., 330 Pfingsten Road, Northbrook, Ill. 60062.

Note.—Discussion open until July 1, 1981. To extend the closing date one month, a written request must be filed with the Manager of Technical and Professional Publications, ASCE. Manuscript was submitted for review for possible publication on March 12, 1980. This paper is part of the Journal of the Geotechnical Engineering Division, Proceedings of the American Society of Civil Engineers, ©ASCE, Vol. 107, No. GT2, February, 1981. ISSN 0093-6405/81/0002-0167/$01.00.

Effect of Source Energy

The magnitude of the vibration at a fixed distance from a source is a function of the energy at the source. This relationship may be established by increasing the energy at the source and determining the rate at which the vibration increases.

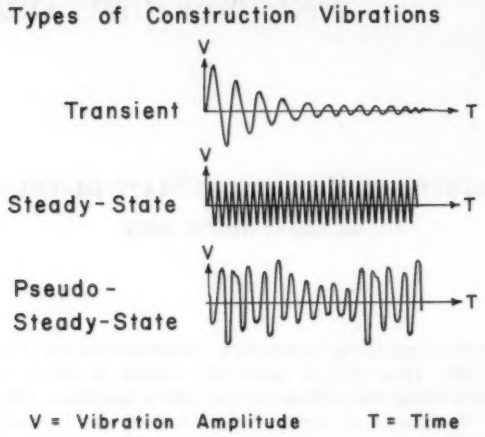

FIG. 1.—Construction Vibration Waveforms

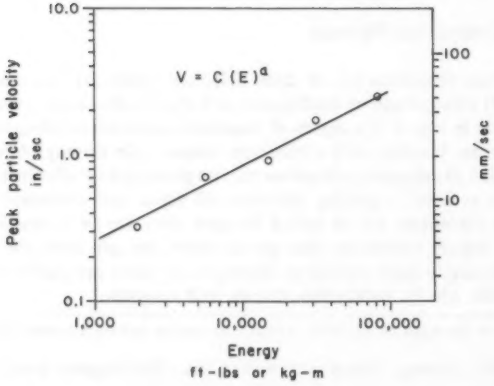

FIG. 2.—Typical Form: Peak Particle Velocity Versus Energy

The form of typical data (Fig. 2) can be approximated by a straight line on a log-log plot. A regression analysis will define the slope of this line. Increasing the energy can be accomplished by dropping a wrecking ball of a known weight from increasing heights. The energy in foot-pounds is the product of the weight and drop height.

Although the vibration magnitude may be expressed as particle displacement, velocity, or acceleration, it has been found by most investigators (9,22,31) that the peak particle velocity is most useful as concerns damage and human evaluation of transient vibration. The relationship between the peak particle velocity and energy may be expressed as

$$V = C(E)^{\alpha} \quad \ldots\ldots\ldots\

on a straight line. A regression analysis of these data can be used with a propagation equation (see Fig. 3) of the form

$$V = kD^{-n} \quad \ldots \ldots \ldots

D = distance, in feet; E = energy in foot-pounds for impacts or charge weight per delay for explosives-pounds; n = slope or attenuation rate; and $D/\sqrt{E}$ = scaled distance. The value of n in this expression generally lies between 1.0 and 2.0 with a relatively common value of 1.5.

Construction Vibration Intensities

Typical intensities of vibration from the operation of construction equipment are presented graphically in Fig. 5. All of the data used to prepare Fig. 5

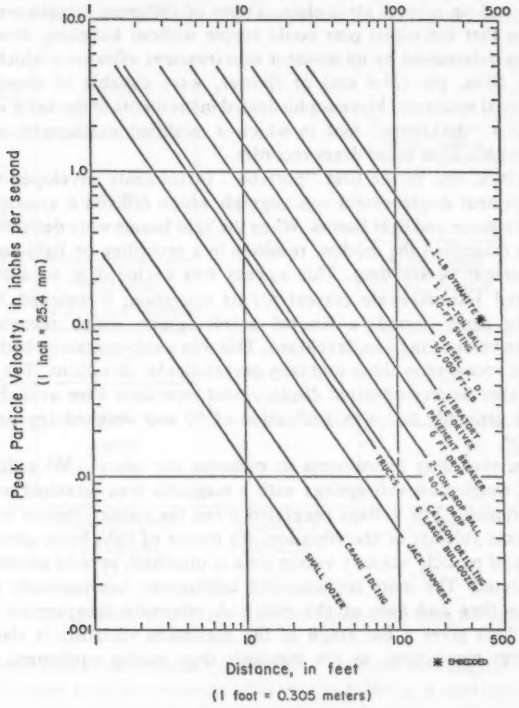

FIG. 5.—Relative Intensities of Construction Vibrations

were obtained by field measurements during actual construction operations (29). The vibration intensities reported in this figure are based on data recorded on the surface of the earth or in residential or relatively small commercial buildings. The response of more massive or subsurface structures may be different, depending on frequency of input and natural frequency of the structure.

It is of interest to note that the intensities involved in these construction activities are spread over a range of three orders of magnitude. It should be

recognized that this graph represents approximate values, but does illustrate the relative intensities of the several sources. The lines shown are for a particular set of soil conditions. The locations and slopes of lines for other conditions may be different.

Vibration Instruments

One of the early instruments used in the 1930s to indicate the intensity of impulse vibrations was the falling-pin seismometer. It consisted of 1/4-in. (6.4-mm) round pins of different lengths 4 in.–15 in. (10 cm–38 cm) which were placed on end on a level glass plate. Tubes of different lengths were bundled together so that individual pins could topple without knocking down adjacent pins. It was determined by its inventor that transient vibrations which "knocked over" the 10-in. pin (25.4 cm) or shorter, were capable of causing damage to a residential structure. More sophisticated instruments in the same era required the use of a "darkroom" tent in which a modified earthquake seismograph was used with a light beam drum recorder.

In the 1940s, one of the first "portable" instruments developed was a Leet three-component displacement seismograph which utilized a system of spring-suspended masses and light beams. When the light beams were deflected, multiple reflections magnified the motion, resulting in a recording on light-sensitive film of displacement versus time. This system was enclosed in an aluminum box and required 110v 60-cycle current for its operation; it weighed 70 lbs (31.8 kg). In the same period, a Knobel accelerograph which recorded particle acceleration versus time was developed. This was a self-contained battery-operated unit that recorded in three mutually perpendicular directions. Ten years later (1950), smaller battery-operated displacement recorders were available for field use. These generally had a magnification of 50 and weighed approximately 35 lbs (15.9 kg).

Vibration recording instruments in common use since 1960 utilize coils as suspended weights on soft springs with a magnetic core attached to the frame of the instrument. The voltage generated when the frame vibrates is a function of the particle velocity of the vibration. By means of light beam galvanometers, a recording of particle velocity versus time is obtained; several sensitivity levels can be selected. The more sophisticated instruments automatically trigger and identify the time and date of the event. A relatively inexpensive strip chart recorder which gives a bar graph of the maximum vibration is also available for long-term monitoring, as are magnetic tape analog equipment and digital recorders.

Criteria for Limiting Vibrations

Vibrations from construction operations are important primarily because of their potential to cause complaints or damage to a variety of structures, or both, above and below ground. They may also cause damage to building contents such as china collections, exhibits in museums, or more commonly, TV sets or glasses. Vibrations have resulted in complaints that they are disturbing to people in the enjoyment of their homes or interference with the performance of their jobs.

The most frequent complaints are from the owners of structures (particularly residential) who claim that damage has been done to their interior walls or exterior walls and foundations, or both. It is probably for this reason that most attention has been focused on residential-type construction. Investigators on this continent and abroad have suggested criteria for limiting such vibration. Some are simple, some are quite complex. The United States Bureau of Mines (USBM) (22) and Edwards and Northwood (9) recommended safe levels of 2.0 ips (50.8 mm/s) for residential structures (see Fig. 6). One investigator (4) classifies buildings in four categories based on their age and condition, and recommends criteria (Table 1) that range from 0.5 ips–4.0 ips (12 mm/s–100 mm/s), the former for old residential structures in very poor condition, the

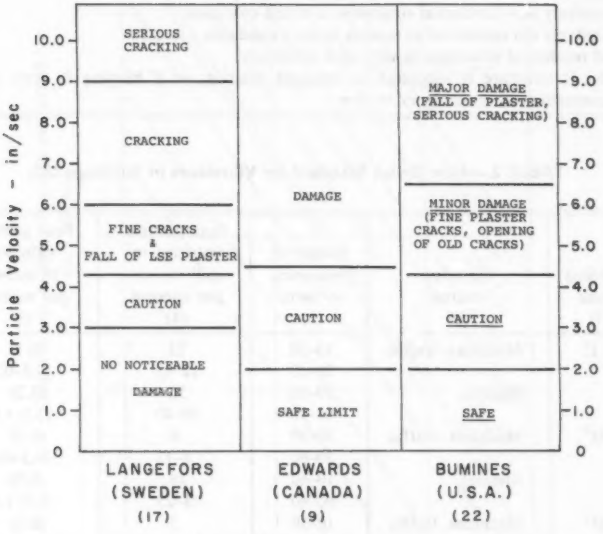

FIG. 6.—Comparison of Damage Criteria: Residential-Type Structures

latter for structures of substantial construction. Another investigator (6) recommends criteria that take into account whether the building is ancient or modern, specific construction details, and degree of distress for both ancient and modern buildings, type of building, type of soil, the cumulative effect of vibration, and an "importance factor." The latter ranges from light industrial to sensitive, ancient, historical buildings, on a scale of 1–10.

The new Swiss standard for vibration (32) differentiates between machines, traffic, and blasting, categorizing all buildings in four classes. For each class of building, permissible levels vary with frequency, as shown in Table 2. The Swiss criteria are more restrictive than the criteria for Langefors (17), Edwards and Northwood (9), and the United States Bureau of Mines (22).

To relate construction vibrations to damage criteria, Fig. 7 is presented. Fig.

TABLE 1.—Criteria Recommended by Chae (4)

Class (1)	Peak particle velocity, in inches per second (2)	Peak particle velocity, in millimeters per second (3)
I[a]	4	100
II[b]	2	50
III[c]	1	25
IV[d]	0.5	12

[a]Structures of substantial construction.
[b]Relatively new residential structures in sound condition.
[c]Relatively old residential structures in poor condition.
[d]Old residential structures in very poor condition.
Note: If structure is subjected to repeated blasting, or if blasting is done without instrumentation, lower category by one.

TABLE 2.—New Swiss Standard for Vibrations in Buildings (32)

Building class (1)	Vibration source (2)	Range of frequency, in hertz (3)	Peak particle velocity, in millimeters per second (4)	Peak particle velocity, in inches per second (5)
I[a]	Machines, traffic	10–30	12	(0.5)
		30–60	12–18	(0.5–0.7)
	Blasting	10–60	30	(1.2)
		60–90	30–40	(1.2–1.6)
II[b]	Machines, traffic	10–30	8	(0.3)
		30–60	8–12	(0.3–0.5)
	Blasting	10–60	18	(0.7)
		60–90	18–25	(0.7–1.0)
III[c]	Machines, traffic	10–30	5	(0.2)
		30–60	5–8	(0.2–0.3)
	Blasting	10–60	12	(0.5)
		60–90	12–18	(0.5–0.7)
IV[d]	Machines, traffic	10–30	3	(0.12)
		30–60	3–5	(0.12–0.2)
	Blasting	10–60	8	(0.3)
		60–90	8–12	(0.3–0.5)

[a]Buildings in steel or reinforced concrete, like factories, retaining walls, bridges, steel towers, open channels; underground chambers and tunnels with and without concrete alignment.
[b]Buildings with foundation walls and floors in concrete, walls in concrete or masonry; stone masonry retaining walls; underground chambers and tunnels with masonry alignments; conduits in loose material.
[c]Buildings as mentioned previously but with wooden ceilings and walls in masonry.
[d]Construction very sensitive to vibrations; objects of historic interest.

7 is the same as Fig. 5, previously presented, but has superimposed upon it the levels of vibration intensities which generally are considered by investigators in the United States to be thresholds of possible damage for both commercial buildings and for residential-type structures. These are 4.0 ips for commercial buildings and 2.0 ips for residential structures. It should be recognized that some of the sources are transient (impulsive) vibrations, others represent steady-state, and others are pseudo-steady-state vibrations. For purposes of

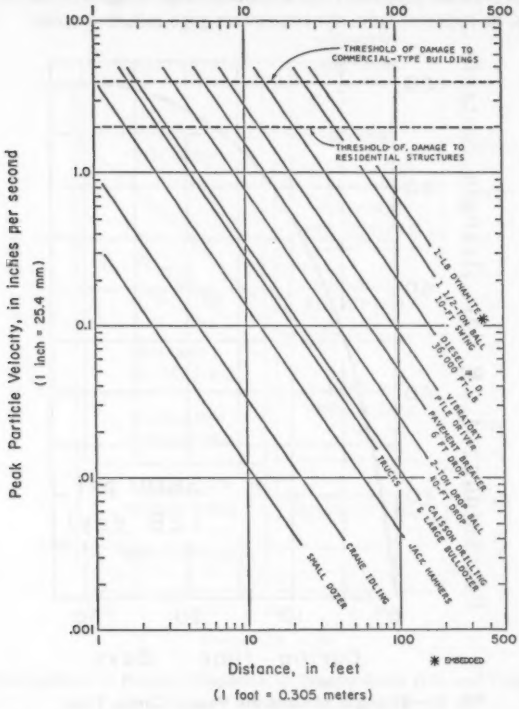

FIG. 7.—Construction Vibration Intensities Related to Damage Criteria

this presentation, they have been lumped together. It is emphasized that these are "threshold" values which generally must be exceeded before damage is likely to occur.

It is generally acknowledged that the ratio of the frequency of the vibrations transmitted to the natural frequency of the structure is an important parameter. The closer this ratio is to unity, the greater the response of the structure, therefore the lower should be the criteria. Since residences have natural frequencies in the range of 4 Hz–10 Hz, lower criteria have been suggested

for lower frequency ground vibration than for higher frequency vibration.

Several investigators (7,20,21) have been and are working on the response spectrum. By this method, the amplitude of the vibrations induced in a structure is a function of the natural frequency and damping characteristics of the structure and the frequency composition and magnitude of the ground motion.

Published criteria for underground utilities are not available. Such utilities include tile or concrete drainpipe, sewer and water mains, and pipelines. In our experience, particle velocities of 3 ips have not damaged pipes and mains. Further, high pressure pipelines have withstood 10 ips–20 ips without experiencing any distress, as apparent from dynamic strain gage measurements.

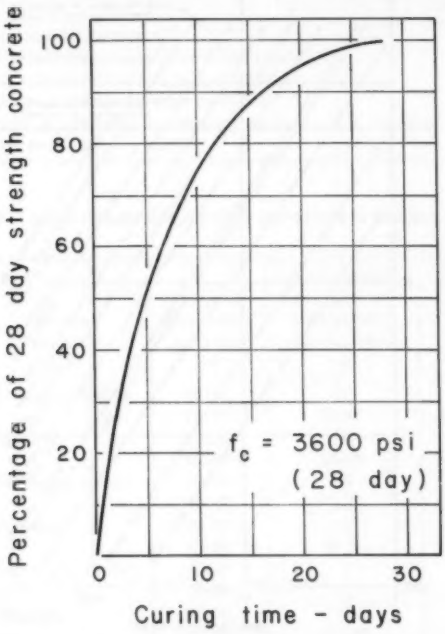

FIG. 8.—Strength of Concrete Versus Curing Time

Another problem that frequently arises on construction jobs is the safe level of transient vibration in the vicinity of young concrete. The primary sources of such are pile driving and excavation blasts. With young concrete, we are dealing with a material which increases in strength with time, thus, so must the criteria. The writer (27) considers the concrete to be essentially at full strength after 28 days, Ontario Hydro (unpublished) 90 days. A decision must then be made as to the particle velocity that full-strength concrete can withstand. The writer (27) says 5 ips, Atkins and Dixon (1) 4 ips, Ontario Hydro (unpublished) 3 ips. Because stress level is proportional to particle velocity, the criteria can be established when it is known how the concrete attains strength with time

(see Fig. 8), e.g., when the concrete attains 10% of its strength, the permissible level for vibration would be 0.5 ips, 0.4 ips, or 0.3 ips. When it attains 50% strength, the permissible level would be 2.5 ips, 2.0 ips, or 1.5 ips.

The effects of transient vibrations upon soils is another area that is of concern to engineers. Some work has been done on the effect of steady-state vibrations on soils (24). Little, if any, quantitative information is available on the effects of short-duration transient vibrations on soils. At best, the literature (5) states that cohesive soils are least affected, e.g., compacted, by vibration, while cohesionless soils are most sensitive to vibration.

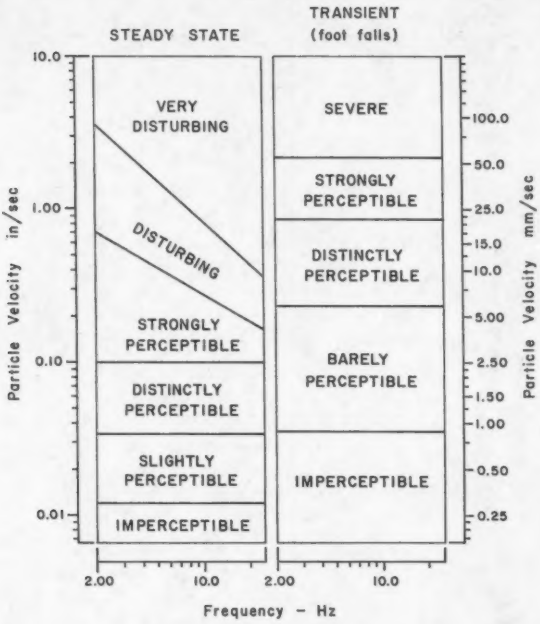

FIG. 9.—Comparison of Human Response to Steady State (23) and Transient Vibrations (28)

Information is available on the effect of cyclic loading on various materials. These have been experimentally determined for complete reversals of stress of several magnitudes and for partial reversals of stress. The studies have involved repetitious or steady-state reversals. There is no information on repeated transient loading. The difference is that in a transient, the peak stress occurs but once or twice with the remaining cycles being of reduced magnitudes. As far as is known, there is virtually no published information on fatigue studies of any kind on plaster or masonry materials used in building construction.

An investigation into the fatigue of plain concrete (15) reveals that the fatigue strength for a life of 10,000,000 cycles is roughly about 50% of static strength

for large-amplitude stress cycles, and approximately 85% for smaller cyclic stress amplitudes. Reinforced concrete exhibits a practical fatigue limit in the vicinity of 1,000,000 cycles and an endurance limit in excess of 20 ksi (1,409 kg/sq cm).

Human Response to Vibration

Regardless of the "safe" criteria that apply to transient vibration, it is rare that the criteria can be reached before complaints or claims are filed. The human body is an excellent detector of vibration, but a poor measuring device.

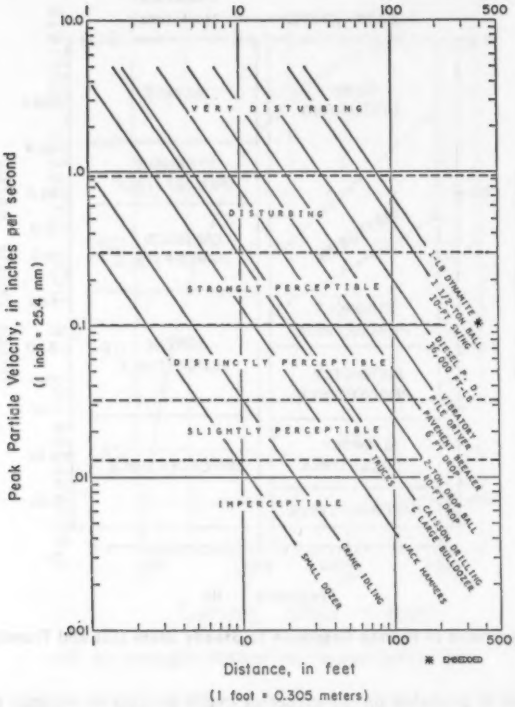

FIG. 10.—Construction Vibration Intensities Related to Human Evaluation of Vibrations (23)

Considerable work has been done on the human evaluation of steady-state vibrations (14,23), but very little has been done on transient vibrations. The only study found on transient vibrations (28) was concerned with impact vibrations which simulated footfalls while walking across a floor. The waveform is sufficiently similar to those resulting from impact pile driving or from single-hole blasts that the criteria would apply. Multidelay blasts do not have a waveform

that is similar to the footfall vibrations. The human evaluation of the transient vibration study compared to those ratings reported from steady-state vibration studies is shown in Fig. 9.

To relate construction vibrations to human response to steady-state vibrations, Fig. 10 is presented. Fig. 10 is the same as Fig. 5 previously presented but has superimposed upon it the normal subjective evaluation of the vibration intensity. It is apparent by comparison of Figs. 7 and 10 that the vibration intensities which are subjectively classified as "disturbing" or "very disturbing" are well below the intensities required to cause damage. Levels in the "disturbing" range may result in complaints or claims of damage.

Needed Research

It is considered that the instrumentation needed to measure and document vibration during construction operations is presently available. Although expensive, competition will bring the costs down.

The development of "practical," yet not overly conservative criteria is needed. This specifically applies to residences, buildings (both low-rise and high-rise), and other structures, as well as underground utilities. Those currently in use are either too simple or too complex. The criteria should be based on available and future controlled tests and not by arbitrary evaluations.

Studies to evaluate the criteria to be used for young concrete can be made in the field or in the laboratory by simulating transient vibrations on a hydraulic shaker. The effects of transient vibration on soils can be studied in the field with laboratory tests providing support information.

The effect of fatigue on common building materials, particularly plaster and masonry, should be investigated. This should be done for both continuous stress reversals, as well as transients. It is acknowledged that, when dealing with transients, the problem is more complex. When dealing with continuous reversals, only the frequency, amplitude, and time are parameters. With transients, there are the additional parameters of damping, duration of individual pulses, rate of occurrence, and complex waveforms.

Human response to transient vibration is being studied in a research program entitled "Human Response to Blast and Noise and Ground and Structure Vibrations," presently underway by a contractor for the United States Bureau of Mines. This is a 2-yr program which consists of attitude surveys and field and laboratory tests. It should provide meaningful results to the construction industry, even though the blasts investigated in the USBM program will be at surface coal mines and quarries.

Summary and Conclusions

The generation and propagation of vibrations due to construction have been considered. The relative intensity of the vibration produced by many construction operations and equipment are identified, based on more than a quarter century of field tests. Instruments suitable for the measurement of these vibrations have been described. The large differences in current damage criteria are revealed. Research is needed on the effects of vibration, both transient and steady-state, on young concrete, soils, and underground utilities. Fatigue data on building

materials for both transient and steady-state vibrations are needed. Additional research is needed in the human response to transient vibrations.

The state of the art has come a long way in the last 50 yr. With sufficient funding, all of the required research can be done; priorities will be established by the need. Hopefully, it will not take the next 50 yr for the required research.

Appendix I.—References

1. Atkins, K. P., and Dixon, D. E., "Concrete Structures and Construction Vibrations," *Vibrations of Concrete Structures*, SP-60, American Concrete Institute, 1979, pp. 213–247.
2. Attewell, P. B., and Farmer, I. W., "Attenuation of Ground Vibrations from Pile Driving," *Ground Engineering*, Vol. 3, No. 7, July, 1973.
3. Brown, L. M., "Measurements of Vibrations Caused by Construction Equipment and Blasting," *Report No. RR172*, Department of Highways, Ontario, Canada, Apr., 1971.
4. Chae, Y. S., "Design of Excavation Blasts to Prevent Damage," *Civil Engineering*, ASCE, Vol. 48, No. 4, Apr., 1978, pp. 77–79.
5. Chellis, R. B., "Pile Foundations," McGraw-Hill Book, Co., Inc., New York, N.Y., 1961.
6. Crockett, J. H. A., "Piling Vibrations and Structural Fatigue," *Recent Developments in the Design and Construction of Piles*, Institute of Civil Engineering, London, England, 1979.
7. Dowding, C. H., "Ground-Structure Response to Blasting Vibrations," *Proceeding of the 14th Annual Meeting, Society of Engineering Sciences*, Lehigh University, Nov., 1977, pp. 1085–1098.
8. Dym, C. L., "Attenuation of Ground Vibration," *Sound and Vibration*, Apr., 1976, pp. 32–34.
9. Edwards, A. T., and Northwood, T. D., "Experimental Studies of the Effects of Blasting on Structures," *The Engineer*, Vol. 210, Sept., 1960, pp. 538–546.
10. Ferahian, R. H., and Hurst, W. D., "Vibration and Possible Building Damage due to Operation of Construction Machinery," *Proceedings of the 1968 Public Works Congress and Equipment Show*, Oct., 1968, pp. 144–155.
11. Ferahian, R. H., "Vibrations Caused by Pile Driving," *Bibliography No. 35*, National Research Council of Canada, Division of Building Research, Ottawa, Canada.
12. Ferahian, R. H., and Ward, H. S., "Vibration Environment in Laboratory Buildings," *Technical Paper No. 329*, Division of Building Research, National Research Council, Ottawa, Canada, Oct., 1970.
13. Forssblad, L., "Ground Vibrations and the Damage They Cause, the Effects of Vibratory Compactors," Swedish Geotechnical Institute, May, 1973.
14. Goldman, D. E. A., "A Review of Subjective Responses to Vibratory Motion of the Human Body in Frequency Range 1 to 70 cps," *Report NM-004-00*, Naval Medical Research Institute, Washington, D.C., 1948.
15. Hanson, J. M., Ballinger, C. A., American Concrete Institute Committee 215, "Considerations for Design of Concrete Structures Subjected to Fatigue Loading," *Journal of the American Concrete Institute*, Vol. 71, No. 3, Mar., 1974, pp. 97–121.
16. Heckman, W. S., and Hagerty, D. J., "Vibrations Associated with Pile Driving," *Journal of the Construction Division*, ASCE, Vol. 104, No. CO4, Proc. Paper 14205, Dec., 1978, pp. 385–394.
17. Langefors, U., Kihlström, B., and Westerberg, H., "Ground Vibrations in Blasting," *Water Power*, Feb., 1958.
18. Liu, T. K., and Kinner, E. B., Yegian, M. K., "Ground Vibrations," *Sound and Vibration*, Oct., 1974, pp. 26–32.
19. Luna, W. A., "Ground Vibration Due to Pile Driving," *Foundation Facts*, Vol. 3, No. 2, Raymond International, Houston, Tex., 1967.
20. Medearis, K., "The Development of Rational Damage Criteria for Low-Rise Structures Subjected to Blasting Vibration," *Proceedings of the 18th U.S. Symposium on Rock Mechanics*, June, 1977, pp. 1A2-1–1A2-6.

21. Naik, T. R., "Predictions of Damage to Low-Rise Buildings Due to Ground Vibrations Created by Blastings," *Vibrations of Concrete Structures,* SP-60, American Concrete Institute, 1979, pp. 249–264.
22. Nicholls, H. R., Johnson, C. F., and Duvall, W. I., "Blasting Vibrations and their Effects on Structures," *BuMines Bulletin 656,* 1971.
23. Reiher, H., and Meister, F. J., "The Effects of Vibration on People," (In German) *Forschung auf dem Gebeite der Ingenieurwesens,* Vol. 2, No. II, 1931, p. 381.
24. Richart, F. E., Hall, J. R., and Woods, R. D., "Vibration of Soils and Foundations," Prentice-Hall, Inc., Englewood Cliffs, N.J., 1969.
25. Steffens, R. J., "Some Aspects of Structural Vibration," *Proceedings of the Symposium on Vibration in Civil Engineering,* Imperial College of Science and Technology, Apr., 1965.
26. Sutherland, H. B., "A Study of Vibrations Produced in Structures by Heavy Vehicles," *Proceedings of the Thirteenth Annual Meeting of the Highway Research Board,* Dec., 1950, pp. 406–419.
27. Wiss, J. F., "Damage Effects of Pile Driving Vibrations," *Highway Research Board Record 155,* 1967, pp. 14–20.
28. Wiss, J. F., and Parmelee, R. A., "Human Perception of Transient Vibrations," *Journal of the Structural Division,* ASCE, Vol. 100, No. ST4, Proc. Paper 10495, Apr., 1974, pp. 773–787.
29. Wiss, J. F., "Vibrations During Construction Operations," *Journal of the Construction Division,* ASCE, Vol. 100, No. CO3, Proc. Paper 10798, Sept., 1974, pp. 239–246.
30. Wiss, J. F., "How Much Vibration," *World Construction,* Oct., 1974, pp. 24–26.
31. Wiss, J. F., "A Study of Damage to a Residential Structure from Blast Vibrations," *Special Publication,* ASCE, 1974.
32. "Effects of Vibration on Construction," Swiss Association of Standardization, Seefeldstrasse 9, CH 8008, Zurich, Switzerland.

Appendix II.—Notation

The following symbols are used in this paper:

D = distance, in feet (meters);
E = energy in foot-pounds (kilogram-meter) or explosive, in pounds (kilograms);
V = peak particle velocity, in inches per second (millimeters per second);
C, k, K = coefficients; and
α, n = exponents.

JOURNAL OF THE GEOTECHNICAL ENGINEERING DIVISION

RESPONSE OF BURIED STRUCTURES TO TRAVELING WAVES

By Richard N. Hwang[1] and John Lysmer,[2] M. ASCE

INTRODUCTION

The response of underground structures, mainly pipelines, is receiving more and more attention because of the impact of such lifelines as water mains and sewer lines upon the health and safety of people served and also because of the hazardous consequences of the failure of gas or oil lines. Procedures are available for analyzing these structures subjected to earthquake loadings (1,2,3, 6,7,11,13). However, all these procedures were developed on the assumption that soil-structure interaction effects on the response of structures are negligible, i.e., structures move with the surrounding soils during earthquakes.

It is reasonable to assume that the soil-structure interaction effects are negligible for small and flexible structures. For large structures, such as subways, the potential errors introduced by ignoring the interaction effects can certainly not be overlooked. It is the object of this study to evaluate the interaction effects on the response of large structures to traveling seismic waves. A new approach is introduced for computing the response of these structures using the finite element method. In analyses using this new approach the soil-structure systems are represented by three-dimensional finite elements; however, by using a special type of wave-transmitting element, a three-dimensional system can be reduced to a plane of finite elements with three degrees-of-freedom at each node while the traveling effects of waves are faithfully retained.

[1]General Mgr., Kiso-Jiban Consultants Co., Ltd., 60 Kallang Pudding Road, Singapore 1334.

[2]Prof., Dept. of Civ. Engrg., Univ. of California, Berkeley, Calif.

Note.—Discussion open until July 1, 1981. To extend the closing date one month, a written request must be filed with the Manager of Technical and Professional Publications, ASCE. Manuscript was submitted for review for possible publication on September 13, 1979. This paper is part of the Journal of the Geotechnical Engineering Division, Proceedings of the American Society of Civil Engineers, ©ASCE, Vol. 107, No. GT2, February, 1981. ISSN 0093-6405/81/0002-0183/$01.00.

Wave-Transmitting Element

Fig. 1(*a*) shows a typical interaction system of interest. The system is represented by a three-dimensional finite element model. For particular cases in which the geometry and material properties remain unchanged along the longitudinal axis of the structure, the system can be modeled into identical planes of finite elements at equal spacings. All these planes are parallel to each other and perpendicular to the longitudinal axis of the structure as shown in the figure.

Consider a brick element bound by two parallel planes A and B, as shown in Fig. 1(*b*). Let the four nodes in plane A be denoted as *I*, *J*, *K*, and *L*,

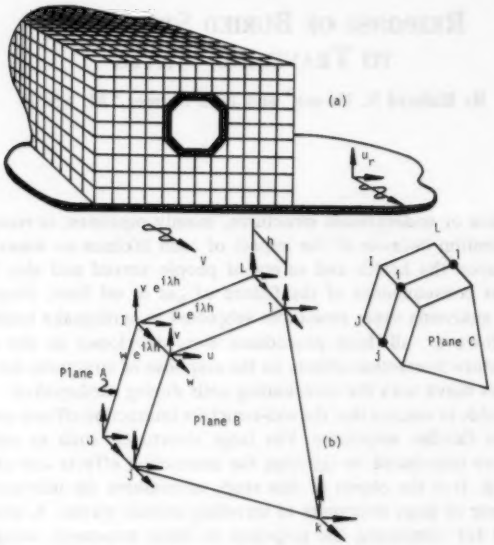

FIG. 1.—Finite Element Representation of Soil-Structure Interaction System of Typical Buried Long Structure: (*a*) Three-Dimensional Model; (*b*) Wave-Transmitting Element

and the corresponding nodes in plane B as *i*, *j*, *k*, and *l*. For simplicity only three translational degrees-of-freedom at each node will be considered. A 24 by 24 stiffness matrix [*K*] can be formed for this element and the forces acting on these nodes can be related to the nodal displacements by

$$\begin{Bmatrix} f_a \\ f_b \end{Bmatrix} = \begin{bmatrix} K_{aa} & K_{ab} \\ K_{ba} & K_{bb} \end{bmatrix} \begin{Bmatrix} u_a \\ u_b \end{Bmatrix} \quad \ldots\ldots\ldots\ldots\ldots\ldots\ldots\ldots\ldots\ldots (1)$$

in which $\mathbf{f}_a$ and $\mathbf{f}_b$ = vectors containing forces acting on nodes in planes A and B, respectively; similarly, u_a and u_b = nodal displacements at these nodes; K_{aa}, K_{ab}, K_{ba}, and K_{bb} = 12 by 12 submatrices of [*K*]. The forces acting

on nodes in plane B, i.e., nodes i, j, k, and l, due to the deformations of this element alone, are

$$\{f_b\} = [K_{ba}]\{u_a\} + [K_{bb}]\{u_b\} \quad \ldots (2)$$

For waves traveling in the longitudinal direction at a constant velocity, the following relationship exists:

$$\{u_a\} = e^{i\lambda h}\{u_b\} \quad \ldots (3)$$

in which λ = the wave number; and h = the thickness of the element or the spacing between two consecutive planes.

The wave number, λ, is related to the velocity, C, and frequency, f, of the wave by the following expression:

$$\lambda = \frac{f}{C} \quad \ldots (4)$$

It should be noted that the wave number used here is a global wave number refering to the frequency and the velocity of the wave propagating through the entire profile and does not relate to the wave velocity in the material making up the element. However, readers are reminded that an assumption that the geometry and the material properties remain unchanged along the longitudinal direction of the structure has been made for Eq. 3 to be valid. This aspect is further considered at the end of this paper.

Substitution of Eq. 3 in Eq. 2 yields:

$$\{f_b\} = (e^{i\lambda h}[K_{ba}] + [K_{bb}])\{u_b\} \quad \ldots (5)$$

Similarly, the additional forces acting on nodes in plane B due to the deformations of the neighboring element bound by planes B and C [see Fig. 1(*b*)] are

$$\{f_b\} = (e^{-i\lambda h}[K_{bc}] + [K_{bb}])\{u_b\} \quad \ldots (6)$$

The total forces acting on nodes in plane B can thus be obtained by combining these two equations, giving

$$\{f_b\} = (2[K_{bb}] + e^{i\lambda h}[K_{ba}] + e^{-i\lambda h}[K_{bc}])\{u_b\} \quad \ldots (7)$$

The preceding expression relates the forces at and the displacements of the four nodes in a single plane; therefore, by definition, the stiffness matrix for the wave-transmitting element formed by these four nodes is

$$[L] = 2[K_{bb}] + e^{i\lambda h}[K_{ba}] + e^{-i\lambda h}[K_{bc}] \quad \ldots (8)$$

The stiffness matrices for all the elements in the same plane can thus be formed and the global stiffness matrix can easily be obtained by assembling the element stiffness matrices. The three-dimensional system is therefore reduced to a plane of finite elements.

It can be noted that although the submatrix $[K_{bb}]$ is a symmetric matrix, the submatrices $[K_{ba}]$ and $[K_{bc}]$ are not; therefore the element stiffness matrix $[L]$ is not longer a symmetric matrix. Furthermore, because of the presence of the imaginary terms, $[L]$ is not even a real matrix, as is the one commonly used in plane strain analyses. As a matter of fact, because the two elements on the two sides of the plane are identical

$$[K_{bc}] = [K_{ba}]^T \quad \ldots \quad (9)$$

$$l^{ij} = 2(k_{bb}^{ij}) + e^{i\lambda h}(k_{ba}^{ij}) + e^{-i\lambda h}(k_{bc}^{ij}) = \text{Conjugate of } l^{ji} \quad \text{for} \quad i \neq j \quad \ldots \quad (10)$$

in which the terms in parentheses are the corresponding terms in the submatrices $[K_{bb}]$, $[K_{ba}]$ and $[K_{bc}]$, respectively. The element stiffness matrices, and therefore the global stiffness matrix, are thus Hermitian matrices if material damping is ignored.

The foregoing procedure is straightforward and easy to understand. However, it is difficult to form the submatrices $[K_{bb}]$ and $[K_{ba}]$ for an arbitrary brick element without first forming the full element stiffness matrix $[K]$ which is a 24 by 24 matrix. The formation of full stiffness matrices for all the elements is very costly. A simpler method for forming the stiffness matrices for wave-transmitting elements is given in the next few paragraphs.

It is standard practice in forming the stiffness matrix for a quadrilateral element to transform the x-y system to a new coordinate system so that the coordinates of an arbitrary point in the element can be expressed in terms of the coordinates of the four nodes at the corners, thus

$$x(x,t) = \sum_{i=1}^{4} h_i \cdot x_i; \; y(s,t) = \sum_{i=1}^{4} h_i \cdot y_i \quad \ldots \quad (11)$$

in which $h_1 = (1 - s)(1 - t)/4$; $h_2 = (1 + s)(1 - t)/4$; $h_3 = (1 + s)(1 + t)/4$; and $h_4 = (1 - s)(1 + t)/4$. The corrdinates x_i and y_i = the x and y coordinates of the ith node of the element. Similarly, the displacements can also be expressed in terms of nodal displacements

$$u = \sum_{i=1}^{4} h_i \cdot u_i; \; v = \sum_{i=1}^{4} h_i \cdot v_i; \; w = \sum_{i=1}^{4} h_i \cdot w_i \quad \ldots \quad (12)$$

in which u, v, and w = displacements in the x, y, and z directions, respectively. For waves traveling in the longitudinal direction, the z direction, the displacement field for the entire system can be expressed as

$$u = e^{-i\lambda z} \sum_{i=1}^{4} h_i \cdot u_i; \; v = e^{-i\lambda z} \sum_{i=1}^{4} h_i \cdot v_i; \; w = e^{-i\lambda z} \sum_{i=1}^{4} h_i \cdot w_i \quad \ldots \quad (13)$$

From calculus, the following relationship exists:

$$\begin{Bmatrix} \frac{\partial}{\partial s} \\ \frac{\partial}{\partial t} \\ \frac{\partial}{\partial z} \end{Bmatrix} = \begin{bmatrix} \frac{\partial x}{\partial s} & \frac{\partial y}{\partial s} & 0 \\ \frac{\partial x}{\partial t} & \frac{\partial y}{\partial t} & 0 \\ 0 & 0 & 1 \end{bmatrix} \begin{Bmatrix} \frac{\partial}{\partial x} \\ \frac{\partial}{\partial y} \\ \frac{\partial}{\partial z} \end{Bmatrix} \quad \ldots \quad (14)$$

Therefore

$$\begin{Bmatrix} \frac{\partial}{\partial x} \\ \frac{\partial}{\partial y} \\ \frac{\partial}{\partial z} \end{Bmatrix} = \frac{1}{J} \begin{bmatrix} \frac{\partial y}{\partial t} & \frac{\partial y}{\partial s} & 0 \\ \frac{\partial x}{\partial t} & \frac{\partial x}{\partial s} & 0 \\ 0 & 0 & J \end{bmatrix} \begin{Bmatrix} \frac{\partial}{\partial s} \\ \frac{\partial}{\partial t} \\ \frac{\partial}{\partial z} \end{Bmatrix} = [D] \begin{Bmatrix} \frac{\partial}{\partial s} \\ \frac{\partial}{\partial t} \\ \frac{\partial}{\partial z} \end{Bmatrix} \quad \ldots\ldots (15)$$

in which the Jacobian $J = \frac{\partial x}{\partial s} \cdot \frac{\partial y}{\partial t} - \frac{\partial x}{\partial t} \cdot \frac{\partial y}{\partial s}$ . . . . . (16)

Differentiation of Eq. 13 yields

$$\begin{Bmatrix} \frac{\partial}{\partial s} \\ \frac{\partial}{\partial t} \\ \frac{\partial}{\partial z} \end{Bmatrix} (u, v, \text{ or } w) = [P] \begin{pmatrix} u_1 & v_1 & & w_1 \\ u_2 & v_2 & & w_2 \\ u_3, & v_3, & \text{or} & w_3 \\ u_4 & v_4 & & w_4 \end{pmatrix} \quad \ldots\ldots (17)$$

in which $[P]$

$$= \frac{e^{-i\lambda z}}{4} \begin{bmatrix} -(1-t) & (1-t) & (1+t) & -(1+t) \\ -(1-s) & -(1+s) & (1+s) & (1-s) \\ -i\lambda(1-s)(1-t) & -i\lambda(1+s)(1-t) & -i\lambda(1+s)(1+t) & -i\lambda(1-s)(1+t) \end{bmatrix} \quad (18)$$

Substitution of Eq. 7 in Eq. 15 leads to

$$\begin{Bmatrix} \frac{\partial}{\partial x} \\ \frac{\partial}{\partial y} \\ \frac{\partial}{\partial z} \end{Bmatrix} (u, v, \text{ or } w) = [T] \begin{pmatrix} u_1 & v_1 & & w_1 \\ u_2 & v_2 & & w_2 \\ u_3, & v_3, & \text{or} & w_3 \\ u_4 & v_4 & & w_4 \end{pmatrix} \quad \ldots\ldots (19)$$

in which $[T] = [D]\,[P] = \begin{bmatrix} T_{11} & T_{12} & T_{13} & T_{14} \\ T_{21} & T_{22} & T_{23} & T_{24} \\ T_{31} & T_{32} & T_{33} & T_{34} \end{bmatrix}$ . . . . . (20)

Strains are related to displacements by

$$\epsilon_x = \frac{\partial u}{\partial x};\ \epsilon_y = \frac{\partial v}{\partial y};\ \epsilon_z = \frac{\partial w}{\partial z};\ \epsilon_{xy} = \frac{\partial u}{\partial y} + \frac{\partial v}{\partial x};\ \epsilon_{yz} = \frac{\partial v}{\partial z} + \frac{\partial w}{\partial y};$$

$$\epsilon_{zx} = \frac{\partial w}{\partial x} + \frac{\partial u}{\partial z} \quad \ldots\ldots (21)$$

Using the relationships in Eqs. 9 and 21, one can obtain the following expression:

$$\{\epsilon\} = [B]\{u\} \quad \ldots\ldots (22)$$

in which $\{\epsilon\} = \begin{Bmatrix} \epsilon_x \\ \epsilon_y \\ \epsilon_z \\ \epsilon_{xy} \\ \epsilon_{yz} \\ \epsilon_{zx} \end{Bmatrix}$ $\ldots\ldots (23)$

$$\{u\} = \begin{Bmatrix} u_1 \\ v_1 \\ w_1 \\ u_2 \\ v_2 \\ w_2 \\ u_3 \\ v_3 \\ w_3 \\ u_4 \\ v_4 \\ w_4 \end{Bmatrix} \quad \ldots\ldots (24)$$

$$[B] = \begin{bmatrix} T_{11} & 0 & 0 & T_{12} & 0 & 0 & T_{13} & 0 & 0 & T_{14} & 0 & 0 \\ 0 & T_{21} & 0 & 0 & T_{22} & 0 & 0 & T_{23} & 0 & 0 & T_{24} & 0 \\ 0 & 0 & T_{31} & 0 & 0 & T_{32} & 0 & 0 & T_{33} & 0 & 0 & T_{34} \\ T_{21} & T_{11} & 0 & T_{22} & T_{12} & 0 & T_{23} & T_{13} & 0 & T_{24} & T_{14} & 0 \\ 0 & T_{31} & T_{21} & 0 & T_{32} & T_{22} & 0 & T_{33} & T_{23} & 0 & T_{34} & T_{24} \\ T_{31} & 0 & T_{11} & T_{32} & 0 & T_{12} & T_{33} & 0 & T_{13} & T_{34} & 0 & T_{14} \end{bmatrix} \quad (25)$$

For a linear elastic isotropic material the stress-strain relationship is given by Hooke's Law

$$\{\sigma\} = [H]\{\epsilon\} \quad \ldots\ldots (26)$$

in which $[H]$

$$= \frac{E}{(1+\nu)(1-2\nu)} \begin{bmatrix} 1-\nu & \nu & \nu & 0 & 0 & 0 \\ \nu & 1-\nu & \nu & 0 & 0 & 0 \\ \nu & \nu & 1-\nu & 0 & 0 & 0 \\ 0 & 0 & 0 & \frac{1-2\nu}{2} & 0 & 0 \\ 0 & 0 & 0 & 0 & \frac{1-2\nu}{2} & 0 \\ 0 & 0 & 0 & 0 & 0 & \frac{1-2\nu}{2} \end{bmatrix} \quad (27)$$

where E = the Young's modulus; and ν = the Poisson's ratio.

Using the virtual work approach the expression for the stiffness matrix is

$$[L] = \int_{\text{vol}} [B]^T [H] [B] \, dv \quad (28)$$

The integration is usually carried out by using Gauss quadrature formulas which turn the integration into the summation of a finite number of terms. It should be carried out through the entire volume of the element. However, it is possible to form the matrix in such a way, see Eq. 7, that

$$[B(s,t,z,\lambda)] = e^{-i\lambda z} [B^*(s,t,\lambda)] \quad (29)$$

the stiffness matrix for an element like the one shown in Fig. 1(*b*) can then be obtained as follows:

$$[L] = \int_0^h e^{-2i\lambda z} \, dz \int_{\text{area}} [B^*]^{TC} [H] [B^*] \, dA$$

$$= \frac{-1}{2i\lambda} (e^{-2i\lambda h} - 1) \int_{\text{area}} [B^*]^{TC} [H] [B^*] \, dA \quad (30)$$

in which $[B^*]^{TC}$ = the transpose conjugate (or called tranjugate) of $[B^*]$. If these slices are sufficiently thin, implying a continuous system, this equation reduces to

$$[L]_{h \to 0} = h [L^*] \quad (31)$$

in which $[L^*] = \int_{\text{area}} [B^*]^{TC} [H] [B^*] \, dA$. Because only the four nodes in plane B are involved in the formulation, the matrix $[L^*]$ can be imagined as the stiffness matrix for a plane element bound by these four nodes while waves are free to pass through. The formulation of element stiffness matrices using this method is much easier than the formulation using Eq. 10 because of the smaller number of degrees-of-freedom involved. It is also more rigorous because Eq. 13 is an exact representation of the variations of displacements in the longitudinal direction once the assumption that the geometry and the material properties remain unchanged is made. In forming the stiffness matrix for an arbitrary three-dimensional element, it is usually assumed that displace-

ments vary linearly with space. Therefore, strictly speaking, Eq. 1 is not exact. However, as the thickness of element, h, approaches, the two methods approach the same results.

It should be noted that, because of the presence of the imaginary terms in the third row of the matrix $[P]$, the matrix $[B^*]$ is a complex matrix and matrix $[L]$ is no longer real and symmetric. As it has been shown previously, the stiffness matrix $[L]$ now is a Hermitian matrix if material damping is ignored. This becomes clear after the matrix operation in Appendix I is followed.

Material damping can easily be incorporated in analyses by using the complex response method (5). The stiffness matrix for an element for which the damping ratio is β thus is

$$[L] = h\,[L^*]\,e^{2i\beta} \quad \ldots\ldots\ldots\ldots\ldots\ldots\ldots\ldots\ldots\ldots \quad (32)$$

In such cases the matrix $[L]$ is no longer Hermitian.

Equation of Motion

After the stiffness matrices for all the elements in a plane have been formed, a global stiffness matrix can be obtained by assembling all these element stiffness matrices. The equation of motion for a slice of elements thus is

$$h\,[M]\,\{\ddot{u}\} + h\,[K]\,\{u\} = \{p\} \quad \ldots\ldots\ldots\ldots\ldots\ldots\ldots\ldots \quad (33)$$

in which $[M]$ = the mass matrix; $[K]$ = the stiffness matrix; and $\{p\}$ = external forces. The mass matrix $[M]$ is the same as the one usually seen in plane strain analyses and can be formed using the lumped-mass method, the consistent-mass method, or the combination of the two. The external forces are zero at free nodes and nonzero at nodes on the base of the finite element model. Given the displacements at nodes on the base, the motions at the free nodes can be obtained by solving the equation

$$h\,[M_{ff}]\,\{\ddot{u}_f\} + h\,[K_{ff}]\,\{u_f\} = -h\,[M_{fr}]\,\{\ddot{u}_r\} - h\,[K_{fr}]\,\{u_r\} \quad \ldots\ldots\ldots \quad (34)$$

which reduces to

$$[M_{ff}]\,\{\ddot{u}_f\} + [K_{ff}]\,\{u_f\} = -[M_{fr}]\,\{\ddot{u}_r\} - [K_{fr}]\,\{u_r\} \quad \ldots\ldots\ldots\ldots\ldots \quad (35)$$

The subscript f in the foregoing expression refers to free nodes and r to the nodes on the base. This equation is commonly seen and techniques are available for solving it for response (5). Because of the presence of complex numbers, transient response will best be solved in the frequency domain using the Fourier techniques by decomposing the input motions into a serious of harmonic motions

$$\{u_r\} = \sum_{j=1}^{n} \{U_r\}_j \cdot e^{i\omega_j t} \quad \ldots\ldots\ldots\ldots\ldots\ldots\ldots\ldots\ldots\ldots \quad (36)$$

$$\{\ddot{u}_r\} = -\sum_{j=1}^{n} \omega_j^2 \{U_r\}_j \cdot e^{i\omega_j^2 t} \quad \ldots\ldots\ldots\ldots\ldots\ldots\ldots\ldots\ldots\ldots \quad (37)$$

The same treatment can be applied to the response

$$\{u_f\} = \sum_{j=1}^{n} \{U_f\}_j \cdot e^{i\omega_j t} \quad \ldots\ldots\ldots\ldots\ldots\ldots\ldots\ldots\ldots\ldots \quad (38)$$

$$\{\ddot{u}_f\} = -\sum_{j=1}^{n} \omega_j^2 \{U_f\}_j \cdot e^{i\omega_j t} \quad \ldots \ldots \ldots

response of a three layer system, Fig. 2, was computed and compared with that obtained in the previous studies. The system was first analyzed by Stoneley (9), later by Stoneley and Hochstrasser (10), and again by the second writer (4).

The results obtained using the code STABLE are compared with the results published by Stoneley in Table 1. In this particular case analyzed, a harmonic wave travels at a phase velocity of 12,441 fps (3.79 km/s) and at a frequency of 2.48 Hz. As can be noted, the agreement between the two sets of results is excellent. Since Stoneley's results are closed-form solutions, the comparison provides a vital test of the proposed theory.

TABLE 1.—Computed Response for Stoneley's Problem

Depth, in feet (1)	From Stoneley (9)		This Study	
	Horizontal (2)	Vertical (3)	Horizontal (4)	Vertical (5)
0	−0.8049	1.0000	−0.8043	0.9988
200	−0.5800	1.0313	−0.5793	1.0304
400	−0.4034	1.0254	−0.4028	1.0245
600	−0.2733	0.9895	−0.2728	0.9888
800	−0.1890	0.9312	−0.1887	0.9307
900	−0.1437	0.9097	−0.1436	0.9094
1,000	−0.1089	0.8848	−0.1088	0.8846
1,100	−0.0841	0.8572	−0.0841	0.8572

Note: 1 ft = 0.305 m.

Solutions for more complicated problems, unfortunately, are not available. Therefore, although it is desirable, it is not possible to test the code for problems such as soil-structure interaction problems for which the code was developed.

Demonstration Example

To demonstrate the potential applications of the proposed procedure the response of a 28-ft by 20-ft (8.5-m by 6.1-m) tunnel was analyzed. The lining of the tunnel is made of 2-ft (0.6-m) thick reinforced concrete for which the Young's modulus = 5.2×10^6 psi (0.366×10^6 kg/cm^2) and the Poisson's ratio = 0.24. The finite element model used in the analyses is shown in Fig. 3. Also shown in the figure are the soil profile and soil properties.

The time history of the input motion at the base of the finite element model is shown in Fig. 4. It is an artificial acceleration time history generated in accordance with Regulatory Guide 1.60 spectra (8) to give a broad frequency content in the frequency range of interest. Although it is possible to specify input motions in all the three directions, for this particular case, the motion is assumed to be horizontal and travels in the longitudinal direction of the tunnel. The phase velocity of the waves is assumed to be 2,000 fps (610 m/s).

To fully investigate the effects of wave travelling on the response of the soil-structure system, the following cases have been analyzed:

1. Free field soils only, assuming the foundation rock is perfectly rigid.
2. Soil-tunnel interaction system, assuming the foundation rock is perfectly rigid.
3. Free field soils only, assuming the foundation rock is flexible and waves are traveling at a velocity of 2,000 fps (610 m/s).
4. Soil-tunnel interaction system, assuming the foundation rock is flexible and waves are traveling at a velocity of 2,000 fps (610 m/s).

The assumption that the foundation rock is perfectly rigid implies an infinite speed of wave traveling. In such cases, the analyses are essentially the same as the conventional two-dimensional plane strain analyses commonly performed.

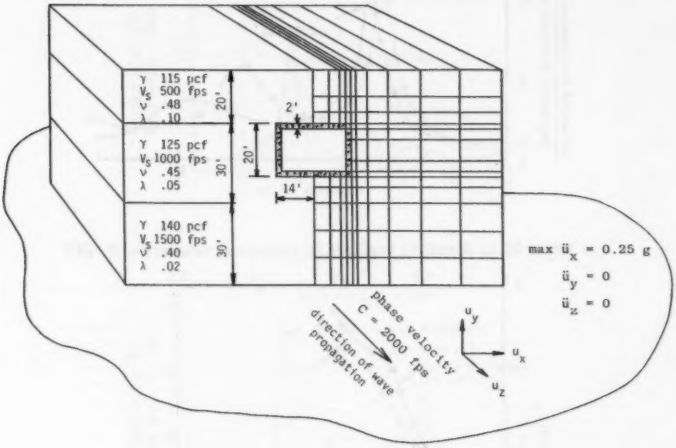

FIG. 3.—Demonstrating Example

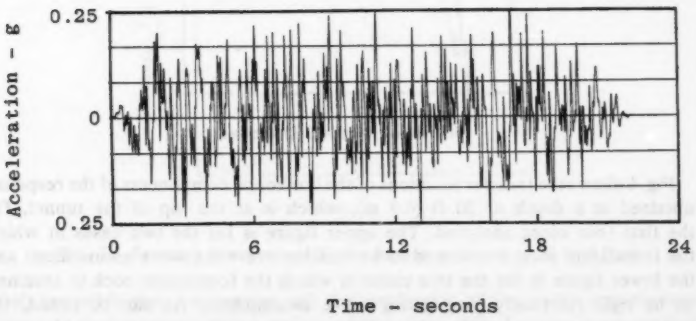

FIG. 4.—Input Motion at Base

Therefore, the computer code FLUSH (5) was used to compute the response for these cases.

The distributions of peak accelerations in the free field and the transfer functions, defined as the ratios between the computed response and the input motion as a function of frequency, of the motions at the surface are shown in Fig. 5. The effects of wave traveling can readily be seen. In the two cases shown, no vertical response was induced.

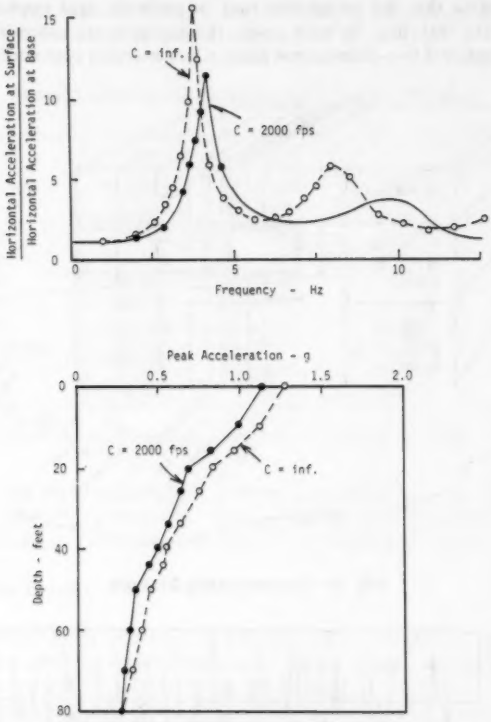

FIG. 5.—Free Field Response

Fig. 6 shows the transfer functions of the horizontal components of the response obtained at a depth of 20 ft (6.1 m), which is at the top of the tunnel, for the first four cases analyzed. The upper figure is for the two cases in which the foundation rock is assumed to be flexible (traveling wave assumption) and the lower figure is for the two cases in which the foundation rock is assumed to be rigid (vertically propagating wave assumption). As can be noted, the soil-tunnel interaction effects on the response are not significant. However, the wave-traveling effects, as can be evaluated by comparing the upper and

the lower figures, on the response can not be ignored. In general, it can be concluded that, if traveling waves are assumed, peaks in transfer functions

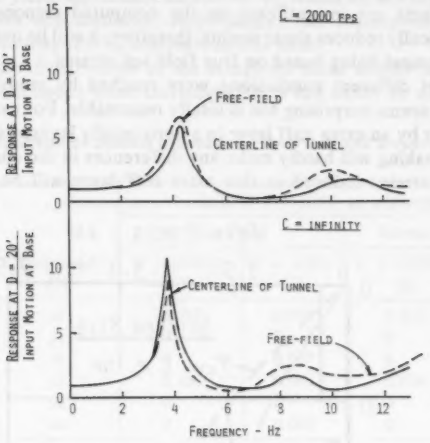

FIG. 6.—Transfer Functions of Motions at Depth of 20 ft (6.1 m)

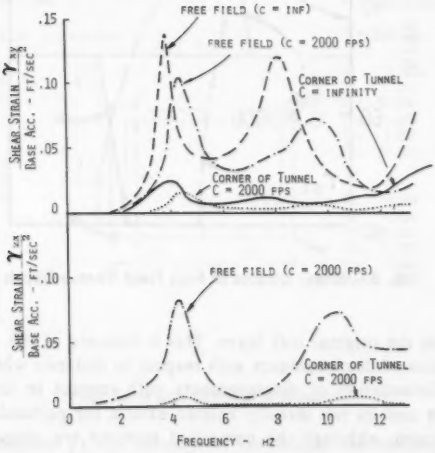

FIG. 7.—Transfer Functions of Shear Strains at Depth of 20 ft (6.1 m)

shift toward higher frequencies and the amplitudes of the peaks become less. This conclusion agrees with previous observations (12). For the cases studied, the vertical response caused by soil-tunnel interaction is quite small.

The transfer functions of the shear strains, γ_{xy} and γ_{zx}, computed at the upper corner of the tunnel are compared with those induced at the same depth in the free field in Fig. 7. Contradictory to the conclusion just made that soil-tunnel interaction effects are insignificant on the computed response, the presence of tunnel drastically reduces shear strains; therefore, it will be overly conservative to design the tunnel lining based on free field soil strains.

The fact that different conclusions were reached by studying the motions and the strains seems surprising but is totally reasonable. For example, replacing a thin soft layer by an extra stiff layer in a horizontally layered system subjected to horizontal shaking will hardly make any differences in the computed motions. But the shear strains induced in this extra stiff layer will be much less than

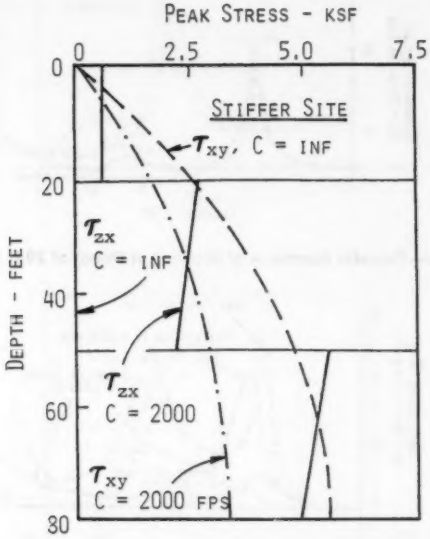

FIG. 8.—Shear Strains in Free Field Versus Depth

those induced in the original soft layer. This is because of the fact that strains are differentiation of displacements with respect to distance while accelerations are double differentiation of displacements with respect to time. Strains and acceleration are usually not directly related except for particular cases. In the example mentioned, although the computed motions are almost the same for the two systems, they are not identical. Because of the stress equilibrium at the interfaces between adjacent layers, the strains induced in the extra stiff layer and the original soft layer will be inversely proportional to the shear moduli of the two layers. Therefore it will be wrong to reach conclusions on the significance of soil-structure interaction effects by comparing motions obtained if strains, instead of motions, are the design parameters of interest.

Unfortunately, this important fact has not been well recognized in the past.

Another observation which can be made by studying Fig. 7 is that the traveling wave assumption yields significant amount of γ_{zx} which do not exist if vertically propagating waves are assumed. Accordingly, the assumption of vertically propagating waves may not be adequate in this case.

Fig. 8 shows the distributions of the computed shear strains in the free field versus depth. Pronounced wave-traveling effects can easily be noted. The peak

TABLE 2.—Comparison of Strains Induced in Free Field and Structural Response

Depth, in feet (1)	Component (2)	SHEAR STRAINS, as a percentage			
		Free Field		Corner of Tunnel	
		C = infinity (3)	C = 2,000 (4)	C = infinity (5)	C = 2,000 (6)
21	xy	0.067	0.044	0.013	0.007
	yz	0	0	0	0.002
	zx	0	0.067	0	0.004
39	xy	0.106	0.064	0.014	0.007
	yz	0	0	0	0.001
	zx	0	0.060	0	0.003

Note: 1 ft = 0.305 m.

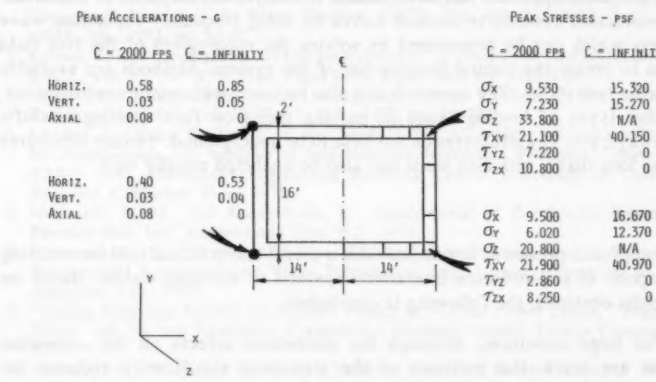

FIG. 9.—Peak Structural Response

shear strains obtained at the corners of the tunnel are summarized in Table 2. Also shown in the table are the corresponding free field strains. In general the strains at the corners of the tunnel are less than one fifth of those in the free field except ϵ_{yz} for which the free field values are zero.

The peak stresses computed at the corners of the tunnel are listed in Fig. 9. It is interesting to see that the traveling wave assumption also yields high normal axial stresses σ_z as a result of the bending of the tunnel as waves

travel along its longitudinal axis. For vertically propagating waves, some amount of axial stresses are caused by Poisson effects because of the plane strain assumption. Their magnitudes are not readily available but are limited to $\nu(\sigma_x + \sigma_y)$ which gives 7,340 psf (351,586 Pa) at the upper corners and 6,970 psf (333,863 Pa) at the lower corners. These amounts are significantly lower than those obtained for traveling waves.

As expected, the presence of tunnel produces some amount of vertical motions and the traveling of waves also causes some longitudinal movements. However, these induced motions are relatively small compared to the horizontal motions because this is a case for SH-wave propagation.

Analysis

The proposed approach is subjected to a couple of limitations. First of all, the geometry and the material properties have to remain the same along the longitudinal axis of a structure in order for Eq. 3 to be valid. This is rarely the case. Therefore, in most cases, representative soil profiles will have to be used. This is in line with almost all the analyses involving soils, even static problems, and should not present any difficulties for practical purposes. Secondly, the analyses using this approach are essentially linear analyses because responses are solved in the frequency domain instead of the time domain. The nonlinearity of material properties will have to be incorporated in the analyses using the equivalent linear method in conjunction with an iterative scheme.

The proposed approach can be expanded to analyze the response of soil-structure interaction systems to surface waves by using frequency-dependent wave numbers which can be determined by solving the eigenvalues of the free field system to obtain the natural frequencies of the system. Methods are available for such a task (4,14). The approach can also be used, with minor modifications, for other types of loadings such as moving trains on rails, landing aircrafts on runways, etc. The structures do not have to be underground. Surface structures such as long dikes, retaining walls can also be analyzed equally well.

Conclusion

The approach presented herein provides a useful and practical tool for studying the respone of soil-structure interaction systems to traveling waves. Based on the results obtained, the following is concluded:

1. For large structures, although the interaction effects on the computed motions are small, the presence of the structures significantly reduces the computed strains because the rigidities of the structures provide much resistance to deformations. Therefore, it may be overly conservative to design such structures based on the strains developed in the free field.
2. The assumption of vertically propagating waves are not adequate for predicting stresses and strains induced in underground structures. Proper considerations should be given to the traveling effects of waves in the design.

Appendix I.—Matrix Algebra

The multiplication of matrices in Eq. 30 is carried out herein. Let the matrix

$[B^*]$ be separated into the real and the imaginary parts so that

$$[B^*] = [A] + i\lambda [C] \quad \ldots \quad (41)$$

then the multiplication can be carried out as follows

$$[B^*]^{TC}[H][B^*] = ([A]^T - i\lambda [C]^T)[H]([A] + i\lambda [C])$$

$$= ([A]^T[H][A] + \lambda^2 [C]^T[H][C])$$

$$- i\lambda([C]^T[H][A] - [A]^T[H][C]) \quad \ldots \quad (42)$$

Because $[H]$ is a real and symmetric matrix, the real part of the result shown on the right hand side of this expression will be a symmetric matrix. Furthermore, because of the fact that

$$[A]^T[H][C] = ([C]^T[H][A])^T \quad \ldots \quad (43)$$

the imaginary part of the result will be an antisymmetric matrix. Therefore, the product of $[B^*]^{TC}[H][B^*]$ is a Hermitian matrix as stated previously.

Appendix II.—References

1. Azar, J. J., Bomba, J. G., and Randolph, V G., "Pipeline Stress Analyses," *Transportation Engineering Journal*, ASCE, Vol. 101, No. TE1, Proc. Paper 11122, Feb., 1975, pp. 163–170.
2. Hemant, S. H., and Chu, S. L., "Seismic Analysis of Underground Structural Elements," *Journal of the Power Division*, ASCE, Vol. 100, No. PO1, Proc. Paper 10648, July, 1974, pp. 53–62.
3. Kuesel, T. R., "Earthquake Criteria for Subways," *Journal of the Structural Division*, ASCE, Vol. 95, No. ST6, Proc. Paper 6616, June, 1969, pp. 1213–1231.
4. Lysmer, J., "Lumped Mass Method for Rayleigh Waves," *Bulletin of the Seismological Society of America*, Vol. 60, No. 1, Feb., 1970, pp. 89–104.
5. Lysmer, J., Udaka, T., Tsai, C.-F, and Seed, H. B., "FLUSH—A Computer Program for Approximate 3-D Analysis of Soil-Structure Interaction Problems," *Report No. EERC 75-30*, Earthquake Engineering Research Center, University of California, Berkeley, California, Nov., 1975.
6. Newmark, N. M., and Rosenblueth, E., *Fundamental of Earthquake Engineering*, Prentice-Hall, Inc., Englewood Cliffs, N.J., 1971.
7. Newmark, N. M., "Problems in Wave Propagation in Soil and Rock," *Proceedings*, International Symposium on Wave Propagation and Dynamic Properties of Earth Materials, Aug., 1967.
8. "Design Response Spectra for Seismic Design of Nuclear Power Plants," *Regulatory Guide 1.60*, Nuclear Regulatory Commission (formerly Atomic Energy Commission), 1973.
9. Stoneley, R., "Rayleigh Waves in a Medium with Two Surface Layers," *Monthly Notices, Geophysical Supplement*, Royal Astronomical Society, No. 7, 1955, pp. 71–75.
10. Stoneley, R., and Hochstrasser, U., "The Attenuation of Rayleigh Waves with Depth in a Medium with Two Surface Layers," *Monthly Notices, Geophysical Supplement*, Royal Astronomical Society, No. 7, 1957, pp. 279–288.
11. Tamura, C., "Design of Underground Structures by Considering Ground Displacements during Earthquakes," *Proceedings of U.S.-Japan Seminar on Earthquake Engineering Research with Emphasis on Lifeline Systems*, Nov., 1967, pp. 417–433.
12. Udaka, T., Lysmer, J. and Seed, H. B., "Dynamic Response of Horizontally Layered Systems Subjected to Traveling Seismic Waves," *Proceedings*, Second U.S. National Conference on Earthquake Engineering, Aug. 22–24, 1979.
13. Yeh, G., "Seismic Analysis of Slender Buried Beams," *Bulletin of the Seismological Society of America*, Oct., 1974, pp. 1551–1562.

14. Waas, G., and Lysmer, J., "Vibrations of Footings Embedded in Layered Media," *Proceedings*, WES Symposium on Applications of the Finite Element Method in Geotechnical Engineering, May, 1972.

Appendix III.—Notation

The following symbols are used in this paper:

A = area;
C = phase velocity of waves;
E = Young's modulus;
f = forces, or frequency;
h = thickness of slices;
J = Jacobian;
$\mathbf{K}$ = stiffness matrices;
$\mathbf{L}$ = stiffness matrices;
$\mathbf{M}$ = mass matrices;
p = forces;
s, t, z = transformed coordinates;
u, v, w = absolute displacements in the x, y, and z directions;
V = volume;
x, y, z = original coordinates;
β = damping ratio;
ϵ = strains;
λ = wave number;
ν = Poisson's ratio; and
σ = stresses.

JOURNAL OF THE GEOTECHNICAL ENGINEERING DIVISION

AT-REST LATERAL PRESSURE OF PEAT SOILS

By Tuncer B. Edil,[1] M. ASCE and Abdulmohsin W. Dhowian[2]

INTRODUCTION

The coefficient of lateral earth pressure under conditions of no lateral deformation, K_0, has been of interest to geotechnical engineers for many years for its role in reconstructing the geotechnical history of soil deposits and for its being an essential parameter in the design or analysis of many conventional problems. The number of situations requiring a knowledge of K_0 has increased, especially during the last decade or two, as a result of the increase in types of structures and situations which now require a great deal more rigour and thoroughness in their analysis. Although not readily amenable to mathematical formulation in terms of other soil parameters, K_0 is a complex function of soil microstructure (fabric), strength, and stress history. These parameters are, in general, interdependent to a certain extent. The range of values of K_0, and its relationship to a number of basic soil parameters, have been reported for sand and clay soils (see Abdelhamid and Krizek (1) for a comprehensive list of references); however, there are very few reports of K_0 for peat soils (2). Peat, encountered extensively in many parts of the world, is a fragmented organic material derived from vegetation which has been chemically changed and fossilized. It is formed in wetlands under appropriate climatic and topographic conditions. Today, some of the marginal sites are old wetlands that have been drained. Because of development in some parts of the world where peat deposits are extensive, methods of improving engineering properties of peats in situ and thus utilizing them as foundation materials, are becoming more and more

[1] Prof., Depts. of Civ. & Environmental Engrg. and Engrg. Mechanics, Univ. of Wisconsin, 2318 Engineering Building, 1415 Johnson Dr., Madison, Wisc. 53706.

[2] Asst. Prof., Dept. of Civ. Engrg., Riyad Univ., Riyad, Saudi Arabia.

Note.—Discussion open until July 1, 1981. To extend the closing date one month, a written request must be filed with the Manager of Technical and Professional Publications, ASCE. Manuscript was submitted for review for possible publication on May 6, 1980. This paper is part of the Journal of the Geotechnical Engineering Division, Proceedings of the American Society of Civil Engineers, ©ASCE, Vol. 107, No. GT2, February, 1981. ISSN 0093-6405/81/0002-0201/$01.00.

common (12). It is of prime importance for the success of such procedures to understand and quantify various engineering properties of peat soils. In an attempt made in this direction, this study presents the results of an experimental program directed towards evaluating K_0 and its dependence on stress history and other parameters of peat soils.

Peats Investigated

Fiber content appears to be a major compositional factor in determining the way in which peat soils behave. For this program, three types of peat with fiber contents ranging from about 20%–60% were investigated. The sampling sites of the peats used in this study are located in the following places in Wisconsin: Fon du Lac county, the city of Portage, and the city of Middleton (5), and the peat samples are designated after these locations. Fond du Lac Peat is an amorphous granular peat in which the soil particles are mainly of colloidal size and the other two peats are fibrous peats which have essentially an open structure with interstices filled with a secondary structural arrangement

TABLE 1.—Average Properties of Peat Samples

Source of samples (1)	Water content, as a percentage (2)	Unit weight, in kilonewtons per cubic meter (3)	Ash content, as a percentage (4)	Specific gravity (5)	Fiber content, as a percentage (6)	pH (7)	Vane shear strength, in kilopascals (8)	Sensitivity (9)	Classification	
									Lynn, et al. (Ref. 11) (10)	MacFarlane and Radforth (Ref. 13) (11)
Fond du Lac County, Wisc.	240	10.2	39.8	1.94	20	6.24	27.0	9.0	Sapric	Amorphous granular
Portage, Wisc.	600	9.6	19.5	1.72	31	7.30	14.4	3.0	Hemic	Fibrous
Middleton, Wisc.	510	9.1	12.0	1.41	64	7.00	22.0	4.4	Fibric	Fibrous

of nonwoody fine fibrous material (13). At all of the sites, the peat deposit occurred at the ground surface, and sampling was achieved by using a 76-mm OD Shelby tube (thin-wall sampling tube with a very sharp leading edge) (5). A portion of the sample in each tube was used to determine the characteristics of the peat. The average properties obtained for the three types of peat used in this study are given in Table 1. These properties were determined largely in accordance with the procedures suggested in Ref. 12. Fiber content was determined in accordance with the procedure suggested by Lynn, et al. (11).

In order to develop a visual appreciation of the peats tested, their microstructure was examined under a scanning electron microscope. An examination of the scanning electron micrographs of the peat samples, given in Fig. 1, indicates that Middleton Peat is made of relatively uniformly shaped fibers with little amount of soil grains or particles in between. Fond du Lac Peat, on the other hand, has a higher amount of soil grains and particles than the other two types of peat. The differences in fiber content are reflected in the micrographs as they were determined in the laboratory. It was noted that Portage Peat contains certain woody pieces larger than the fibers (not shown in Fig. 1).

MIDDLETON PEAT

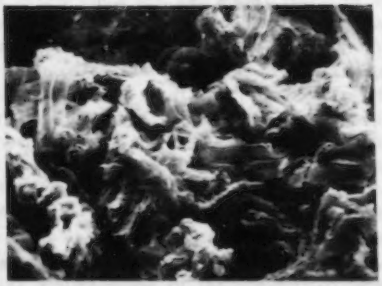

PORTAGE PEAT

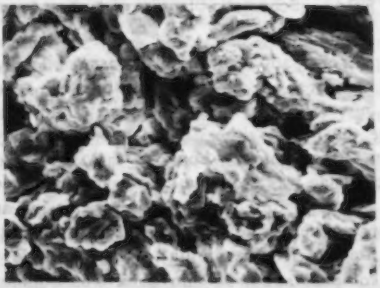

FOND DU LAC PEAT

100 μ

FIG. 1.—Scanning Electron Micrographs of Peat Samples

Test Equipment and Procedure

Available laboratory and in situ techniques to determine K_0 were classified and presented in a summary form by Abdelhamid and Krizek (1). Within the framework of their classification system, the technique employed in this investigation can be categorized as a direct approach of the semirigid ring type with continuous measurement of K_0 throughout the entire consolidation history of the peat, from its natural state with a high water content to a consolidated block with relatively low water content. The custom-built test apparatus consisted of a stainless steel "K_0-test tube" with strain gages mounted on its wall to monitor the time dependent history of the lateral pressure.

K_0-Test Tube.—Essentially, the apparatus consists of a honed stainless steel cylindrical tube (72.5-mm ID, 250 mm in height, and 2 mm in thickness) that is sealed by a lower end plate and a piston which is sealed against the cylinder

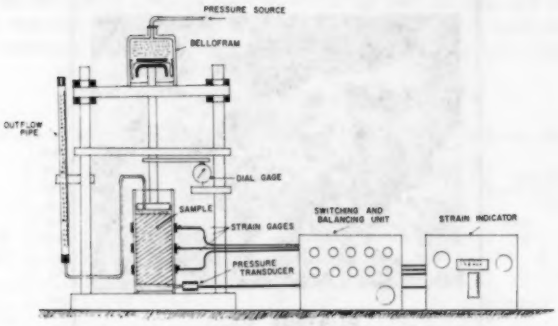

FIG. 2.—Schematic Diagram of K_0-Test Setup

wall by an O-ring. A schematic diagram of the assembled K_0-test tube is shown in Fig. 2. Vertical pressures are applied by means of an air cylinder (bellofram) connected to the piston. A pressure difference of approx 7 kPa was found sufficient to move the piston either up or down in the cylinder. The piston friction was taken into account in applying the vertical loads by calibrating the cell. Vertical drainage was provided by a cast-in-place porous stone located in the piston and the pore pressure was monitored using an integrated circuit pressure transducer connected to a cast-in-place porous stone located in the lower end plate. Starting from an initial average sample thickness of about 150 mm, a block of peat about 90 mm thick was obtained at the end of a typical K_0 test.

The side friction force between the K_0-test tube and the soil specimen was measured by determining the difference between the applied vertical load and the load transferred to the bottom of the specimen. The transferred load was measured by a load cell placed under a plate below the specimen inside the K_0-test tube which, in turn, rested on the loading table. The side friction force determinations were made for 20-30 Ottawa sand, Hydrite PX clay, and Middleton

Peat using this setup. The test results indicated that side friction increased with strain and pore pressure dissipation. Side friction force corresponding to "consolidated equilibrium," defined in terms of complete dissipation of measureable excess pore pressure, was linearly related to the applied vertical stress in a logarithmic plot with an average slope of 1 for all three soil types. The ratio of the maximum side friction force to the applied load increment per millimeter of specimen height was, on the average, 0.45–0.53 (corresponding to $e = 0.53$ and $e = 0.66$, respectively) for Ottawa sand, 0.58 for Hydrite PX clay, and 0.56 for Middleton Peat. These values fall below the values reported for bare steel and slightly above the values for teflon-lined rings (10); this may be due to honing and lubrication with grease of the steel tube surface.

Measurement of Total Lateral Pressure.—The hoop strains induced by the consolidating sample against the tube wall were measured by electrical resistance strain gages. They were 6.35-mm foil type strain gages with self-temperature compensation (Micromeasurements Model EA-06-250 BF-350). The gage resistance was 3.50.0 ± 0.15% ohms and had a gage factor of 2.12 ± 0.5% ohms at 24° C. They were mounted on the outside surface of the K_0-test tube at three levels (50 mm, 90 mm, and 140 mm from the base). At each level, four strain gages were mounted so that each pair of strain gages (one axial and one circumferential) placed 180° apart. The strain gages at each level were connected together, thus forming full bridge arrangement with circumferential gages wired in opposite arms of the bridge. This arrangement provides bridge completion as well as temperature compensation while eliminating bending and torsional effects. The advantage of having the four gages connected together is that the strain sensed by each strain gage is added together and, thus, the total strain indicated by the strain indicator is twice the actual hoop strain assuming axial strain from the soil-tube friction is negligible. This procedure, of course, increases the accuracy of the determined lateral pressure and, consequently, the K_0 coefficient. The magnitude of strain was measured by a strain indicator (Baldwin-Lima Hamilton Model 120C) in connection with a switching and balancing unit (Baldwin-Lima Hamilton Model 225). The pore-water pressure was measured by a hybrid integrated-circuit type pressure transducer (National Semiconductors Model LX1730GB). This relatively new transducer offers sufficient accuracy with lower cost, smaller volume change, and greater flexibility over the conventional strain gage-type transducer. Furthermore, it requires only simple and inexpensive read-out and recording systems.

Calibration.—The strain gages have to be calibrated accurately in order to determine the lateral pressure exerted by the soil specimen normal to the wall of the consolidation tube when a vertical pressure is applied. In order to calibrate the strain gages a known value of fluid pressure (air or water) is applied inside the tube and, since the fluid pressure is equal in all directions, the magnitude of the strain measured by the strain gage, corresponds to the known value of that lateral pressure. The calibration procedure indicated that all strain gages at all levels produced linear relationships maintaining a calibration factor constant throughout the range of applied pressures (5). No hysteresis effects were noticed during the cycling of load and the strain gages at all levels produced approximately the same calibration curve despite the difference in their locations. The calibrations performed before and after each K_0 test showed that the electronics of the system was stable without any significant long-term drifts.

The thickness of the K_0-test tube was chosen to assure that the tube was sufficiently thin so that the hoop deformations would be accurately sensed by the strain gages and also sufficiently thick to satisfy the K_0 condition (no lateral deformation). Computations based on the theory of elasticity using the tube dimensions and properties, as well as the characteristics of the strain gages, suggested a thickness of 1.31 mm as compatible with the level of sensitivity desired (7 kPa of lateral pressure). The tube selected had a wall thickness of about 2 mm. The radial strain at the maximum soil stress is computed to be on the order of 2×10^{-5} which is significantly less than the values given by Terzaghi (16) and Bishop (3) for the coefficient of lateral earth pressure to drop to the active state.

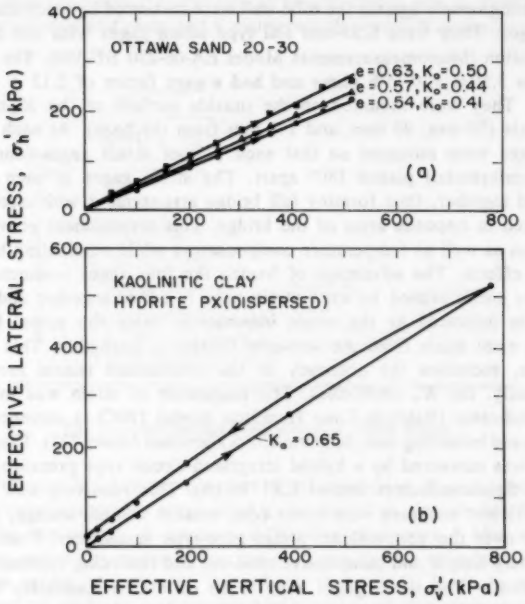

FIG. 3.—K_0 Response of a Sand and a Clay

In order to further verify that the K_0 condition is satisfied, two inorganic soils for which the K_0 values had been reported in the literature were also tested using the K_0-test tube. Furthermore, these tests provided a basis for the comparison of the K_0 response of peat soils. The two soils chosen were 20-30 Ottawa Sand, a cohesionless soil, and Hydrite PX, a kaolinitic clay. A linear relationship between applied vertical pressure and resulting lateral pressure is obtained at three different initial void ratios as shown in Fig. 3(*a*) for Ottawa Sand. The slope of these lines indicates the value of K_0 for normal loading at the corresponding void ratio. The measured values of K_0 appear reasonable

for this sand and compare well with the values calculated using Jaky's expression (Table 2) given in Ref. (8) as

$$K_0 = 1 - \sin \phi' \quad \ldots \ldots \ldots

vertical deformation, vertical stress, total lateral stress, pore-water pressure at the base and effluent outflow. Loading was applied to the peat specimen using a pressure increment ratio of 1. For certain increments, the top and bottom drainage were initially prevented, thereby permitting the sample to deform by compressing the gas within the soil mass, thus allowing the pore-water pressure to build to its maximum value. When the highest value of pore-water pressure was reached, and the deformation ceased, the consolidation was commenced by opening only the top drainage line. The effluent drained from the top of the specimen was collected in a burette. Each increment was left on the specimen for a period of approx 30 days which usually was sufficient to complete the primary consolidation and a considerable amount of secondary compression. At the advanced increments of pressure, because of the drastic decrease in permeability, a longer time was needed for the completion of pore-water pressure dissipation and, therefore, the final pressure increments were left on the specimen a much longer period of time than was the case in the conventional consolidation tests. For example, in Portage Peat, the final pressure increment (400 kPa–800 kPa) was maintained on the specimen for about 4 months. The same loading procedure adopted for Portage Peat was followed for the other two types of peak except, in the latter two peats, loading was carried out only to 400 kPa rather than to 800 kPa. The effect of overconsolidation was investigated by unloading 50% of the existing vertical pressure at a time and maintaining the specimen under that reduced pressure for a period of 1 day–2 days. Before and after each test, the K_0-test tube was calibrated to evaluate the variation, if any, in strain gage response to applied pressure. This procedure indicated that only slight changes took place, and they were within the accepted experimental variability.

Test Results

From the measured quantities, the total vertical and horizontal stresses, as well as the vertical strain, can be determined at any stage. The effluent outflow is normalized by dividing it with the initial volume of the specimen at the beginning of the stress increment application and is referred to as normalized outflow, $\Delta V/V_0$. After excess pore-water pressure dissipates under a given vertical stress increment, the measured vertical and horizontal stresses can be considered effective stresses and a value of K_0 can be computed.

Time-dependent response during a typical consolidation stage for Middleton Peat is given in Fig. 4. In this test the drainage was allowed as soon as the pressure increment was applied. Also shown in this figure is the ratio of lateral to vertical pressure increments, K, versus the logarithm of time. The pressure ratio, K, gradually decreases from an immediate value of 0.60 with time until it reaches a value of 0.32, at which it stabilizes. The value of K continues to decrease with time even after pore-water pressure has dissipated. This behavior is dissimilar to the one observed for inorganic soils where K is found to be constant after complete dissipation of excess pore-water pressure. Newlin (14) observed that lateral pressure values for a compacted clay specimen stabilized at almost exactly the same time excess pore pressure reached a negligible value. As shown in Fig. 4, the pore pressure dissipates after about 3,000 min, but the K value does not reach its final value before 14,000 min, thus, even under

the same effective pressure, K continues to decrease. The continuing decrease of lateral pressure indicates that considerable soil structure creep takes place. Apparently, the pore-water pressure associated with this process is very small to be sensed at the specimen boundary. The water continues to flow out of the specimen even after measurable pore pressure is completely dissipated. This also supports the contention that pore-water pressure exists in the specimen

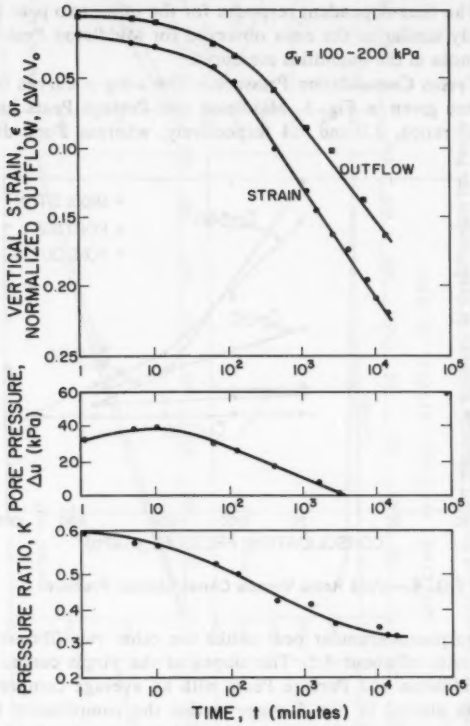

FIG. 4.—Time-Dependent Response during Typical Consolidation Stage

even though it may be very small to measure. The vertical strain (ϵ) and normalized outflow ($\Delta V/V_0$) curves generally have the same shape except that the rate of outflow is slightly lower than the rate of strain. For example, under this particular pressure increment, the deformation that can be accounted for by water outflow is about 20 mm, whereas the total deformation is 32 mm. The difference between the outflow and total deformation is partially due to the fact that the specimen was not saturated. However, the compressibility of the solid phase (fibers) could also contribute to this difference. The usual shape of the primary consolidation curve observed for inorganic soils is not apparent

in an ϵ-log t compression curve. The second straight line portion which may be termed "tertiary" compression (6) indefinitely continues even after the pressure ratio, K, stabilizes. In some other tests, a period of nearly a year was required before the measureable vertical strain ceases (6). The behavior shown in Fig. 4 was observed for other pressure increments with certain notable changes. For example, the time for complete dissipation of measurable pore pressure increases in the higher pressure increments due to the drastic decrease in permeability. The time-dependent response for the other two peat samples was also qualitatively similar to the ones observed for Middleton Peat with certain notable differences in the quantities measured.

Void Ratio Versus Consolidation Pressure.—The ϵ-log σ curves for the three types of peat are given in Fig. 5. Middleton and Portage Peats had relatively high initial void ratios, 8.0 and 7.4 respectively, whereas Fond du Lac Peat,

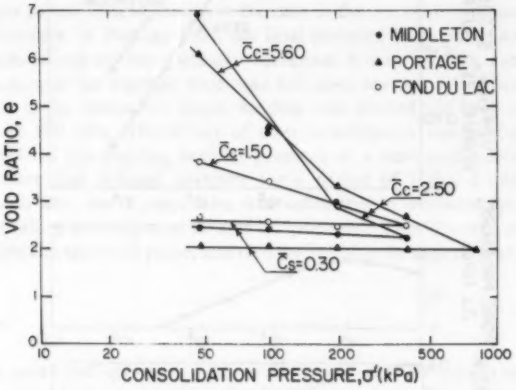

FIG. 5.—Void Ratio Versus Consolidation Pressure

which is an amorphous granular peat unlike the other two fibrous peats, had an initial void ratio of about 4.5. The slopes of the virgin curves are almost identical for Middleton and Portage Peats with an average compression index of 5.6. The data plotted in Fig. 5 suggests that the compression behavior of the fibrous peat samples during virgin consolidation can be divided into two distinct phases. The compression index decreases to an average value of 2.5 for these two peats after a consolidation pressure of 200 kPa. Fond du Lac Peat, on the other hand, exhibits a constant compression index of 1.5. In the unloading stage, all peats exhibited relatively low rebound with an average swell index of about 0.3. The void ratios decreased drastically during consolidation and they were 2.35, 2.70, and 2.50 at a vertical pressure of 400 kPa respectively for Middleton, Portage and Fond du Lac Peats.

K_0 Response.—The final values of lateral pressure ratio, K, when it stabilizes at a constant value, is defined as K_0 for the peat samples; K stabilizes at a time beyond the "consolidated equilibrium" defined in terms of the complete dissipation of measurable excess pore pressure. Several important aspects of

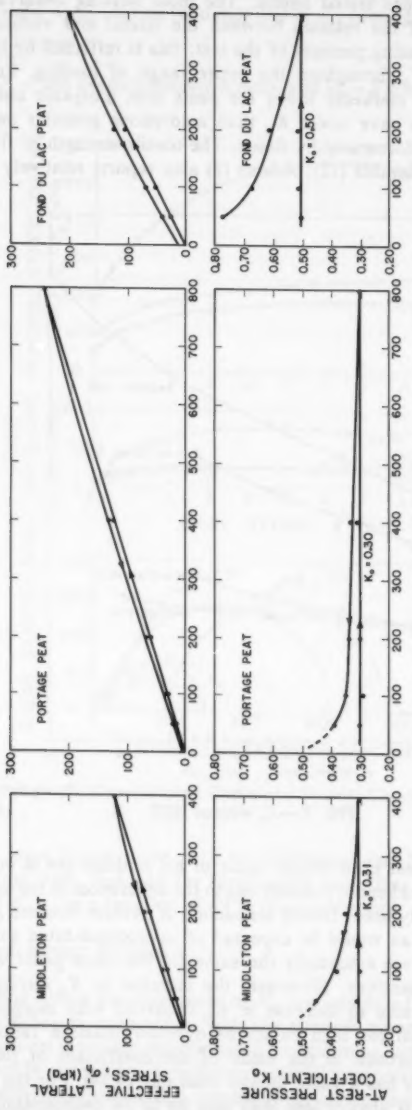

FIG. 6.—Lateral and Vertical Effective Stresses at Stabilization for Peats

the nature and variation of K_0 with stress history are manifested in Fig. 6 for the three peat types tested herein. The most striking observation is the nearly linear trend of the relation between the lateral and vertical effective stresses during the loading portions of the test; this is reflected by the virtually constant values of K_0 throughout the entire range of loading. Furthermore, the values of K_0 are markedly lower for peats than inorganic cohesive soils and the fibrous peats have lower K_0 than amorphous granular peat possibly due to the lateral reinforcement by fibers. The tensile strength of fibrous peats is known to be considerable (12). Adams (2) also reports relatively low values

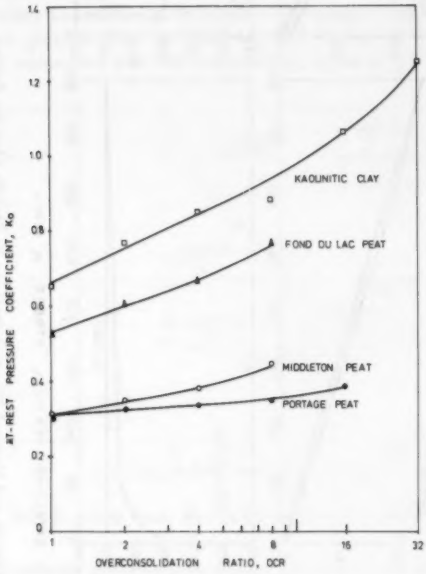

FIG. 7.—K_0 Versus OCR

of K_0 for a fibrous peat even though some of his findings are in contradiction with the trends reported herein, possibly due to the differences in the measurement techniques respectively used. During unloading, K_0 values become greater than those during loading, as would be expected of overconsolidated soils, and the qualitative responses are essentially the same for the three peats with notable differences in the quantities. However, the increase in K_0 during unloading is in no way comparable to increase in K_0 observed with inorganic soils. It has been reported that for high values of overconsolidation ratio, the value of K_0 appears to approach to the value of the coefficient of passive earth pressure and generally has a value greater than one (4,14). For the three peats tested, the K_0 value is always less than one up to an overconsolidation ratio of 16 as shown in Fig. 7. Despite the possibility of tube wall contraction resulting

in higher values of K_0 during unloading than really exist in the soil, the qualitative trends are probably quite reasonable. Schmidt (15) has proposed the following formula to relate $K_{0(rb)}$ (during rebound) and $K_{0(nc)}$ (during normal loading):

$$K_{0(rb)} = K_{0(nc)}(\mathrm{OCR})^{h_1} \quad \ldots \ldots \ldots

pore pressures are shown in Fig. 8 along with the total and effective failure envelopes for a sample of Middleton Peat. The general patterns indicated in Fig. 8 were observed for the other peats. The induced pore pressures during undrained shear were found to be relatively low and the pore pressure parameter, A_f, was generally less than 0.5 for all peats. The shear strength is mainly frictional with exceptionally high values of the effective angle of internal friction, ϕ' (50°–57°) compared to those of inorganic soils. Similarly high values of ϕ' were also reported by Adams (2) indicating that the shear strength of peat greatly increases by consolidation.

A number of expressions, mostly based on semiempirical considerations, have been suggested to evaluate K_0 from measured values of ϕ'. Value of K_0 obtained from each of these expressions, which were developed basically for inorganic soils, for the measured values of ϕ', are given in Table 3 along with the measured values of K_0. A comparison of the calculated values with those measured directly

TABLE 3.—Indirect Determination of K_0 from Shear Strength Parameters

Equation (1)	Most appropriate soil type (2)	Middleton Peat ($\phi' = 57.4°$) (3)	Portage Peat ($\phi' = 53.8°$) (4)	Fon du Lac Peat ($\phi' = 50.2°$) (5)
$K_0 = 1\text{-}\sin\phi'$ (Ref. 8)	Cohesionless	0.16	0.19	0.23
$K_0 = 0.95\text{-}\sin\phi'$ (Ref. 4)	Cohesive	0.11	0.14	0.18
$K_0 = 1\text{–}1.2\sin\phi'$ (Ref. 17)	Cohesive	−0.01	0.03	0.08
$K_0 = \frac{1}{2}\frac{\left[1 + \frac{\sqrt{6}}{8} - 3\frac{\sqrt{6}}{8}\sin\phi'\right]}{\left[1 - \frac{\sqrt{6}}{8} + 3\frac{\sqrt{6}}{8}\sin\phi'\right]}$ (Ref. 7)	Cohesionless	0.18	0.20	0.21
Direct Measurement of K_0	Peat	0.31	0.30	0.53

suggests that none of these equations are satisfactory for peat soils. Such discrepancy could be attributed to many factors including the argument that the empirical equations are valid only for a certain range of ϕ' values and for certain soil types. Lambe (9) suggests that the original theoretical derivation of K_0 given by Jaky in the form

$$K_0 = 1 - \frac{2}{3}\sin\phi' \quad \ldots\ldots\ldots\

as amorphous granular, according to the classification by MacFarlane and Radforth (13). It is, therefore, suggested that a low K_0 value of about 0.30 is associated with fibrous peats, whereas amorphous granular peats have a higher K_0 of about 0.53. This sort of broad distinction between fibrous and amorphous granular peat groups was also observed in an investigation of compression behavior involving large number of tests and four different peats (6) and supports the contention that this classification is meaningful for engineering purposes.

Conclusions

In view of the experimental results and the analyses presented in this investigation, the following conclusions can be advanced:

1. The K_0-test tube instrumented to measure lateral stresses and pore water pressures during one-dimensional consolidation provides a unique experimental capability for investigating the K_0 behavior of a wide variety of soils from sands to clays to peats.
2. The ratio of the horizontal stress to vertical stress at the time it stabilizes at a constant value (usually some time after the consolidated equilibrium is reached) is defined as the coefficient of lateral earth pressure at-rest, K_0, for peat soils; K_0 is constant throughout the range of virgin loading.
3. Significant difference is observed between the K_0 values of peats and clays, with the former being much lower due to the presence of fibers; furthermore, peat type exerts significant influence on the measured value of K_0 during loading, which is 0.53 for amorphous granular peat and about 0.30, a markedly low value, for fibrous peats.
4. The relationship between the horizontal and vertical effective stresses during unloading is nonlinear, and the value of K_0 is, therefore, not constant; however, the increases in K_0 during unloading is not as significant as those observed for clays.
5. The effective friction angle of peats is much higher than that for inorganic soils (about 50° for amorphous granular and 53°–57° for fibrous peats); the use of the effective friction angle to determine K_0 indirectly from empirical expressions was found to give unacceptable values of K_0 when compared with those measured in the laboratory. The use of the classical soil mechanics strength theory to explain the behavior of peats is limited due to the presence of fibers.
6. Classification of peats broadly into the categories of fibrous and amorphous granular peats appears meaningful for engineering purposes; this is supported by the K_0 behavior reported herein as well as by the compression behavior reported previously (6).

The value of K_0 of a soil determines the magnitude of in situ shear stresses in a soil deposit. The relatively low values of K_0 for peat soils implies the presence of higher in situ shear stresses for a given effective vertical stress than those in clay deposits. It is important to recognize this both with respect to the stability problems in the field involving peats as well as the usefulness of isotropically consolidated triaxial compression testing of peats in the laboratory. The effect of fibers on ϕ' observed for fibrous peat and certain industrial sludges (such as papermill sludge) leads one to conclude that normal soil mechanics

parameters cannot be used for such materials. The writers further recognize that environmental changes could have an effect on fiber quality and strength and consequently the parameters examined could be affected over time or with certain environmental changes.

Acknowledgments

The assistance of N. H. Severson and J. W. Dreger, Jr. in the design and construction of the K_o-test tube is gratefully acknowledged. G. B. Lee is acknowledged for his assistance in locating the sampling sites and providing background information on peat characteristics. G. H. Bahmanyar assisted in certain phases of sampling and triaxial compression testing. The second writer was supported by a fellowship from the University of Riyad during this study.

Appendix I.—References

1. Abdelhamid, M. S., and Krizek, R. J., "At-Rest Lateral Earth Pressure of Consolidating Clay," *Journal of the Geotechnical Engineering Division*, ASCE, Vol. 102, No. GT7, Proc. Paper 12240, July, 1976, pp. 721–738.
2. Adams, J. I., "Laboratory Compression Tests on Peat," *Proceedings of the Seventh Muskeg Research Conference*, National Research Council of Canada, Technical Memorandum No. 71, 1961, pp. 36–54.
3. Bishop, A. W., "The Test Requirement for Measuring the Coefficient of Earth Pressure at-Rest," *Proceedings of Brussels Conference on Earth Pressure Problems*, Vol. 1, 1958, pp. 2–14.
4. Brooker, E. Q., and Ireland, H. O., "Earth Pressure at-Rest Related to Stress History," *Canadian Geotechnical Journal*, Vol. 2, No. 1, 1965, pp. 29–38.
5. Dhowian, A. W., "Consolidation Effects on Properties of Highly Compressive Soils-Peats," thesis presented to the University of Wisconsin, at Madison, Wisc., in 1978, in partial fulfillment of the requirements for the degree of Doctor of Philosophy.
6. Dhowian, A. W., and Edil, T. B., "Consolidation Behavior of Peats," *Geotechnical Testing Journal*, American Society for Testing and Materials, Vol. 12, No. 3., Sept., 1980, in press.
7. Hendron, A. J., "The Behavior of Sand in One-Dimensional Compression," *Technical Documentary Report RTD-TDE-63-3089 to the United States Air Force*, University of Illinois, Urbana, Ill., 1963.
8. Jaky, J., "State of Stress at Great Depth," *Proceedings of the Second International Conference of Soil Mechanics and Foundation Engineering*, Vol. 1, 1948, pp. 103–107.
9. Lambe, T. W., "Methods of Estimating Settlement," *Journal of the Soil Mechanics and Foundations Division*, ASCE, Vol. 90, No. SM5, Proc. Paper 4060, Sept., 1964, pp. 47–71.
10. Leonards, G. A., and Girault, P., "Study of the One-Dimensional Consolidation Test," *Proceedings of the Fifth International Conference of Soil Mechanics and Foundation Engineering*, Vol. 1, 1961, pp. 213–218.
11. Lynn, W. C., McKinzie, W. E., and Grossman, R. B., "Field Laboratory Tests for Characterization of Histosols," *Histosols: Their Characteristics, Classification, and Use*, Soil Science Society of America, Special Publication No. 6, 1974.
12. MacFarlane, I. C., *Muskeg Engineering Handbook*, National Research Council of Canada, University of Toronto Press, Toronto, Canada, 1969.
13. MacFarlane, I. C., and Radforth, N. W., "A Study of the Physical Behavior of Peat Derivatives Under Compression," *Proceedings of the Tenth Muskeg Research Conference*, National Research Council of Canada, 1965.
14. Newlin, C. W., "Lateral Stresses During One-Dimensional Consolidation," thesis presented to Northwestern University, at Evanston, Ill., in 1965, in partial fulfillment of the requirements for the degree of Doctor of Philosophy.
15. Schmidt, B., "Lateral Stresses in Uniaxial Strain," *Danish Geotechnical Institute Bulletin*, No. 23, 1967, pp. 5–12.

16. Terzaghi, K., "Large Retaining Wall Test," *Engineering News-Record*, Vol. 112, 1934, pp. 136–140.

Appendix II.—Notation

The following symbols are used in this paper:

A_f = pore pressure coefficient;
$\bar{C}_c$ = compression index;
$\bar{C}_s$ = swell index;
c' = effective cohesion intercept;
e = void ratio;
h_1 = coefficient;
K = ratio of lateral to vertical pressure;
K_0 = coefficient of earth pressure at-rest;
$K_{0(nc)}$ = coefficient of earth pressure at-rest during normal loading;
$K_{0(rb)}$ = coefficient of earth pressure at-rest during rebound;
OCR = overconsolidation ratio;
Δu = excess pore pressure;
$\Delta V/V_0$ = normalized outflow;
ϵ = axial strain;
σ_1 = major principal stress;
σ_{1c} = vertical consolidation pressure;
σ_3 = minor principal stress;
σ'_h = effective horizontal stress;
σ'_v = effective vertical stress;
ϕ_{cu} = consolidated undrained angle of friction; and
ϕ' = effective angle of friction.

JOURNAL OF THE
GEOTECHNICAL
ENGINEERING DIVISION

TECHNICAL NOTES

Note.—Discussion open until July 1, 1981. To extend the closing date one month, a written request must be filed with the Manager of Technical and Professional Publications, ASCE. This paper is part of the Journal of the Geotechnical Engineering Division, Proceedings of the American Society of Civil Engineers, ©ASCE, Vol. 107, No. GT2, February, 1981.

Technical Notes

To provide a place within ASCE for publication of technical ideas that have not advanced, as yet, to the point where they warrant publication as a Proceedings paper in a *Journal*, the publication of Technical Notes was authorized by the Board of Direction on October 16–18, 1967, under the following guidelines:

1. An original manuscript and two copies are to be submitted to the Manager of Technical and Professional Publications, ASCE, 345 East 47th Street, New York, N.Y., 10017, along with a request by the author that it be considered as a Technical Note.
2. The two copies will be sent to an appropriate Technical Division or Council for review.
3. If the Division or Council approves the contribution for publication, it shall be returned to Society Headquarters with appropriate comments.
4. The technical publications staff will prepare the material for use in the earliest possible issue of the *Journal*, after proper coordination with the author.
5. Each Technical Note is not to exceed 4 pages in the *Journal*. As an approximation, each full manuscript page of text, tables, or figures is the equivalent of one-half a *Journal* page.
6. The Technical Notes will be grouped in a special section of each *Journal*.
7. Information retrieval abstracts and key words will be unnecessary for Technical Notes.
8. The final date on which a Discussion should reach the Society is given as a footnote with each Technical Note.
9. Technical Notes will not be included in *Transactions*.
10. Technical Notes will be included in ASCE's annual and cumulative subject and author indexes.

The manuscripts for Technical Notes must meet the following requirements:

1. Titles must have a length not exceeding 50 characters and spaces.
2. The author's full name, Society membership grade, and a footnote reference stating present employment must appear on the first page of the manuscript. Authors need not be Society members.
3. The manuscript is to be submitted as an original copy (with two duplicates) that is typed double-spaced on one side of 8-1/2-in. (220-mm) by 11-in. (280-mm) white bond paper.
4. All mathematics must be typewritten and special symbols must be properly identified. The letter symbols used must be defined where they first appear, in figures or text, and arranged alphabetically in an Appendix.—Notation.
5. Standard definitions and symbols must be used. Reference must be made to the lists published by the American National Standards Institute and to the *Authors' Guide to the Publications of ASCE*.
6. Tables must be typed double-spaced (an original ribbon copy and two duplicate copies) on one side of 8-1/2-in. (220-mm) by 11-in. (280-mm) paper. An explanation of each table must appear in the text.
7. Figures must be drawn in black ink on one side of 8-1/2-in. (220-mm) by 11-in. (280-mm) paper. Because figures will be reproduced with a width of between 3 in. (76 mm) to 4-1/2 in. (110 mm), the lettering must be large enough to be legible at this width. Photographs must be submitted as glossy prints. Explanations and descriptions must be made within the text for each figure.
8. References cited in text must be typed at the end of the Technical Note in alphabetical order in an Appendix.—References.
9. Dual units, i.e., U.S. Customary followed by SI (International System) units in parentheses, should be used throughout the paper.

Statistical Analysis of Marine Clay Deposits

By Hin Fatt Cheong,[1] M. ASCE
and R. V. Subrahmanyam[2]

Introduction

Extensive deposits of marine clay are found around the coastal regions of Singapore where several projects are currently in progress. The wide variations observed in physical properties of such marine clays make a statistical approach a useful tool.

Skempton (4) suggested a relation $c/\sigma = 0.11 + 0.0037\ (w_L - w_P)$ in which σ = effective overburden pressure; w_L = liquid limit, and w_P = plastic limit. Osterman (3) also proposed a similar linear relationship between the plasticity index and c/σ for marine clays. Koutsoftas and Fischer (2) reported graphically the relation among the undrained shear strength, overconsolidation ratio, and the effective consolidation stress for marine clays along the New Jersey coast in the United States. Balasubramaniam, et al., (1) expressed the undrained strength of Bangkok clays in terms of natural water content, unit weight, and effective overburden pressure.

In the present investigation, the main objective is to find a dimensionless regression equation for the normalized undrained strength of Singapore marine clays in terms of other normalized properties easily determined in the laboratory.

Fig. 1 summarizes the sequence of analytical operations and the reasons for the same.

Analysis

Preliminary analyses of the data obtained from bore logs indicate that the mean values of the same soil property for marine clay deposits at the various sites are significantly different. The soil parameters can be studied by normalizing each soil property according to the equation

$$Y_i^* = \frac{Y_i - \bar{Y}}{\Theta_Y} \quad \ldots\ldots\ldots\ldots\ldots\ldots\ldots\ldots\ldots\ldots\ldots\ldots\ldots\ldots\ldots\ldots\ldots\ldots (1)$$

[1]Sr. Lect., Dept. of Civ. Engrg., National Univ. of Singapore, Kent Ridge, Singapore 0511, Republic of Singapore.

[2]Sr. Lect., Dept. of Civ. Engrg., National Univ. of Singapore, Kent Ridge, Singapore 0511, Republic of Singapore.

Note.—Discussion open until July 1, 1981. To extend the closing date one month, a written request must be filed with the Manager of Technical and Professional Publications, ASCE. Manuscript was submitted for review for possible publication on March 2, 1980. This paper is part of the Journal of the Geotechnical Engineering Division, Proceedings of the American Society of Civil Engineers, ©ASCE, Vol. 107, No. GT2, February, 1981. ISSN 0093-6405/81/0002-0221/$01.00.

in which Y_i = ith observation of the soil property, Y, Θ_Y = standard deviation of Y; $\bar{Y}$ = mean of the observed values of Y; and Y_i^* = normalized value of Y_i. Normalization of the data from the various sites will give rise to normalized data sets from each site.

Since the normalized variable Y_i^* has expected zero mean and unit variance irrespective of the site, it is conceivable that the sets of Y_i^* for each site are statistically similar. In other words, it is possible that Y^* for each site can be described by the same probability law.

The assumption is first made that the sets of $\{Y_i^*\}$ describing any soil property for the various sites are statistically similar. The sets of $\{Y_i^*\}$ from the different

FLOW CHART
Raw data
H-test on raw data
To ascertain whether raw data from various sites belong to the same population
Normalisation of raw data
It is possible that normalised variates with zero mean and unit variance are from the same general population
Combined normalised data
If the above postulate is true, combining the normalised data is valid and this results in a larger sample for statistical analysis
Stepwise regression analysis
To check if postulate is acceptable, a multiple regression equation obtained through stepwise analysis is made. The residuals are then determined. Kruskal-Wallis H-test is required to determine whether the residuals are from the same population. If H-test is affirmative, then normalisation and grouping of normalised data is acceptable.
Randomness test on residuals
A basic requirement in the H-test is that the residuals are random variables
H-test on residuals
To determine whether the residuals from various sites belong to the same population
Frequency distribution
Necessary for sequential analysis
Sequential analysis
To check validity of regression analysis at a new site
Construction of confidence intervals

FIG. 1.—Flow Chart

sites are then grouped together to form a larger set $\{Y_i^*\}_\Sigma$, in which

$$\{Y_i^*\}_\Sigma = \{Y_i^*\}_A \, U \{Y_i^*\}_B \, U \{Y_i^*\}_C \, U \ldots \quad \ldots \ldots \ldots \ldots \ldots \ldots \ldots \ldots \ldots \ldots \quad (2)$$

The set of residuals $\{r_i\}_A$ of the normalized cohesion, c^*, for a given site, A, is obtained according to the following equation

$$r_i = c_i^* - f_i^*; \quad \text{site A values} \quad \ldots \ldots \ldots \ldots \ldots \ldots \ldots \ldots \ldots \ldots \ldots \ldots \quad (3)$$

in which f_i^* = predicted value of c_i^* obtained from the stepwise regression equation. The set of residuals are analyzed to ascertain: (1) If they are random;

(2) their frequency distribution; and (3) if they are independent of the normalized variates in the regression equation.

The Wald-Wolfowitz Runs test is being used to ascertain the randomness of the set of residuals at a given site with the residuals taken in order of occurrence with increasing effective stress. The test of randomness has to be applied to every set of residuals from all the sites before the application of the Kruskal-Wallis H-test for deciding whether the residuals of the normalized data sets from the different sites come from identical populations. The amount of data collected in a new site where marine clay is concerned is generally quite limited, especially if the area under development is not extensive. If these data values are normalized and can be grouped with normalized values of the sites from which the regression equation is obtained, then the dimensionless stepwise regression equation derived earlier may also apply to the new site. The sequential probability ratio (SPR) test may be used to ascertain the expected number of samples required to establish whether grouping is justified or not.

Let $\{r_i\}_E$ be the set of residuals for the new site, E, and $P_0(r)$ and $P_1(r)$ be the probability density functions of r with unit variance and means 0 and Θ, respectively. It is desired to test the hypothesis H_o that the observed set $\{r_i\}_E$ came from the distribution $P_0(r)$ against the possibility that it came from another distribution $P_1(r)$. The proposed sequential test employs the likelihood ratios sequentially. It presupposes that $\{r_i\}_E$ constitutes a random sample; i.e., the $r_i s$ are independent and identically distributed. The procedure entails the definition of the likelihood ratio

$$\lambda_m = \frac{\prod_{i=1}^{m} P_0(r_i)}{\prod_{i=1}^{m} P_1(r_i)}; \quad m = 1, 2, \ldots \quad \ldots\ldots\ldots\ldots\ldots\ldots\ldots\ldots\ldots\ldots (4)$$

and the sequential computation of computing these ratios. At each step in the computation, it is necessary to determine if the ratio lies within the interval (k_0, k_1) for preassigned Type I and Type II errors (α and β, respectively). The value α = the probability of rejecting H_o when it is true, and β = the probability of accepting H_o when it is false. The choice of α and β fixes k_0, k_1 since

$$k_0 \simeq \frac{\alpha}{1-\beta}; \quad k_1 \simeq \frac{1-\alpha}{\beta} \quad \ldots\ldots\ldots\ldots\ldots\ldots\ldots\ldots\ldots\ldots (5)$$

The test continues beyond the jth step as long as $k_0 < \lambda_j < k_1$ and stops at the mth step when $\lambda_m < k_0$ or $\lambda_m > k_1$. The hypothesis H_o is rejected if $\lambda_m < k_0$ and accepted if $\lambda_m < k_1$.

For the case in which $P_0(r)$ and $P_1(r)$ are both Gaussian distributed with means 0 and $\pm\Theta$ and standard deviation

$$\lambda_m = \prod_{i=1}^{m} e^{1/2} - V_i = e^{m/2} - \Sigma V_i \quad \text{for mean} \quad \Theta \quad \ldots\ldots\ldots\ldots\ldots\ldots (6)$$

$$\text{and} \quad \lambda_m = \prod_{i=1}^{m} e^{1/2} + V_i = e^{m/2} + \Sigma V_i \quad \text{for mean} \quad -\Theta \quad \ldots\ldots\ldots\ldots (7)$$

with $V_i = \frac{r_i}{\Theta}$ . . . . . (8)

Results and Examination

Data from three different geographical sites, namely Changi, Buona Vista, and East Lagoon in Singapore are analyzed. Since different testing methods on the soil samples yield different results, only those data covered by the undrained

TABLE 1.—Results of Stepwise Regression Analysis Based on Linear Combinations of Independent Variables

Variable (1)	Standard error of estimate S (2)	Computed F statistic (3)	$F_{0.05}(p,^b n^* - p - 1)$ $n = 130$ (4)
		(*a*) Step 1	
$R(\sigma^*) = 44.7$	0.80	69.78	3.92
$R(w^*) = 27.8$	0.88	35.97	3.92
$R(w_L^*) = 6.3$	0.97	6.69	3.92
$R(I_L^*) = 20.9$	0.91	25.27	3.92
$R(I_P^*) = 4.6$	0.98	4.82	3.92
		(*b*) Step 2	
$R(w^*/\sigma^*) = 3.65$	0.78	5.91	3.00
$R(w_L^*/\sigma^*) = 0.61$	0.80	0.95	3.00
$R(I_L^*/\sigma^*) = 2.05$	0.79	3.26	3.00
$R(I_P^*/\sigma^*) = 0.294$	0.80	0.46	3.00
$R(\sigma^*/w^*) = 20.57$	0.78	33.3	3.00
$R(\sigma^*/w_L^*) = 39.07$	0.80	48.8	3.00
$R(\sigma^*/I_L^*) = 25.89$	0.79	41.1	3.00
$R(\sigma^*/I_P^*) = 40.45$	0.80	63.2	3.00
		(*c*) Step 3	
$R(w_L^*/\sigma^*, w^*) = 0.32$	0.78	0.52	2.60
$R(I_L^*/\sigma^*, w^*) = 0.28$	0.79	0.46	2.60
$R(I_P^*/\sigma^*, w^*) = 0.43$	0.78	0.69	2.60

[a] n = number of observations.

[b] p = number of independent variables.

Note: Regression equation: $c^* = 0.48\sigma^* - 0.2w^*$; multiple regression coefficient = 0.62.

triaxial test are considered. The normalized engineering properties considered are effective stress, σ^*; cohesion, c^*; bulk density, γ^*; water content, w^*; liquid limit, w_L^*; plastic limit, w_P^*; liquid index, I_L^*; and plasticity index, I_P^*. Bore log data on marine clay without information on all of the aforementioned properties are not considered. Ambiguous data that accrued from tests performed on samples near boundaries of stratification are also discarded. In summary, there are 77, 38, and 15 data sets from Changi, Buona Vista, and East Lagoon,

respectively. The maximum depths at which samples have been taken is about 32 m, while 80% of the samples are from depths less than 10 m below ground level. Overconsolidated clays have not been included. For all sites, the bulk density exhibits the lowest variability about the mean value. Consequently, the use of the average value in the estimation of the effective stress at any prescribed depth due to the overlying surcharge will not incur serious errors.

The results of the stepwise regression analysis are summarized in Table 1 and the analysis is based on equations expressing c^*, the dependent variable, in terms of linear combinations of the independent normalized variables.

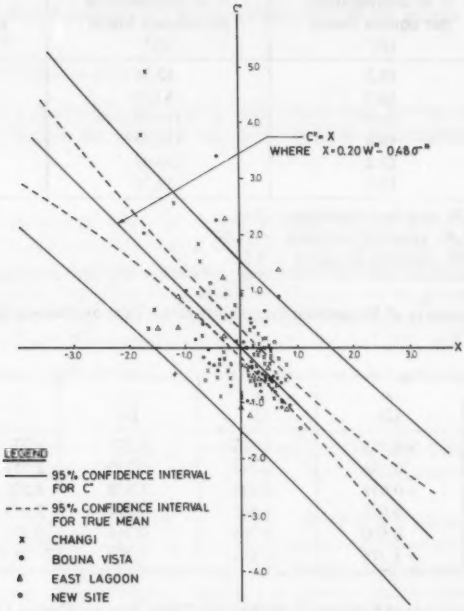

FIG. 2.—Plot of Regression Equation

The stepwise regression equations (SRE) are found to be

$$c^* = 0.48\sigma^* - 0.2w^* \quad \ldots \quad (9)$$

and

$$c^* = 0.52\sigma^* - 0.15I_L^* \quad \ldots \quad (10)$$

with multiple regression coefficients of 0.62 and 0.61, respectively. Eq. 9 is preferred, as it does not involve the determination of Atterberg limits. The graph of the regression equation with the confidence intervals are shown in Fig. 2 with the normalized data from the various sites plotted for comparison.

For each site, the residuals of the normalized variates about the SRE are obtained and the Kruskal-Wallis H-test is performed for the three sets of residuals

from Changi, Buona Vista, and East Lagoon. The computed H-statistic is 0.62, which is less than the critical value of 5.99 at the 5% level of significance. This test result indicates that the grouping of the three sets of residuals is justified. In the Two-Way Contingency Table tests, the residuals are ascertained to be independent of σ^* and w^* at the 5% level of significance.

TABLE 2.—Summary of Sequential Probability Ratio Test on Marine Clay Parameters at New Site

Data (1)	c, in kilonewtons per square meter (2)[a]	σ, in kilonewtons per square meter (3)[b]	w, as a percentage (4)[c]
1	10.5	42.38	69
2	14.4	64.35	64
3	14.4	111.83	61
4	16.8	130.47	59
5	17.2	150.09	58
6	12.9	169.71	58

[a]Mean = 14.37; standard deviation = 2.49.
[b]Mean = 111.47; standard deviation = 49.47.
[c]Mean = 61.50; standard deviation = 4.32.

TABLE 3.—Summary of Sequential Probability Ratio Test on Marine Clay Parameters at New Site

Data (1)	r (2)	v (3)	λ_i (4)	λ_m (5)
1	−0.536	−0.687	3.277	3.277
2	0.584	0.748	0.780	2.557
3	−0.014	−0.018	1.678	4.293
4	0.675	0.865	0.694	2.979
5	0.600	0.769	0.764	2.277
6	−1.316	−1.687	8.908	20.28 (Stop)

TABLE 4.—Summary of Sequential Probability Ratio Test on Marine Clay Parameters at New Site

Data (1)	r (2)	v (3)	λ_i (4)	λ_m (5)
1	−0.536	−0.687	0.829	0.829
2	0.584	0.748	3.483	2.887
3	−0.014	−0.018	1.619	4.675
4	0.675	0.865	3.915	18.305
5	0.600	0.769	3.557	65.11 (Stop)

As an illustration in the application of the SRE for estimating the cohesion values of marine clay at a new locality, the residuals from the SRE are determined and the SPR test is used to determine if the normalized values at the new

site can be incorporated into the total grouping. The results of such an analysis based on Gaussian assumption for residuals is given in Tables 2–4. In Table 2, the set of the first six data is taken. In Tables 3 and 4, the residuals are normalized using $\Theta = 0.78$ and the likelihood ratios, λ_i, are computed.

These results are obtained on the basis of limiting the Type I and Type II errors in the SPR test to 5% for which $k_0 = 0.053$ and $k_1 = 19.0$. It is seen that at least five or six samples are required to ascertain if the normalized variates of marine clay at the chosen new site can be grouped into the SRE; five samples are required for the case in which $P_1(r)$ is postulated to have a mean of $-\Theta$ and variance, Θ, and six for the case in which $P_1(r)$ is postulated to have mean Θ and variance Θ. Upon substitution of the means and variances for c, σ, and w

$$c = 0.024\sigma - 0.115w + 18.7 \quad \ldots \quad (11)$$

This approach is especially use if there are limited data for the new site where lack of adequate data can render a regression analysis meaningless.

Conclusions

Marine clay properties from the various geographical areas in Singapore could not be grouped together for statistical analysis in their raw form. This necessitated normalization at the areal level and the application of the Kruskal-Wallis H-test on the residuals showed that the normalized variates can be grouped for further statistical analyses. The final forms of the stepwise regression analysis which involved the independent variables σ^*, γ^*, w_L^*, w_P^*, w^*, I_P^*, and I_L^* are

$$c^* = 0.48\sigma^* - 0.2\,w^* \quad \ldots \quad (11a)$$

and

$$c^* = 0.52\sigma^* - 0.15I_L^* \quad \ldots \quad (11b)$$

in which the multiple correlation coefficients are 0.62 and 0.61, respectively. The validity of these equations has not been tested for overconsolidated and cemented clays.

For the 5% Type I and Type II errors, the SPR test shows that a small number of samples is sufficient to infer whether the normalized variates of the new site can be grouped with the total sample used earlier for regression analysis. This test, if affirmative, also permits the use of the stepwise regression equation for reduction to a simple predictive equation for cohesion at the new site.

Acknowledgments

The research described herein was sponsored by the Ministry of Science and Technology of the Republic of Singapore, under Grant MS/RG2/77. This support is gratefully acknowledged.

Appendix.—References

1. Balasubramanian, A. S., Adikari, G. S. N., and Sivandran, C., "Statistical Evaluation of the Strength Characteristics of Bangkok Clay," *Proceedings of the 3rd International Conference on Applications of Statistics & Probability in Soil & Structural Engineering*, Sydney, Australia, 1979.

2. Koutsoftas, D., and Fischer, J. A., "In-situ Undrained Shear Strength of Two Marine Clays," *Journal of the Geotechnical Engineering Division*, ASCE, Vol. 102, No. GT9, Proc. Paper 12431, Sept., 1976, pp. 989–1005.
3. Osterman, J., "Notes on the Shearing Resistance of Soft Clays," *Acta Polytechnica Scandinavica*, Stockholm, Sweden, No. 263, 1959.
4. Skempton, A. W., "Discussion: The Planning and Design of the New Hong Kong Airport," *Proceedings*, Institution of Civil Engineers, London, England, 1957.

Limit Plasticity Approach to Slope Stability Problems

By Ryszard J. Izbicki[1]

Introduction

In slope stability analysis, various limit equilibrium methods are applied, e.g., Fellenius' method (4), Bishop's method (1), Janbu's method (6), Kenney's method (8), the Morgenstern-Price method (11), Madej's method (10), and others. All these methods are generally called "methods of slices." The safety factor is obtained from the conditions of a global equilibrium of forces acting on the vertical rigid slices (see Fig. 1). Thus, the methods are similar to the limit analysis method, which is based on the static equilibrium of the field of forces being associated with the failure mechanism (see Ref. 5). However, application of the slices methods requires various additional assumptions concerning the force distribution on interfaces of slices, since the stability problems are statically indeterminate.

The application of the upper bound theorem to the determination of the safety factor is examined in this paper. The upper bound of the safety factor is compared with those obtained by conventional limit equilibrium methods. The accuracy of limit equilibrium methods is also estimated.

Upper Bound of Safety Factor

A classical measure of the margin of slope safety is the safety factor, F, defined as a relation between shear strength and mobilized shear stress; i.e.

[1]Lect., Inst. of Geotechnics, Technical Univ. of Wrocław, 53-621 Wrocław, Poland.

Note.—Discussion open until July 1, 1981. To extend the closing date one month, a written request must be filed with the Manager of Technical and Professional Publications, ASCE. Manuscript was submitted for review for possible publication on April 8, 1980. This paper is part of the Journal of the Geotechnical Engineering Division, Proceedings of the American Society of Civil Engineers, ©ASCE, Vol. 107, No. GT2, February, 1981. ISSN 0093-6405/81/0002-0228/$01.00.

$$F = \frac{\tau_f}{\tau_o} = \frac{\sigma \tan \phi + c}{\sigma \tan \phi_o + c_o} \quad \ldots \ldots \ldots

Both approaches are equivalent. It can be observed that the equation of the total work balance may be treated as an equation that expresses the condition of global equilibrium of the system consisting of rigid blocks. Also, the local equilibrium of each block may be performed, provided that along the division lines the shear stresses are of limit value.

Let us consider now the system of forces associated with the failure mechanism in which the sliding mass is divided into vertical rigid slices (see Fig. 1). When we introduce the symbols: $\Delta E_i = E_{i+1} - E_i$; and $\Delta X_i = X_{i+1} - X_i$, the equilibrium equations may be written as

$$-\Delta E_i + N_i \sin \alpha_i - T_{oi} \cos \alpha_i = 0 \quad \ldots \ldots \ldots \ldots \ldots \ldots \ldots \quad (4a)$$

$$W_i - N_i \cos \alpha_i - T_{oi} \sin \alpha_i - \Delta X_i = 0 \quad \ldots \ldots \ldots \ldots \ldots \ldots \quad (4b)$$

$$E_i y_i^M - X_i \left(\frac{b}{2}\right) - X_{i+1} \left(\frac{b}{2}\right) - E_{i+1} y_{i+1}^M = 0 \quad \ldots \ldots \ldots \ldots \quad (4c)$$

Eqs. 4*a* and 4*b* express the horizontal and vertical equilibrium; Eq. 4*c* expresses the moments equilibrium about the center point of the slice base.

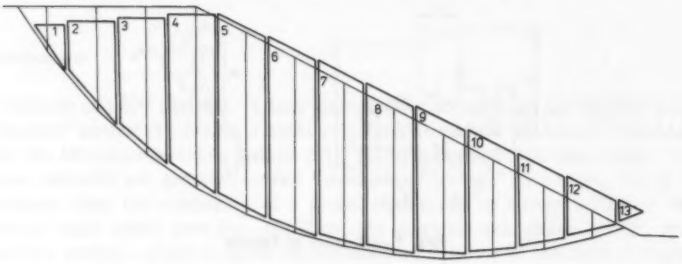

FIG. 2.—Failure Mechanism

Assuming the forces along the interfaces of slices and base to be the same as those for the limit state; i.e.

$$T_{oi} = \frac{N_i \tan \phi + c l_i}{F_k}; \quad X_i = \frac{E_i \tan \phi + c h_i}{F_k}; \quad X_{i+1} = \frac{E_{i+1} \tan \phi + c h_{i+1}}{F_k} \quad (5)$$

and making use of Eqs. 4*a* and 4*b*, we may write the condition of internal force equilibrium for the whole sliding mass, $\Sigma \Delta E_i = 0$, in the following form

$$\Sigma \Delta E_i = \Sigma \frac{1}{F_k} \left\{ -c l_i \cos \alpha_i + \left[F_k W_i - c \Delta h_i + c l_i \left(\frac{1}{F_k} \tan \phi \cos \alpha_i - \sin \alpha_i \right) \right] f_i \right\} = 0 \quad \ldots \ldots \quad (6)$$

in which

$$f_i = \frac{\sin \alpha_i - \frac{1}{F_k} \tan \phi \cos \alpha_i}{\frac{2}{F_k} \tan \phi \sin \alpha_i - \frac{1}{F_k^2} \tan^2 \phi \cos \alpha_i + \cos \alpha_i} \quad \ldots\ldots\ldots\ldots\ldots (7)$$

From these equations we may directly determine the value of the upper bound of the safety factor. The calculation of the increments ΔX_i is unnecessary,

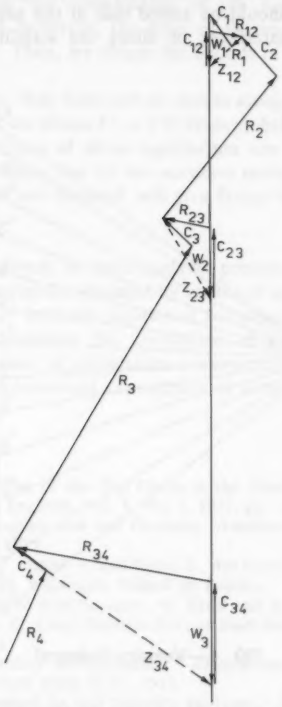

FIG. 3.—Force Polygon

because using Eqs. 5 allows the condition $\Sigma \Delta X_i = 0$ to be written as

$$\Sigma \Delta X_i = \frac{\tan \phi \, \Sigma \Delta E_i + c \Sigma \Delta h_i}{F_k} \quad \ldots\ldots\ldots\ldots\ldots\ldots\ldots\ldots\ldots (8)$$

From the aforementioned, it follows that when $\Sigma \Delta E_i = 0$, the condition $\Sigma \Delta h_i = 0$ is sufficient to satisfy $\Sigma \Delta X_i = 0$.

Calculation Example

For the slope 5 m high (see Fig. 2), with 1:2 inclination and soil parameters $\gamma = 20$ kN/m^3; $c = 10$ kPa; and $\phi = 20°$, it followed from Eq. 6 that $F_k = 2{,}17$. The piecewise linear and circumscribed on the circular arc slip surface, were assumed to be the shear surface bounding the sliding mass.

The satisfaction of equilibrium equations in geometrical interpretation corresponds to the building of the closed polygon of forces which in the case considered may be obtained by building successively the polygons for slices 1, 2, 3 and so on (see Fig. 3). It should be added that at the assumption of limit values of interactions along interfaces of slices the stability problem is statically determinate.

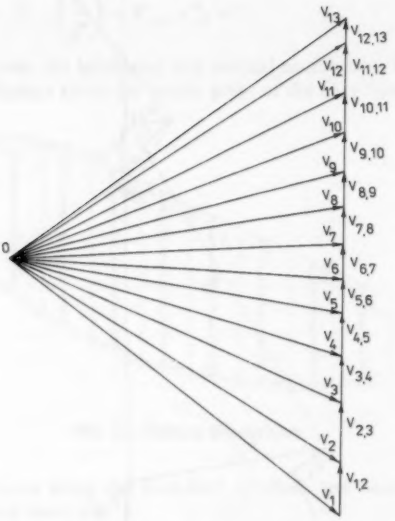

FIG. 4.—Velocity Hodograf

When constructing the hodograf of velocity (see Fig. 4) and making use of the equation of total work balance, we again arrive at the value $F_k = 2{,}17$. The assumed failure mechanism consists in shearing along the shear surface bounding; the sliding mass and along the vertical surfaces dividing the sliding mass into slices (see the translation scheme of Fig. 2). Internal dissipation was calculated from the formula

$$D = (\Sigma V_i l_i + \Sigma V_{i,i+1} h_i)\, c_o \cos \phi_o \quad \ldots\ldots\ldots\ldots\ldots\ldots\ldots\ldots\ldots (9)$$

and total work of body forces was given by

$$L = \Sigma W_i V_i \cos (90° - \alpha_i + \phi_o) \quad \ldots\ldots\ldots\ldots\ldots\ldots\ldots\ldots\ldots (10)$$

in which V_i = velocity of a slice; and $V_{i,i+1}$ determines the velocity discontinuity along the appropriate vertical line separating the neighboring slices.

Conclusions

The calculation example was taken from Ref. 10 (also see Ref. 11), in which the safety factors are given determined by some slices methods. The application of the correction in Kenney's method (10) resulted in $F'_k = 2{,}045$; the correction in Janbu's method gave $F'_k = 2.050$, whereas in Madej's method, $F'_k = 2.048$.

All the methods allow the construction of the associated force field in equilibrium; in this field, however, the state of forces on interfaces of slices lies below the limit state. Thus, we obtain the bounds of safety factor according to Eq. 3.

Assuming, additionally, that there are no forces along the interfaces of slices (as in Fellenius' method), we obtain $F'_k = 1.95$ from global equilibrium conditions. In this case, local conditions of slices equilibrium are satisfied for each slice separately. So, we may state that all the accurate methods of slices, provided that the yield condition is not violated, will give factor bounds in the interval

$$1.95 \leq F_k \leq 2.17 \quad \ldots\ldots\ldots\ldots\ldots\ldots\ldots\ldots\ldots\ldots\ldots\ldots\ldots\ldots \quad (11)$$

The upper bound approach of limit analysis presented in the paper allows the upper bound F_k to be rapidly obtained by means of an analytical or graphical method. The use of other methods mentioned for calculations is in most cases troublesome because it requires the application of an electronic calculation technique, and the increase in calculation accurracy for any of the methods is not proportional to the increased expenditure of work and energy.

Appendix.—References

1. Bishop, A. W., "The Use of the Slip Circle in the Stability Analysis of Slopes," *Geotechnique*, London, England, Vol. 5, No. 1, 1955, pp. 7–17.
2. Chen, W. F., *Limit Analysis and Soil Plasticity*, American Elsevier Publishing Co., Inc., New York, N.Y., 1975.
3. Derski, W., Izbicki, R. J., Kisiel, I., and Mróz, Z., *Rock and Soil Mechanics, Technical Mechanics*, Vol. 7, PWN, Warszawa, Poland (in Polish).
4. Fellenius, W., *Erdstatische Berechnungen*, W. Ernst and Son, Berlin, Germany, 1927.
5. Izbicki, R. J., and Mróz, Z., *Limit States in Soil and Rock Mechanics*, PWN, Warszawa, Poland, 1976 (in Polish).
6. Janbu, N., "Slope Stability Computations," *Embankment Dam Engineering*, John Wiley and Sons, Inc., New York, N.Y., 1973.
7. Karal, K., "Energy Method for Soil Stability Analyses," *Journal of the Geotechnical Engineering Division*, ASCE, Vol. 103, No. GT5, Proc. Paper 12917, May, 1977, pp. 431–445.
8. Kenney, T. C., "An Examination of the Methods of Calculating the Stability of Slopes," thesis presented to the Imperial College, at London, England, in 1956, in partial fulfillment of the requirements for the degree of Master of Science.
9. Livesley, R. K., "Limit Analysis of Structures Formed from Rigid Blocks," *International Journal for Numerical Methods in Engineering*, Vol. 12, No. 12, 1978, pp. 1853–1871.
10. Madej, J., *Analytical Methods of the Stability Calculation of Arbitrary Assumed Slip Surfaces*, PWN, Warszawa, Poland, 1976 (in Polish).
11. Morgenstern, N. R., and Price, V. E., "The Analysis of Stability of General Slip Surfaces," *Geotechnique*, London, England, Vol. 15, No. 1, 1965, pp. 79–93.

JOURNAL OF THE
GEOTECHNICAL
ENGINEERING DIVISION

DISCUSSION

Note.—This paper is part of the Journal of the Geotechnical Engineering Division, Proceedings of the American Society of Civil Engineers, ©ASCE, Vol. 107, No. GT2, February, 1981. ISSN 0093-6405/81/0002-0237/$1.00.

Discussions

Discussions may be submitted on any Proceedings paper or technical note published in any *Journal* or on any paper presented at any Specialty Conference or other meeting, the *Proceedings* of which have been published by ASCE. Discussion of a paper/technical note is open to anyone who has significant comments or questions regarding the content of the paper/technical note. Discussions are accepted for a period of 4 months following the date of publication of a paper/technical note and they should be sent to the Manager of Technical and Professional Publications, ASCE, 345 East 47th Street, New York, N.Y. 10017. The discussion period may be extended by a written request from a discusser.

The original and three copies of the Discussion should be submitted on 8-1/2-in. (220-mm) by 11-in. (280-mm) white bond paper, typed double-spaced with wide margins. The length of a Discussion is restricted to two *Journal* pages (about four typewritten double-spaced pages of manuscript including figures and tables); the editors will delete matter extraneous to the subject under discussion. If a Discussion is over two pages long it will be returned for shortening. All Discussions will be reviewed by the editors and the Division's or Council's Publications Committees. In some cases, Discussions will be returned to discussers for rewriting, or they may be encouraged to submit a paper or technical note rather than a Discussion.

Standards for Discussions are the same as those for Proceedings Papers. A Discussion is subject to rejection if it contains matter readily found elsewhere, advocates special interests, is carelessly prepared, controverts established fact, is purely speculative, introduces personalities, or is foreign to the purposes of the Society. All Discussions should be written in the third person, and the discusser should use the term "the writer" when referring to himself. The author of the original paper/technical note is referred to as "the author."

Discussions have a specific format. The title of the original paper/technical note appears at the top of the first page with a superscript that corresponds to a footnote indicating the month, year, author(s), and number of the original paper/technical note. The discusser's full name should be indicated below the title (see Discussions herein as an example) together with his ASCE membership grade (if applicable).

The discusser's title, company affiliation, and business address should appear on the first page of the manuscript, along with the *Proceedings* paper number of the original paper/technical note, the date and name of the *Journal* in which it appeared, and the original author's name.

Note that the discusser's identification footnote should follow consecutively from the original paper/technical note. If the paper/technical note under discussion contained footnote numbers 1 and 2, the first Discussion would begin with footnote 3, and subsequent Discussions would continue in sequence.

Figures supplied by the discusser should be designated by letters, starting with A. This also applies separately to tables and references. In referring to a figure, table, or reference that appeared in the original paper/technical note use the same number used in the original.

It is suggested that potential discussers request a copy of the *ASCE Authors' Guide to the Publications of ASCE* for more detailed information on preparation and submission of manuscripts.

Static Shear and Liquefaction Potential[a]

Discussion by Yoshiaki Yoshimi,[3] M. ASCE and Kohji Tokimatsu[4]

The authors have made a valuable contribution to resolving some of the conflicting views on the influence of initial static shear stress on the behavior of sand subjected to cyclic shear under constant volume conditions.

The writers admit that the simple shear test apparatus used by the authors is quite suitable for carrying out the constant volume cyclic loading tests. The ability of the apparatus to apply large shear strains at large shear stress ratios may be attributed to the fact that displacements rather than stresses are prescribed along the boundary surfaces of the specimen. In other words, the specimen is forced to deform into a parallelepiped with a well-defined *average* shear strain, at the expense of nonuniform stresses along the boundaries.

On the other hand, the ring torsion shear apparatus developed by the first writer and Oh-Oka (8,10) was designed to reduce the nonuniformity in the boundary shear stresses by making the specimen endless in the direction of shear and by making the height of the specimen proportional to the radius as shown in Fig. 11. As the authors point out, the ring torsion apparatus does impose nonuniform stresses and strains during consolidation. The first writer and Oh-Oka have shown, however, that such nonuniformity was considered insignificant when the geometry of the sample was as shown in Fig. 11 (8).

In order to facilitate comparison, the test results by the authors and those by the first writer and Oh-Oka (8) have been replotted in Fig. 12 in terms of normalized quantities. The ordinate shows the cyclic shear stress ratio, τ_{cy}/σ'_{vo}, required to cause 2%, 5% or 10% shear strain in 10 stress cycles at any value of static to cyclic shear stress ratio, τ_s/τ_{cy}, normalized with respect to that under a condition of total shear stress reversal, or $\tau_s = 0$. As indicated above Fig. 12, $\tau_s = 0$, $0 < (\tau_s/\tau_{cy}) < 1$, and $\tau_s/\tau_{cy} \geq 1$ correspond to conditions of total, partial, and no reversal of shear stress, respectively. The fact that the curves for $D_r = 37\%$ lie below those for $D_r = 50\%$ shows that the test data by the first writer and Oh-Oka are compatible with the authors'. The

[a]October, 1979, by Yoginder P. Vaid and W. D. Liam Finn (Proc. Paper 14909).
[3]Prof., Tokyo Inst. of Tech., 4259 Nagatsuta, Midori-ku, Yokohama 227, Japan.
[4]Asst. Prof., Tokyo Inst. of Tech., 4259 Nagatsuta, Midori-ku, Yokohama 227, Japan.

dimensionless relationship of Fig. 12 confirms the authors' important conclusion that the cyclic shear strength of sand may

> increase, decrease or remain unaltered, depending on the relative density of the sample, the shear strain level of interest and the magnitude of initial static shear stress.

Although Fig. 12 represents constant amplitude cyclic shear tests in which τ_s/τ_{cy} was held constant during each test, the value of τ_s/τ_{cy} varies during

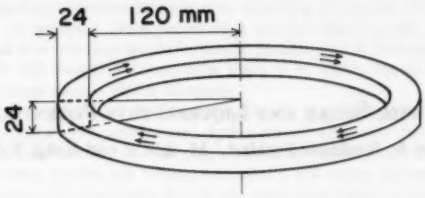

FIG. 11.—Shape of Specimen for Ring Torsion Shear Test by First Writer and Oh-Oka (8)

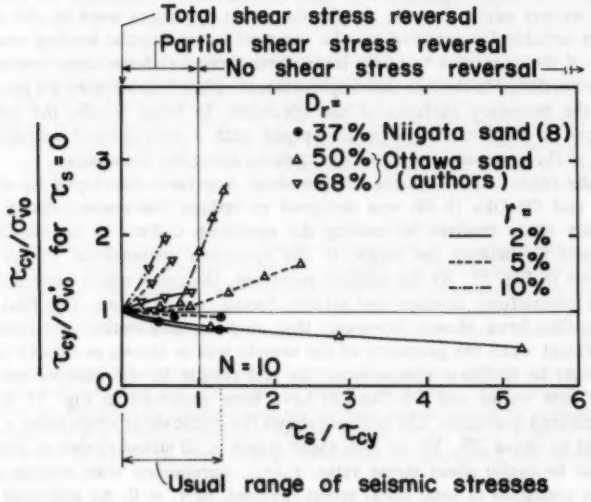

FIG. 12.—Comparison of Test Results by Authors and by First Writer and Oh-Oka (8)

an earthquake because τ_{cy} varies while τ_s remains constant. Therefore, the concept of equivalent uniform cyclic shear stress (9) that has been applied to the completely reversed shear stresses might require a certain modification when static shear stress is present. Nevertheless, if one takes 65% of the maximum

value of irregular dynamic shear stress as the amplitude of equivalent uniform cyclic shear stress, τ_{cy}, the ratio τ_s/τ_{cy} in embankments and in level ground near structures during strong earthquakes seldom exceeds unity, i.e., shear stress reversal usually occurs as indicated at the bottom of Fig. 12.

Appendix.—References

9. Annaki, M., and Lee, K. L., "Equivalent Uniform Cycle Concept for Soil Dynamics," *Journal of the Geotechnical Engineering Division*, ASCE, Vol. 103, No. GT6, Proc. Paper 12991, June, 1977, pp. 549–564.
10. Yoshimi, Y., and Oh-Oka, H., "A Ring Torsion Apparatus for Simple Shear Tests," *Proceedings*, 8th International Conference on Soil Mechanics and Foundation Engineering, 1973, Vol. 1, 2, pp. 501–506.

Technical Papers

Original papers should be submitted in triplicate to the Manager of Technical and Professional Publications, ASCE, 345 East 47th Street, New York, N.Y. 10017. Authors must indicate the Technical Division or Council, Technical Committee, Subcommittee, and Task Committee (if any) to which the paper should be referred. Those who are planning to submit material will expedite the review and publication procedures by complying with the following basic requirements:

1. Titles must have a length not exceeding 50 characters and spaces.

2. The manuscript (an original ribbon copy and two duplicate copies) should be double-spaced on one side of 8-1/2-in. (220-mm) by 11-in. (280-mm) paper. Three copies of all figures and tables must be included.

3. Generally, the maximum length of a paper is 10,000 word-equivalents. As an *approximation*, each full manuscript page of text, tables or figures is the equivalent of 300 words. If a particular subject cannot be adequately presented within the 10,000-word limit, the paper should be accompanied by a rationale for the overlength. This will permit rapid review and approval by the Division or Council Publications and Executive Committees and the Society's Committee on Publications. Valuable contributions to the Society's publications are not intended to be discouraged by this procedure.

4. The author's full name, Society membership grade, and a footnote stating present employment must appear on the first page of the paper. Authors need not be Society members.

5. All mathematics must be typewritten and special symbols must be identified properly. The letter symbols used should be defined where they first appear, in figures, tables, or text, and arranged alphabetically in an appendix at the end of the paper titled Appendix.—Notation.

6. Standard definitions and symbols should be used. Reference should be made to the lists published by the American National Standards Institute and to the *Authors' Guide to the Publications of ASCE*.

7. Figures should be drawn in black ink, at a size that, with a 50% reduction, would have a published width in the *Journals* of from 3 in. (76 mm) to 4-1/2 in. (110 mm). The lettering must be legible at the reduced size. Photographs should be submitted as glossy prints. Explanations and descriptions must be placed in text rather than within the figure.

8. Tables should be typed (an original ribbon copy and two duplicates) on one side of 8-1/2-in. (220-mm) by 11-in. (280-mm) paper. An explanation of each table must appear in the text.

9. References cited in text should be arranged in alphabetical order in an appendix at the end of the paper, or preceding the Appendix.—Notation, as an Appendix.—References.

10. A list of key words and an information retrieval abstract of 175 words should be provided with each paper.

11. A summary of approximately 40 words must accompany the paper.

12. A set of conclusions must end the paper.

13. Dual units, i.e., U.S. Customary followed by SI (International System) units in parentheses, should be used throughout the paper.

14. A practical applications section should be included also, if appropriate.